Aus dem Institut für Neuropathologie
der Medizinischen Fakultät Charité – Universitätsmedizin Berlin

DISSERTATION

Mechanisms of immunotherapy in Alzheimer's disease – testing the peripheral sink hypothesis by restricting Aβ-antibodies to the periphery

zur Erlangung des akademischen Grades
Doctor of Philosophy (PhD)
des
International Graduate Program Medical Neurosciences

vorgelegt der Medizinischen Fakultät
Charité – Universitätsmedizin Berlin

von

Nicole Hentschel

aus Wernigerode

Gutachter/in: 1. Prof. Dr. med. F. Heppner

2. Prof. Dr. rer. nat. A. Radbruch

3. Prof. Dr. rer. nat. A. Waisman

Datum der Promotion: 22. März 2013

ABSTRACT

Alzheimer's disease (AD), a progressive neurodegenerative disease, is the most common form of dementia in later life and a major cause of disability and death in the elderly.[1] Amyloid-β (Aβ) immunotherapy for patients with AD offers an important chance for treating this devastating disease. However the mechanism by which antibodies reduce Aβ deposition in the brain is still unknown. There have been three mechanisms postulated to explain how antibody-directed clearance of Aβ could work – activation of microglial phagocytosis, catalytic dissolution of Aβ fibrils and shift of the Aβ equilibrium from the central nervous system to the blood. The latter was termed the peripheral sink hypothesis, and argues that anti-Aβ antibodies sequester circulating Aβ to either favor increased clearance from the brain or simply to prevent the influx to the brain. The main object of this thesis was to prove or falsify the peripheral sink hypothesis *in vivo*. To accomplish this, I utilized novel transgenic (tg) mice which produce anti-Aβ IgM antibodies (AB9-IgM) and B cell-bound anti-Aβ IgG antibodies (*AB9μ* mice), as well as a novel mouse strain only producing B cell-bound anti-Aβ antibodies (*DelS* mice). Neither B cells nor IgM antibodies are expected to enter the brain during the course of AD,[2] thereby restricting anti-Aβ antibodies to the periphery. *15B3* mice served as control as they harbor the same IgM transgene with a CDR (Complementarity Determining Region) of unknown specificity.

First, the immunophenotype of *AB9μ* and *DelS* mice was assessed through flow cytometric analyses of B cell development, B cell proliferation as well as peripheral blood immune cells and B cells. Further assessment strategies included histological examination and *in vivo* infection assays utilizing vesicular stomatitis viridae (VSV). All *AB9μ* and *DelS* lines contained tg B cells and all *AB9μ* lines elicited anti-Aβ-antibody titers. Both *AB9μ* and *DelS* mice were lacking obvious alterations in the immune system, which has insofar been shown to be crucial, as a growing number of publications report that changes of the systemic immune system influence AD pathology[3-5], which could blur putative specific changes of the transgenes introduced by us (*AB9μ* and *DelS*) in AD mouse models.

Second, we crossed *AB9µ* and *DelS* mice to two different AD mouse models – *APPPS1* and *TgSwDI* mice – as they show biochemical and histological differences in the deposited Aβ. Notably, we observed a reduction of Aβ plaque load at 250 days in *AB9µ-APPPS1* mice and – to some extent – in *DelS-APPPS1* mice with Aβ42 being the prevalent Aβ species reduced. The noted reduction of Aβ burden at 250 days was limited to diffuse plaques and did not involve compact core plaques. At 120 days, we only observed alterations in plaque size distribution in *AB9µ-APPPS1*, which might be due to the fast kinetics of *de novo* plaque generation at this rather early time point which overrules putative anti-Aβ antibody-mediated effects. One key finding providing further evidence for the peripheral sink paradigm is the increase in serum Aβ42 in *AB9µ-APPPS1* mice which is in accordance with the predominant reduction in Aβ42 in the brain of these mice. In *TgSwDI* mice crossed to *AB9µ* and *DelS* mice we could not find any difference in plaque deposition. Yet, the data obtained in *TgSwDI* mice are – in contrast to the data obtained in *APPPS1* mice – not fully conclusive as *TgSwDI* mice – due to the Dutch/Iowa mutations within the Aβ peptide – do not serve as an ideal tool for the herein proposed question. Intracerebroventricular (icv) administered AB9-IgM antibodies did not exhibit an alteration in plaque load, whilst icv administered AB9-IgG significantly ameliorated Aβ pathology. This demonstrated that – even if IgM antibodies can cross the blood brain barrier – AB9-IgM antibodies are less likely to produce the same effect as AB9-IgG due to the fact that IgM effector functions might not be sufficient to reduce plaque load locally and/or that AB9-IgM cannot penetrate that far into the tissue.

Further studies in another AD mouse model, namely APP23 mice, could further help to dissect the contribution of the peripheral sink to immunotherapeutic approaches. Studies focusing on transport and degradation systems involved in the peripheral clearance of Aβ could promote to unravel the mechanism underlying immunotherapy. A better insight into the action of Aβ immunotherapy might help to design and test new combination therapies.

CONTENTS

LIST OF ABBREVIATIONS

3xTg	triple transgenic mice carrying APP, PS1 and tau mutation
AB9µ	transgenic mice expressing Aβ-specific Ab9 IgM antibodies
AD	Alzheimer's disease
AICD	APP intracellular domain
ApoE	apolipoprotein E
APP	amyloid precursor protein
APPPS1	transgenic mice carrying the Swedish APP and the presenilin 1 mutation L166P
Aβ	amyloid β
BBB	blood brain barrier
BM	bone marrow
CAA	cerebral amyloid angiopathy
CAD106	Aβ1-6 peptides covalently conjugated to virus like particles
CFA	complete Freund's adjuvant
CFDA-SE	Carboxyfluorescein diacetate, succinimidyl ester
CNS	central nervous system
CSF	cerebrospinal fluid
CT	computed tomography
CTF	C-terminal fragment
CP	choroid plexus
DeIS	transgenic mice expressing Aβ-specific Ab9 IgM antibodies only on the surface of B cells
Dpi	day post immunisation
DS	Down Syndrom
EAD	early onset Alzheimer's disease
ELISA	Enzyme-linked immunosorbent assay
FAD	familial Alzheimer's disease
FO	follicular
IFA	incomplete Freund's adjuvant
IP	immunoprecipitation
ISF	interstitial fluid
LRP	lipoprotein receptor-related protein
LPS	lipopolysaccharide
LTP	long-term potentiation
MBP	mannan binding protein
MRI	magnetic resonance imaging
MZ	marginal zone
NMDA	N-methyl-D-aspartate

PAGE	polyacrylamide gel electrophoresis
PB	peripheral blood
PCR	polymerase chain reaction
PFTAA	pentameric formyl thiophene acetic acid
P-gp	P-glycoprotein
PRP^c	cellular prion protein
PS	presenilin
PSAPP	transgenic mice carrying PS1 and APP mutations
RAGE	receptor of advanced glycation end products
RH	RPMI 1640 containing 1% Hepes
RT	room temperature
RT-PCR	real-time polymerase chain reaction
sRAGE	soluble receptor of advanced glycation end products
sLRP	soluble lipoprotein receptor-related protein
TgSwDI	transgenic mice carrying the Swedish, Dutch and Iowa mutated APP
Th	T helper
VLP	virus like particle
VSV	vesicular stomatitis virus
WS	Withania somnifera

LIST OF FIGURES

INTRODUCTION

Alzheimer`s disease (AD) is the leading cause of dementia and disability in the aged population. According to the World Health Organization it affects 18 million people worldwide. Prevalence increases exponentially with age[6], affecting about 1% of the population aged 65-69 years up to as much as 30-40% of those aged 90 and older.[7,8] This makes advancing age the greatest risk factor of the disease. Correspondingly, AD represents a significant concern for the future of health care systems due to changing demographic profiles, with an increased proportion of elderly and increased life expectancy. In 2010, the global economic impact of AD and other dementias was US$604 billion. About 70% of the costs occur in Western Europe and North America.[9,10] To date there exists no curative treatment or effective disease-modifying therapy. Approved treatments, including acetylcholine-esterase inhibitors and N-methyl-D-aspartate (NMDA) receptor antagonists, have only modest symptomatic effects.[11] This emphasizes the importance of further research on the pathophysiological mechanisms, as well as the search for novel strategies to combat the disease.

1. Clinical features & diagnosis of Alzheimer's disease

In 1906, the German psychiatrist and neuropathologist Alois Alzheimer published an essay about a 50 year-old delusional woman called Auguste D. with unusual behavioral symptoms and progressive loss of cognitive functions.[12] Auguste D. was the first person who was diagnosed with AD. With his essay Alois Alzheimer provided the classical clinical and anatomical pathological description of the disease.[13,14]

AD is a chronic progressive neurodegenerative brain disorder with most affected patients dying within 3 to 9 years after diagnosis.[15] However, the first pathological changes begin to develop decades before the earliest symptoms set in.[16,17] Consequently the entire disease course may take twenty years, the first half being without overt symptoms. Its clinical manifestation differs between individuals, but the most common early symptom is worsening ability to remember recent information, referred to as mild cognitive impairment (MCI). The disease advances from these minor memory problems to complete loss of

cognitive functions and eventually death. Gradual cognitive dysfunctions are related to language, memory and judgment. In later disease stages, AD can be accompanied by a variety of neuropsychiatric symptoms such as depression, hallucinations and delusions. Along with these symptoms, restrictions in performing activities of everyday life such as dressing, eating and bathing and changes in personality are common.

There are several parameters which serve as the basis for a diagnosis of AD, such as medical and family history together with clinical, neurological, and psychiatric examinations. In addition, brain imaging is an important diagnostic tool in AD. CT (computed tomography) scanning and magnetic resonance imaging (MRI) are especially beneficial to detect brain changes characteristic for later disease stages including cerebral atrophy (see Fig. 1) and to rule out other causes of dementia such as stroke and brain tumors.[18] Several studies showed that amyloid β42 in the cerebrospinal fluid (CSF) was decreased in AD,[19-22] and currently this is an accepted biomarker for AD[23,24] that is frequently used in clinical practice.[25,26] Other emerging biomarkers which are attributed a more prominent role in the diagnostic criteria are total tau and phosphorylated-tau in CSF as well as amyloid tracer uptake and fluorodeoxyglucose (FDG) in positron emission tomography (PET).[27-29] With a combination of these tools AD can be diagnosed with more than 95% accuracy. However, an unequivocal diagnosis can only be made post-mortem via neuropathological autopsy.[30]

2. Pathophysiology of Alzheimer's disease

In AD the symptoms are caused by progressive synaptic degeneration and neuronal loss in the limbic system and neocortex, brain regions critical for thought processing and memory.[31,32] At the microscopic level, neuropathological hallmarks used for final diagnosis of AD are neuritic amyloid plaques, consisting of fibril β-amyloid peptide (Aβ) aggregates and neurofibrillary tangles (NFTs) containing hyper-phosphorylated tau protein filaments (Fig. 1).[15,32] Tau is an intracellular microtubule binding protein which when hyper-phosphorylated will destabilize microtubules and thus will hamper axonal transport and compromise neuronal and synaptic function.[33] Whether tangle formation is a cause or consequence of the disease is still under debate. Importantly, NFTs are implicated in other neurodegenerative diseases besides AD which are called tauopathies and are also associated

with pathological aggregation of tau protein. Neuropil threads are further pathological alterations in AD which occur in dystrophic distal dendrites in the vicinity of amyloid plaques and NFTs and also are composed of hyper-phosphorylated tau.[34] Aβ is an extracellular cleavage product of the transmembrane amyloid precursor protein (APP). Furthermore, amyloid plaques have been reported in individuals that show no symptoms of dementia,[35,36] which also could be due to the fact that plaque deposition occurs prior to clinical decline.[16,17,37] Another pathological feature of Aβ deposition is cerebral amyloid angiopathy (CAA). In CAA Aβ deposition in blood arterioles leads to compromised vessels resulting in hemorrhages.[38] Another pathological attribute of AD is granulovacular degeneration which involves the accumulation of small vacuoles containing basophilic granules most commonly within pyramidal neurons of the hippocampus.[39,40] Among all these pathologic features, synaptic loss and selective neuronal death are best correlated with severity of cognitive impairment.[41-43]

Studies on several pathogenic mechanisms triggering these changes have been undertaken, i.e: on Aβ aggregation and deposition, tau hyperphosphorylation and neurovascular dysfunction.[44,45] Alternatively, mechanisms such as cell-cycle abnormalities[46] acting in concert with oxidative stress[46,47], or inflammatory processes[48,49] and mitochondrial dysfunction[47] are considered as key events in the pathological cascade.[50] For example it has been suggested that both oxidative stress and abnormalities in mitotic signaling can independently serve to initiate disease pathogenesis.[47] However, the dominant theory for the cause of AD is the amyloid cascade hypothesis. According to this hypothesis abnormal metabolism of APP and subsequent accumulation of toxic Aβ species are the primary initiators in AD pathology.[51,52] Hence, this hypothesis suggests that accumulation of Aβ

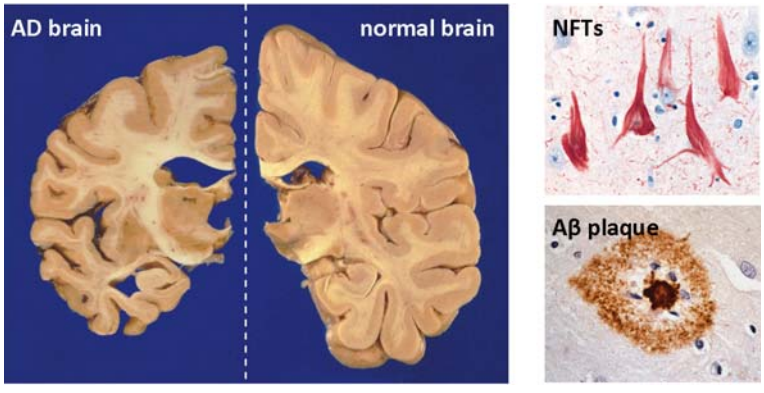

Fig. 1: basic anatomic and histological differences between normal and AD brains: left| basic anatomical differences between a normal and an AD brain: AD brain shows enlarged ventricles, shrinkage in the hippocampus and atrophy in the cerebral cortex. right| neuropathological hallmarks: Aβ plaques and NFTs; adapted from Neuropathology department, Charite

impacts on or even induces tau pathology.[53,54] However, a molecular link between Aβ and tau protein in AD pathology is still missing.

3. APP metabolism & the amyloid cascade hypothesis

APP is a transmembrane protein that is constitutively cleaved by 3 different proteases, designated α-, β- and γ-secretases during cell metabolism. The differential action of these secretases leads to two different pathways, the non-amyloidogenic and amyloidogenic pathway, which are distinguished as follows (Fig. 2):

In the non-amyloidogenic pathway APP is cleaved first by α-secretase to yield a soluble N-terminal domain of APP (sAPPα)[55] and a C-terminal fragment (CTFα). sAPPα may be involved in memory enhancement by promoting synaptogenesis, neurite outgrowth and neuronal survival, and is considered to be neuroprotective.[56-58] The membrane retained C-terminal fragment (CTFα) is then acted upon by presenilin-containing γ-secretase, generating the soluble p3 peptide and a membrane-bound C-terminal fragment (AICD, or APP intracellular domain). AICD may be involved in transcriptional regulation as well as axonal transport and control of cell death.[59]

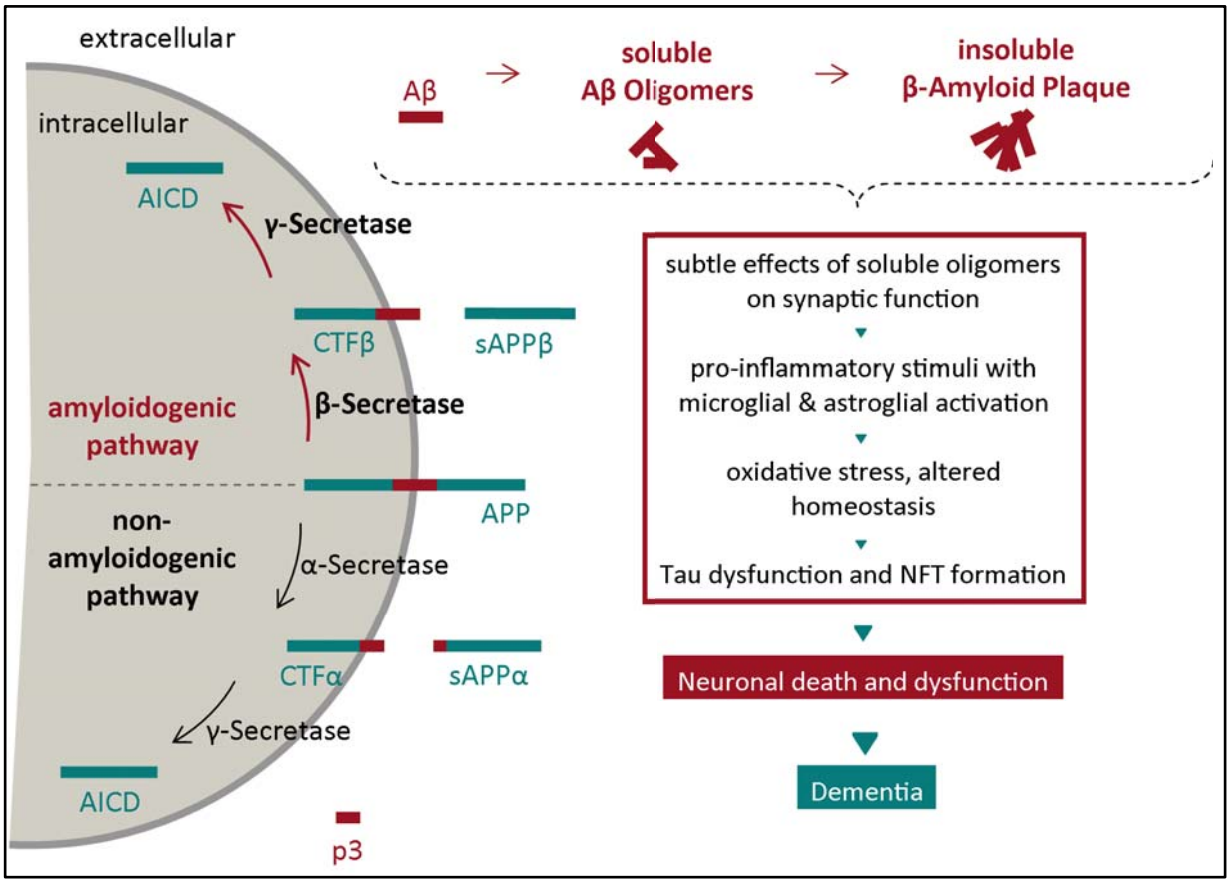

Fig. 2: APP Processing with the non-amyloidogenic and the amyloidogenic pathway: According to the amyloid cascade hypothesis, dominance of the amyloidogenic pathway leads to Aβ aggregation and plaque formation which via several mechanisms leads to neuronal death and dementia.

The amyloidogenic pathway generates Aβ by the sequential action of two proteases, the β- and γ-secretases.[51] The APP derivatives generated by the β-secretase, also known as BACE [14], are the released ectodomain fragment sAPP-β and the cell-associated C-terminal fragment CTFβ. The latter is successively cleaved by the γ -secretase, which, acting at diverse sites, generates peptides of different length with peptides of 40 amino acid residues (Aβ40) and 42 amino acid residues (Aβ42) being the most prevalent. Normally, Aβ is quickly removed from the brain by degrading enzymes[60] or a balanced efflux[61]. This is why Aβ can be detected in both cerebrospinal fluid and plasma in healthy individuals throughout life.[62] However, in the case of excess production[63] or reduced clearance[64], Aβ aggregates as extracellular oligomers, fibrils and eventually plaques, with Aβ42 being much more prone to form aggregates. According to the amyloid cascade hypothesis this ultimately leads to neuronal degeneration and dementia via toxic effects and down-stream events such as tangle formation, oxidative stress and chronic inflammation. Although plaques were originally considered the mediators of neurotoxicity in AD, several reports suggest that the

oligomeric aggregates are the most toxic form of Aβ.[65] This hypothesis is supported by the finding that mutations implicated in the familial disease are present in the genes encoding for both the substrate, APP, and the presenilins, the active center of the γ-secretase.[66] Furthermore, it is proposed that Aβ biomarkers become abnormal first, before biomarkers of tau-mediated neuronal dysfunction, neurodegeneration and cognitive symptoms, suggesting a primary key role of Aβ.[67]

Owing to its putative causative role in AD, Aβ has become an important therapeutic target. The testing of therapeutic approaches to ameliorate AD has been made possible by the existence of numerous transgenic (tg) mouse models which each mirror specific aspects of AD pathology. AD associated pathologies in these tg mouse models are triggered by the overexpression of transgenes carrying mutations which cause autosomal dominant heritable forms of familial AD (FAD) in humans.

4. Heritable causes of Alzheimer's disease

Genetically, AD is a complex disorder; mutations and polymorphisms in multiple genes are involved, together with non-genetic environmental risk factors.[68] Alzheimer's disease is categorized according to its age of onset and/or inheritance pattern. Most cases of AD are part of the late onset type, occurring in individuals over 65 years of age, and are sporadic. About 4-5% of all AD cases develop early onset AD (EAD) and are defined as having an age of onset before 65.[69,70] Among those as many as 20% develop the disease due to autosomal dominant inheritance of mutations in 3 genes encoding for the presenilin 1 (PS1), presenilin 2 (PS2), or amyloid precursor protein (APP). This type of Alzheimer's disease is known as familial Alzheimer's disease (FAD). In fact, after age, family history is the second greatest risk factor for AD.[71] In rare cases patients with FAD may develop symptoms as early as in their 30's or 40's. Mutations in all three of the mentioned pathogenic genes increase Aβ42 production.

The most frequent mutations (>170) causing up to 80% of FAD occur in the gene encoding for PS1 with symptoms apparent before age 50 years.[72-74] Concerning APP, more than 30 mutations have been discovered, all of which lie within or are flanking the Aβ peptide

region.[75-77] These mutations account for only 1% of FAD cases. Whereas Aβ flanking mutations are mainly characterized by excessive Aβ production[73], mutations within Aβ affect Aβ aggregation and distribution[78]. Distinctive for most APP mutations is early-onset of disease (at age 45 to 61 years).[79] Furthermore there are 14 mutations in the PSEN2 gene that have been discovered with a variable age of onset.[74,77,79] A chromosomal cause for developing AD is found in middle-aged patients with Down Syndrome (DS). Development of AD might be related to the extra copy of the chromosome 21 (with the APP gene) leading to overproduction of Aβ peptides.

Apart from these highly penetrant mutations leading to FAD, the apolipoprotein ε4 allele (ApoE ε4) increases susceptibility for the development of sporadic AD. ApoE ε4 is one of 3 common variants of the ApoE gene, whose protein distributes cholesterol in the blood stream. Whereas the ApoE2 protein may exert a protective effect from AD,[80] the ApoE4 isoform increases the risk of developing AD and decreases age of onset. ApoE seems to play a critical role in balancing brain Aβ peptide levels by interacting with the Aβ cascade. There is evidence that ApoE4 mediates amyloid aggregation by promoting fibrillogenesis, facilitating plaque formation and reducing Aβ clearance.[81,82]

The mechanistic contribution of the aforementioned genes in FAD pathogenesis has been studied extensively, but the specific biology involved in the occurrence and progression of sporadic AD remains unclear. Evidence from various methods of genetic analysis strongly implicate multiple different genetic loci predisposing to AD, but only few of them have been confirmed.

5. Transgenic mouse models of AD harboring FAD mutations

Transgenic mouse models harboring mutations found in familial AD represent the most widely used *in vivo* models to study the disease. The first transgenic (tg) mouse models mimicking amyloid plaque pathology were generated by expressing mutated human APP. In addition to age-dependent amyloid pathology, dystrophic neuritis and gliosis, some of these mouse models develop cognitive deficits revealed by behavioural tests.[83] Coexpression of APP with PS1 mutations (PSAPP) dramatically accelerates amyloid deposition[84-86] due to the

increase in Aβ42 production mediated by mutations in *PSEN1*.[87,88] Despite the robust amyloid deposition observed in APP and PSAPP transgenic mice, an important limitation of these models is the lack of an overt neuronal loss and the failure to develop NFTs.[89-91]

Multiple lines of APP and PSAPP mice develop age-dependent amyloid pathology. However, there are significant biochemical differences in the deposited Aβ that largely reflect the expressed APP mutation and the resultant Aβ42:Aβ40 ratio. It is known that the ratio of Aβ42/Aβ40 determines the sites of amyloid deposition meaning a shift towards Aβ40 results in mainly vascular amyloid, while predominant Aβ42 yields amyloid deposition in the parenchyma.[92] In *APPPS1* mice, the APPswe double mutation increases the production of both Aβ40 and Aβ42. In addition, the PS1 (L166P) mutation selectively elevates Aβ42.[93] Cerebral amyloidosis starts at 6–8 weeks. Most of the amyloid lesions consist of dense core plaques with relatively few diffuse deposits. By contrast, in *TgSwDI* mice combination of the APPswe mutations with the APP Dutch E22Q and APP Iowa D23N mutations produces a phenotype in which the Aβ40 species accumulation prevails.[94] Detectable amyloid deposition begins to accumulate at 2 to 3 months of age. *TgSwDI* differ from *APPPS1* mice in the extent of cerebral amyloid angiopathy (CAA); abundant CAA can be observed in *TgSwDI* but is largely absent in the brains of *APPPS1* mice. Hence, these two mouse models mirror distinct pathological features of AD: either CAA and diffuse parenchymal plaques (*TgSwDI*) or only parenchymal but dense core plaques (*APPPS1*). This observation clearly shows that mutant human APP and/or PS1/2 overexpression does not sufficiently reflect the entire pathological cascade in humans. One of the major drawbacks of all above-mentioned tg mouse models is the lack of NFTs.

To overcome this, triple transgenic lines (3xTg) were generated, in which a mutation in the tau gene was inserted, in addition to APP and PS1 mutations.[95] 3xTg AD models form amyloid plaques and NFTs similar to humans in an age-dependent fashion[95-97] and subsequently show synaptic dysfunction, inflammation and impaired learning ability.[98] Besides these positive outcomes, however, 3xTg mice harbor a tau mutation, whereas none has ever been found in AD patients.[99] These observations raise concern about the reliability of the model in terms of AD pathology compared to humans, though it is clearly still extremely useful for investigating the relations between Aβ and tau pathology.

AD mouse models recapitulate only certain aspects of AD pathogenesis – and not the comprehensive pathology of the AD brain – and consequently are of great experimental value despite their limitations. They have been proven to be of advantage for deciphering and understanding the complexity of AD pathogenesis – especially in the context of testing new drugs. However, due to lack of generalizability, multiple AD mouse models should be used as complementary tools to study the contribution of vascular vs. parenchymal amyloid to test certain causative therapies and to decipher their mechanisms of action.[91,100]

6. Immunotherapy in Alzheimer's disease

Present strategies for the treatment of AD provide only minimal effect due limited symptomatic treatment, without targeting the underlying cause of AD. Currently, immunotherapy may be the most promising strategy for a therapeutic intervention that significantly slows or reverses AD progression in the near future.[101-103] Over the past 13 years, Aβ immunotherapy has emerged from preclinical studies in tg mouse models of AD to enter clinical trials in humans. In 1999, Schenk et al. reported the initial evidence that active immunization against Aβ in a murine AD model could prevent or reverse Aβ pathology *in vivo*.[104] These findings have been confirmed and extended in numerous tg mouse models of AD using various strategies including active and passive immunization, as well as diverse adjuvants and routes of administration. These strategies likewise lowered brain Aβ levels effectively[105-109] and attenuated behavioral deficits.[110-112] It became evident that the active factor modulating amyloid load was a serum antibody which recognized aggregated Aβ.[109,113] These anti-Aβ antibodies only reduced pre-established plaques when they recognized the amino-terminal epitopes of Aβ (that is, not the mid-region or carboxy-terminal epitopes).[109]

The striking biological effect of vaccination in preclinical testing and the apparent lack of side-effects in transgenic mice encouraged the company Elan/Wyeth to launch the first clinical trials in 2001. Elderly patients with sporadic AD were immunized with a vaccine that contained pre-aggregated Aβ42 formulated with the T helper (Th) 1 adjuvant QS-21. The trial was halted prematurely because 6% of the patients developed sterile meningoencephalitis.[114] Post-mortem examinations proposed that this post-vaccination inflammation was due to proinflammatory Th1 T-cell responses (mainly CD4+ T cells with

only a few CD8+ T cells) specifically associated with the adjuvant, or an age-associated tendency to generate autoimmune reactions.[115-117] Notwithstanding, vaccination has been shown to lower number of parenchymal plaques[114,118,119] and reduce neuronal pathology[116,120,121] in AD patients. Some reports also describe a slower rate of cognitive decline.[114,122,123] These benefits resulting from vaccination were likely due to the antibody response against Aβ, as the patients with the most dramatic reductions in plaque burden also had the highest antibody titers against Aβ.[122] Likewise, immune responders having robust antibody titers showed significantly slower decline of cognitive functions and daily living capacities as compared to the nonresponders.[114] Subsequent preclinical trials in AD mouse models and clinical trials (i.e. Bapineuzumab) described further side effects such as increased incidence of microhemorrhages and vasogenic edema which might be linked to vascular amyloid.[124-128]

The findings from the first clinical trial as well as adjacent preclinical studies have been useful in designing next generation vaccines. Presently, at least 14 different Aβ immunotherapies are in clinical trials worldwide (Table 1). In these clinical trials several types of immunotherapy for AD are under investigation. Administration of synthetic fragments of Aβ conjugated to a carrier protein represents one possible way to avoid potential problems associated with T-cell responses against Aβ. Another type of immunotherapy under investigation involves passive administration with monoclonal antibodies directed against Aβ.

Drug name	Trial phase	Vaccine	Manufacturer	Estimated completion
ACTIVE VACCINES				
AFFITOPE AD02	II	Mimotope Aβ(1-6)	Affiris	March 2013
UB311	II	Aβ1–14 using UBITh®	United Biomedical	NP
ACC-001 + QS-21	II	Aβ 1-7 coupled to carrier	Wyeth	March 2013
CAD106	II	Aβ1-6 coupled to virus like particle	Novartis	December 2012
V950 (/Iscomatrix)	I	Aβ amino-terminal peptides conjugated to ISCO®MATRIX	Merck	January 2012*
PASSIVE VACCINES				
Bapineuzumab (AAB-001, ELN115727)	III	Antibody recognizing Aβ 1–5	IgG1 Janssen/Elan/	June 2013
Solanezumab (LY2062430)	III	Antibody recognizing Aβ 13–28	Eli Lilly	August 2012

Drug name	Trial phase	Vaccine	Manufacturer	Estimated completion
PASSIVE VACCINES				
Ponezumab (PF-04360365)	II	Antibody recognizing Aβ 33–40	Pfizer	August 2011*
MABT5102A I	II	NP	Genentech	June 2014
Gantenerumab	II	NP	Hoffman-La Roche	January 2017
GSK933776A	I	Antibody recognizing N-terminus of Aβ	GlaxoSmithKline	March 2014
BAN2401	I	antibody recognizing Aβ protofibrils	Eisai Co., Ltd.	October 2012
Octagam (10% IVIG)	II	NA	Octapharma	January 2011*
Gammagard (10% IVIG)	III	NA	Baxter Healthcare	February 2013

Table 1: Ongoing clinical trials on immunotherapy in AD with data from www.alzforum.org and http://clinicaltrials.gov (*no clinical data have been presented to date)

7. Mechanisms of Immunotherapy

Immunotherapies targeting Aβ are auspicious candidates to be the first disease-modifying therapy in AD. Despite all these new approaches and studies, the question of the mechanism of action of immunotherapy in AD remains unanswered. Defining this mechanism in more detail would allow to refine and improve the design of immunotherapeutics and enable the development of novel combination therapies that could act synergistically. Several mechanisms have been proposed (Fig. 3). First, Aβ antibodies may interfere with Aβ aggregation and/or catalytically dissolve preformed Aβ aggregates.[129,130] This idea is supported only by in vitro data demonstrating that anti-Aβ antibodies mixed with Aβ could prevent or reverse aggregation of Aβ fibrils. Second, binding of the Aβ antibodies to Aβ may trigger microglial cells to clear plaques through Fc-receptor-mediated phagocytosis and subsequent peptide degradation.[131] Two findings however indicate that Fc-dependent phagocytosis is not the only mechanism involved as F(ab)2 fragments of Aβ antibodies were as effective in clearance of Aβ as the full-length antibody indicated[132,133], and Aβ vaccination in APP tg mice lacking the Fc-receptor lowered cerebral Aβ.[134] A third proposed mechanism assumes that penetration of the antibodies into central nervous system (CNS) is not necessary and that the presence of circulating antibodies creates a ‘‘peripheral sink’’ which alters the Aβ equilibrium across the blood brain barrier to favor Aβ efflux owing to the reduced free Aβ in blood or to prevent transport of Aβ back into the brain and thereby

enhancing net clearance of Aβ.[108,135] All mentioned mechanisms are not mutually exclusive and may overlap under certain conditions.

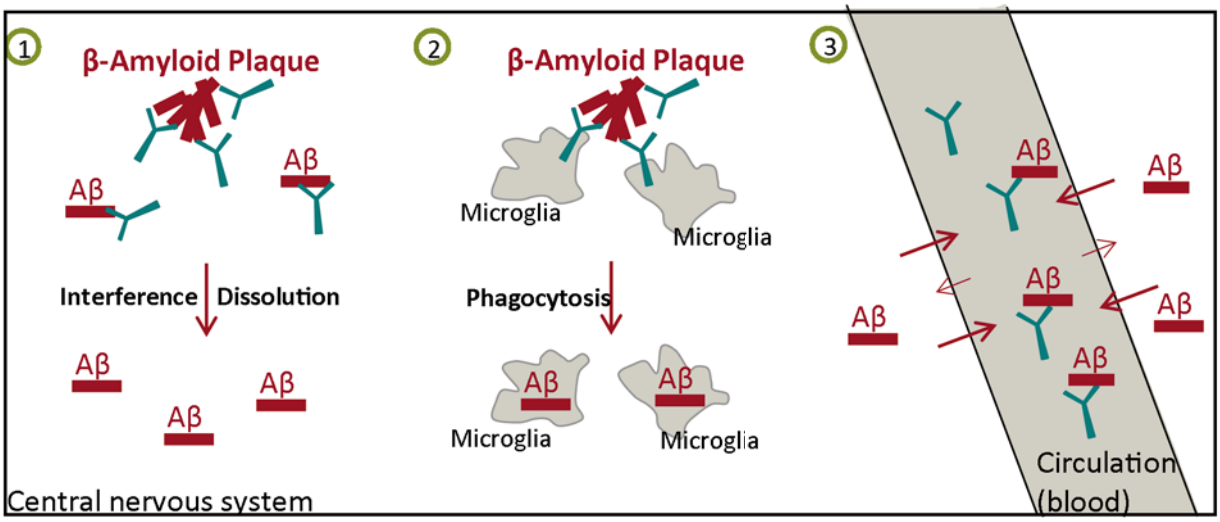

Fig. 3: Models of antibody-mediated amyloid clearance. Three models that are not mutually exclusive have been proposed. 1 | Anti-amyloid antibodies reach amyloid deposits in the brain and resolve them directly through interaction of the antibody with the amyloid deposit and/or interfere with the aggregation of monomeric Aβ. 2 | Small amounts of anti-amyloid antibodies reach amyloid deposits in the brain and trigger a phagocytic response by microglia. 3 | Anti-amyloid antibodies act as a peripheral sink for soluble amyloid-β species, leading ultimately to the resolution of brain deposits.

Molecules that bind Aβ in blood are referred to as Aβ sinks. These molecules reduce the amount of bio-available Aβ in blood, thereby shifting the dynamic equilibrium between Aβ in the periphery versus the CNS to either favor increased clearance from the brain or simply to prevent the influx to the brain. Consistent with this idea are data showing that peripheral injection of Aβ-binding agents including gelsolin[136], ganglioside M1[136], soluble RAGE (sRAGE)[137], soluble LRP (sLRP)[138] and *Withania somnifera* (WS)[139] promote transport of brain derived Aβ into blood, thereby reducing Aβ levels and amyloid load in the CNS. The possibility that anti-Aβ antibodies could also act as a sink was first proposed by DeMattos and colleagues. They observed a rapid and marked increase in plasma Aβ after immunization with anti-Aβ antibodies which correlated with both brain Aβ levels and amyloid burden in the hippocampus.[108,135] Subsequent studies supporting this idea demonstrated reversal of memory impairment in a mouse model of AD with the very same vaccine.[112] The possible role of this peripheral sink hypothesis was further emphasised by active immunisation with a synthetic Aβ peptide conjugated to virus like particles that primarily induces humoral responses with IgM antibodies instead of IgG, which indicates a T-cell-independent immune response[140], that is commonly seen for antigens with a repetitive structure.[141] Although IgM crosses the blood brain barrier much less than IgG, vaccinated mice had both reduction of

amyloid burden and cognitive improvement.[142] However, it was not definitively proven that it was really the IgMs in the periphery that provoked the effect, and not the low amounts of IgG antibodies possibly entering the brain. Furthermore this study did not address the analysis of plasma Aβ. In another report using next generation vaccines also a robust IgM response next to a low IgG response was elicited. Plasma Aβ levels were measured, however no elevation could be observed indicating a rather central effect of the generated antibodies.[143] Thus far it has not been shown that antibodies active in the periphery exclusively can indeed lower plaque burden. The contribution of putative peripheral and central effects has not yet been assessed independently.

Concerning the transport systems at the blood brain barrier (BBB) responsible for the influx and efflux of brain Aβ three molecules have been proposed to regulate this process: receptor for advanced glycation end products (RAGE), low-density lipoprotein receptor-related protein (LRP) and P-glycoprotein (P-gp). Whereas RAGE regulates the influx of Aβ to the brain, LRP-1 and P-gp are responsible for the efflux of Aβ from the brain.[137,144-150] The neurovascular hypothesis of Zlokovic[44,45] states that reduced clearance of Aβ from brain across the blood is a critical pathological event. A large body of work from multiple groups has shown that in animal models of AD and in AD brains, down regulation of LRP-1 and P-gp in concert with up regulation of RAGE may create an unfavorable Aβ gradient across the BBB, resulting in Aβ retention in the brain.[145,150-156] Also, perivascular macrophages were referred to as playing an important role in Aβ clearance.[157] In accordance with these findings, a recent report states that AD is related to impairment in Aβ clearance rather than increase in Aβ production.[64]

Another process which is thought to contribute to level of Aβ in the brain is through bulk flow of interstitial fluid (ISF) into CSF. Bulk flow denotes the reabsorption of CSF into peripheral compartments, including the systemic circulation via the choroid plexus (CP). Accumulating evidence supports the idea that continually decreasing CP function and CSF turnover in advanced ageing exacerbates AD[158-160] which is also emphasized by the fact that CSF Aβ42 is highly decreased in AD patients. The process by which Aβ is transported via the CP however is still unclear and might involve also active transport systems.[161] In support of this conclusion a recent report showed that an aquaporin-4 dependent ISF bulk flow of

soluble Aβ contributes to the clearance of Aβ from the brain.[162] Aβ clearance from the brain is a complex mechanism which might involve several aspects and seems to be disturbed in AD.

Understanding the mechanism of vaccination will help to refine and focus the generation and design of new drugs. This finally will improve AD therapy also in the face of possible combinational treatments.

AIMS OF THE STUDY

Alzheimer's disease (AD), a progressive neurodegenerative disease, is the most common form of dementia of later life and a major cause of disability and death in the elderly[1]. Aβ immunotherapy of patients with Alzheimer's disease offers an important chance for the treatment of this devastating disease. However the mechanism by which antibodies reduce amyloid-β deposition in the brain is still unknown. There have been three mechanisms postulated to explain how antibody-directed clearance of Aβ could work – activation of microglial phagocytosis, catalytic dissolution of Aβ fibrils and induction of an increased efflux of Aβ from the brain. The latter was termed the peripheral sink hypothesis, and postulates that antibodies sequester circulating amyloid-β causing an efflux of Aβ from the brain to the plasma.

Hypothesis:

In my thesis, I aimed to test if the peripheral sink hypothesis is true by transgenic restriction of anti-Aβ antibodies to the periphery. I hypothesise that Aβ binding antibodies reduce the plaque load by sequestering Aβ in the blood stream. To test this hypothesis I utilized transgenic (tg) mice which were generated by my co-workers Dr. Li and Annette Wolf (under supervision of Prof. Dr. Heppner and either produce pentameric anti-Aβ IgM antibodies as well as B cell bound anti-Aβ antibodies (*AB9μ* mice) or only B cells bound antibodies (*DelS* mice). Neither B cells nor IgM antibodies are expected to enter the brain during the course of Alzheimer`s disease,[2] thereby restricting anti-Aβ antibodies to the periphery.

Specific Aim 1 (Fig. 4):

The first aim was to examine the immuno phenotype of *AB9µ* and *DelS* mice, to verify that they show normal B cell physiology, development, or histoarchitecture and cellular composition of germinal centers and peripheral blood. Alterations in the immune system may influence Alzheimer's disease and thereby interfere with the outcome induced by anti-Aβ antibodies. Techniques used include flow cytometry, histology, in vitro proliferation assays, infection with vesicular stomatitis viridae (VSV) and IgM purification. In this part we also wanted to make sure that the transgenic antibodies do indeed recognise Aβ tested. Therefor we developed an anti-Aβ antibody ELISA.

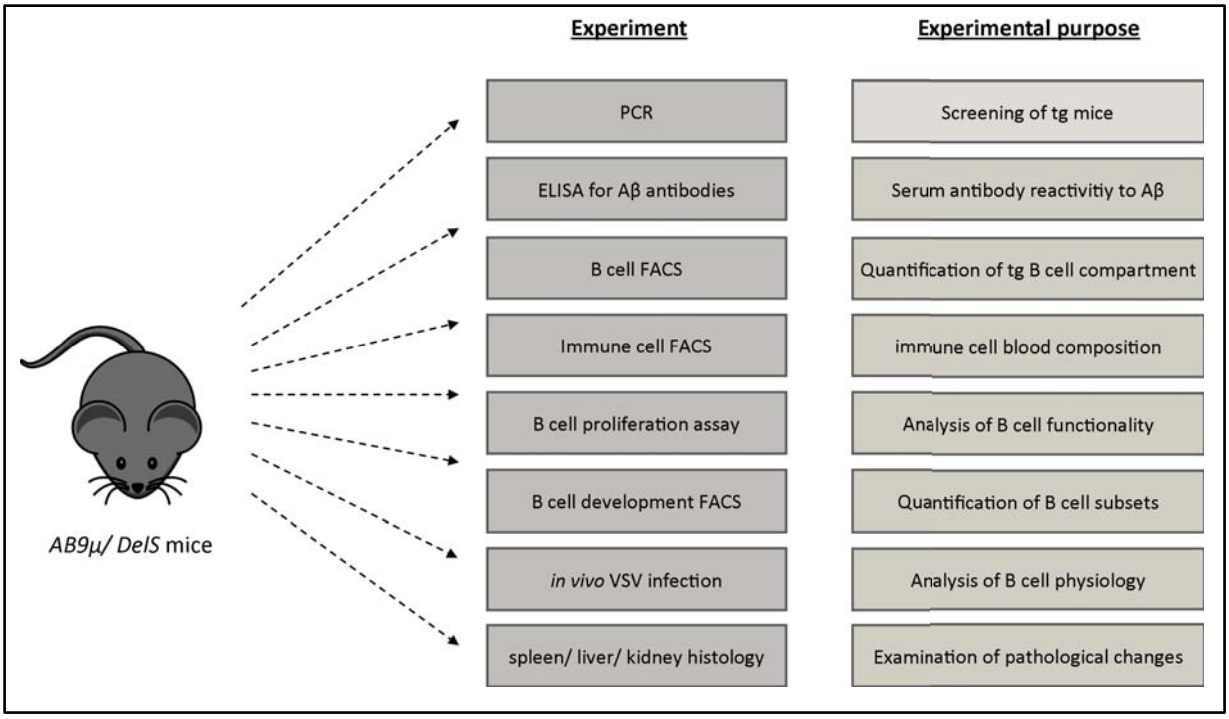

Fig. 4: Experimental setup for the characterization of transgenic (tg) mice: *AB9µ* and *DelS* mice were examined with regard to different read outs in order to identify the best lines.

Specific Aim 2 (Fig. 5):

The next aim was to investigate whether anti-Aβ antibodies – present exclusively in the periphery – can improve cerebral amyloidosis in mouse models with AD-like neuropathology. This was addressed using two different Alzheimer mouse models which differ in the FAD mutations they harbor. These differences lead to distinct plaque-like Aβ deposits in the neocortex and hippocampus. The two mouse models used were *APPPS1* mice[93] and *TgSwDI* mice[94]. The methods to analyse the mice included histological examination, Aβ-ELISA (MesoScale) and Schaegger western blot.

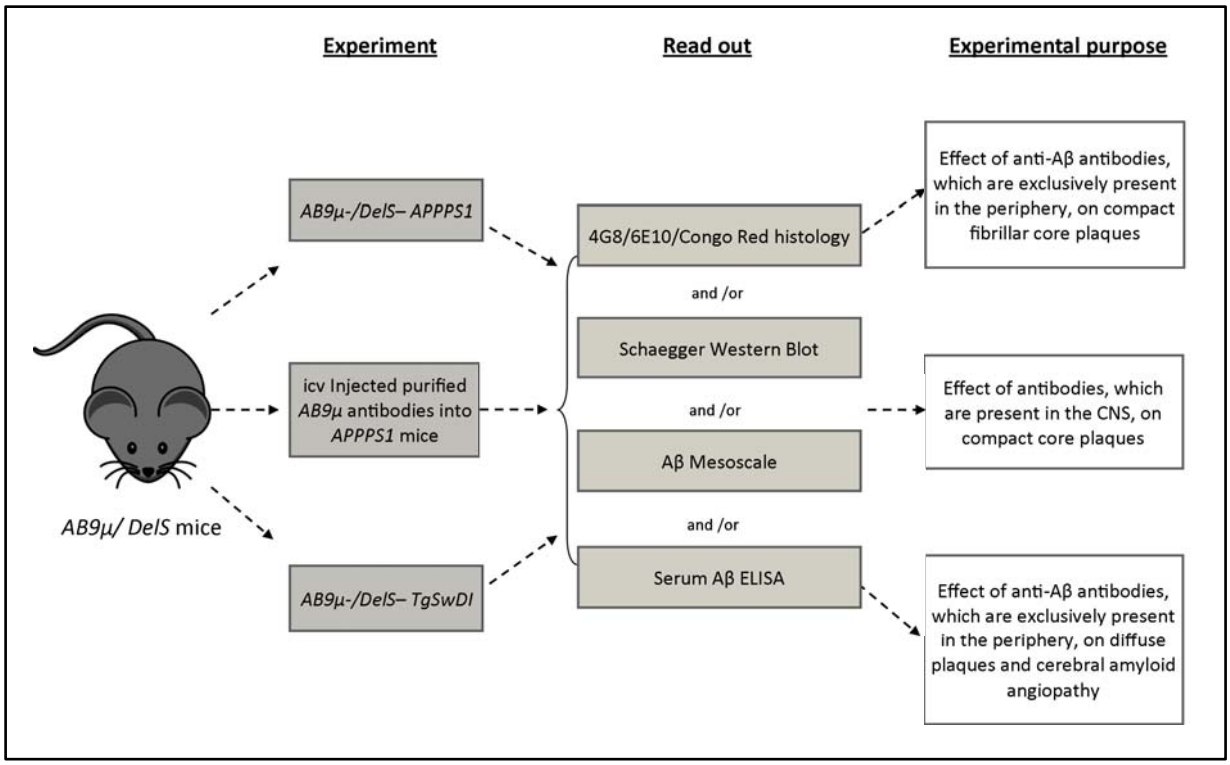

Fig. 5: Experimental setup for the examination of the peripheral sink hypothesis in AD mouse models: We used several AD mouse models as they show biochemical differences in the deposited Aβ. Also Jucker suggested in 2010 that „external validity of mouse studies could benefit from including more than one mouse model".[85] To test whether the antibodies might be more efficient if they are injected directly into the brain of *APPPS1* mice we injected purified IgM as well as AB9-IgG icv.

MATERIAL & METHODS

1. *AB9µ* and *DelS* mice

To test the peripheral sink hypothesis of immunotherapy two transgenic mouse strains were generated in Department of Neuropathology under the supervision of Prof. Heppner (All cloning steps were performed by Dr. Li and Annette Wolf.) as follows:

Several subcloning steps were performed to insert the AB9 VDJ fragment into the 22Kb pSV2neo-6H4µ vector comprising the µ-promoter, the intron enhancer sequence, the constant regions, polyadenylation sites and the membrane anchor of the µ heavy chain. First, the 7kB EcoRI fragment of the pSV2neo-6H4µ vector was cloned into the smaller 3kB pBSSK backbone vector. This vector was digested with EcoRI/NcoI to produce two smaller fragments (1.7 and 4.9kB) out of the aforementioned EcoRI fragment which were separately cloned into two pBSSK vectors. The bigger fragment containing the genomic VDJ sequence of 6H4µ was then cloned into a Litmus vector for better amplification of the fragment. The 6H4 VDJ region was exchanged by the AB9 VDJ region (from the pSecTag2BAB9IgG vector provided by Todd Golde) with the help of an overlapping vector strategy which is based on homology between sequences present in both fragments. The homology consists with only one of the four primers used for amplification of the AB9 VDJ region and the big 6H4 EcoRI/NcoI fragment. After amplification and annealing a PCR product is produced that contains the leader sequence of the 6H4 fragment and the AB9 VDJ region. The smaller EcoRI/NcoI fragment containing the µ-promotor and the newly formed AB9 VDJ fragment were cloned together into the Litmus vector and amplified. The EcoRI fragment comprising the promoter, AB9 VDJ and the intron enhancer sequences was subcloned into the genomic expression vector psV2neo yielding the secreted and membrane bound form of IgMa (Fig. 6).

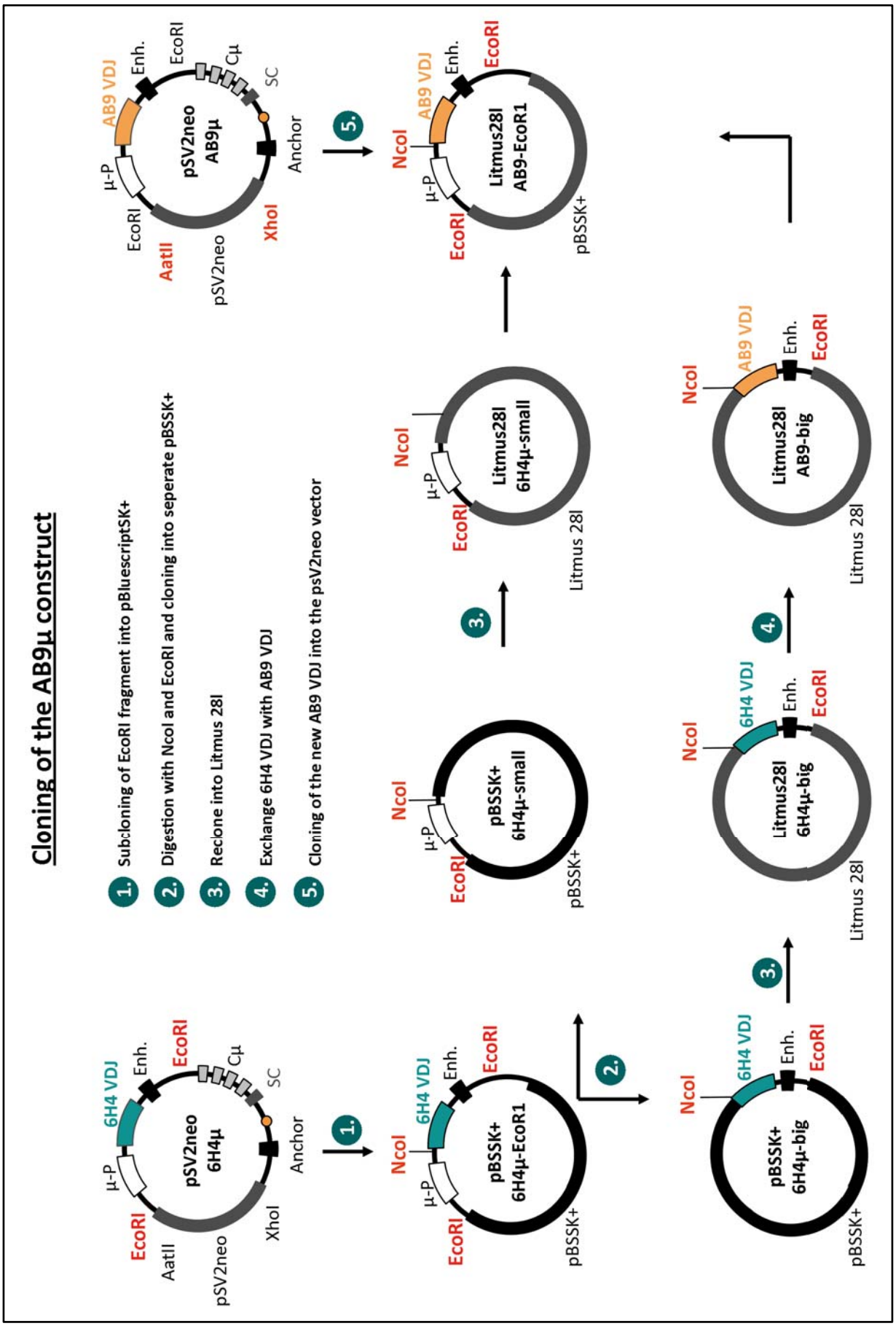

Fig. 6: Cloning strategy of the *AB9µ* vector

In the next cloning steps the polyadenylation site was removed to obtain the *DelS* sequence. The BamHI fragment comprising the polyadenylation site, constant region 3 and 4 and the membrane anchor was subcloned into the pBSSK backbone vector. This vector was restricted with BamHI and HhaI to produce 3 fragments: 1. the BamHI/HhaI fragment with the membrane anchor sequence, 2. the HhaI/Hha fragment with the Polyadenylation sequence and 3. BamHI/HhaI fragment containing the two constant regions. 3-piece-ligation resulted among others in fragments in which the polyadenylation site containing HhaI/HhaI 471 Kb fragment was missing. This fragment was ligated with the pBSSK backbone vector and finally cloned into the genomic expression vector psV2neo yielding the membrane bound form of IgMa (Fig.7). To prepare DNA for microinjection, µ-heavy-chain transgenes of AB9 and *DelS* were excised using restriction endonucleases AatII and XhoI, and injected into male pronuclei of fertilized oocytes of C57BL/6 (B6).

The microinjection (performed by Dr. Ronald Nauman, MPI of Molecular Cell Biology and Genetics, Dresden) resulted in these two mouse strains:

Heterozygous *AB9µ* mice harboring a transgenic Aβ specific IgMa µ chain express anti-Aβ IgM antibodies (*AB9µ*) which due to their large size, cannot cross the blood brain barrier (BBB) and thus will only be present in the periphery. The Ab9-IgG2a antibody was generated and characterized by Levites and Colleagues[163,164]: Ab9 recognizes the aminoterminal amino acids 1-16 in both monomeric and aggregated Aβ as well as Aβ amyloid. Peripheral injection of Ab9 readily prevents Aβ deposition in the brain of specific Alzheimer mouse models.

Heterozygous *AB9µDelS* (*DelS*) mice also express *AB9µ*, however only on the surface of B cells due to deletion of the secretion sequence: since B cells do not enter the CNS in the course of AD and since the latter mice do not secrete anti-Aβ antibodies into the circulation, anti-Aβ antibodies will be restricted to the periphery. These mice serve as a more stringent control.

Both mouse strains were bred on the B6 background, which express IgM/D of the b allotype. This enables us to distinguish endogenous from transgenic B cells (a allotype) to characterize the mice. During my thesis I was allowed to work with *AB9µ* and *DelS* mice in various ways. Some characterization experiments were performed together with Dr. Li.

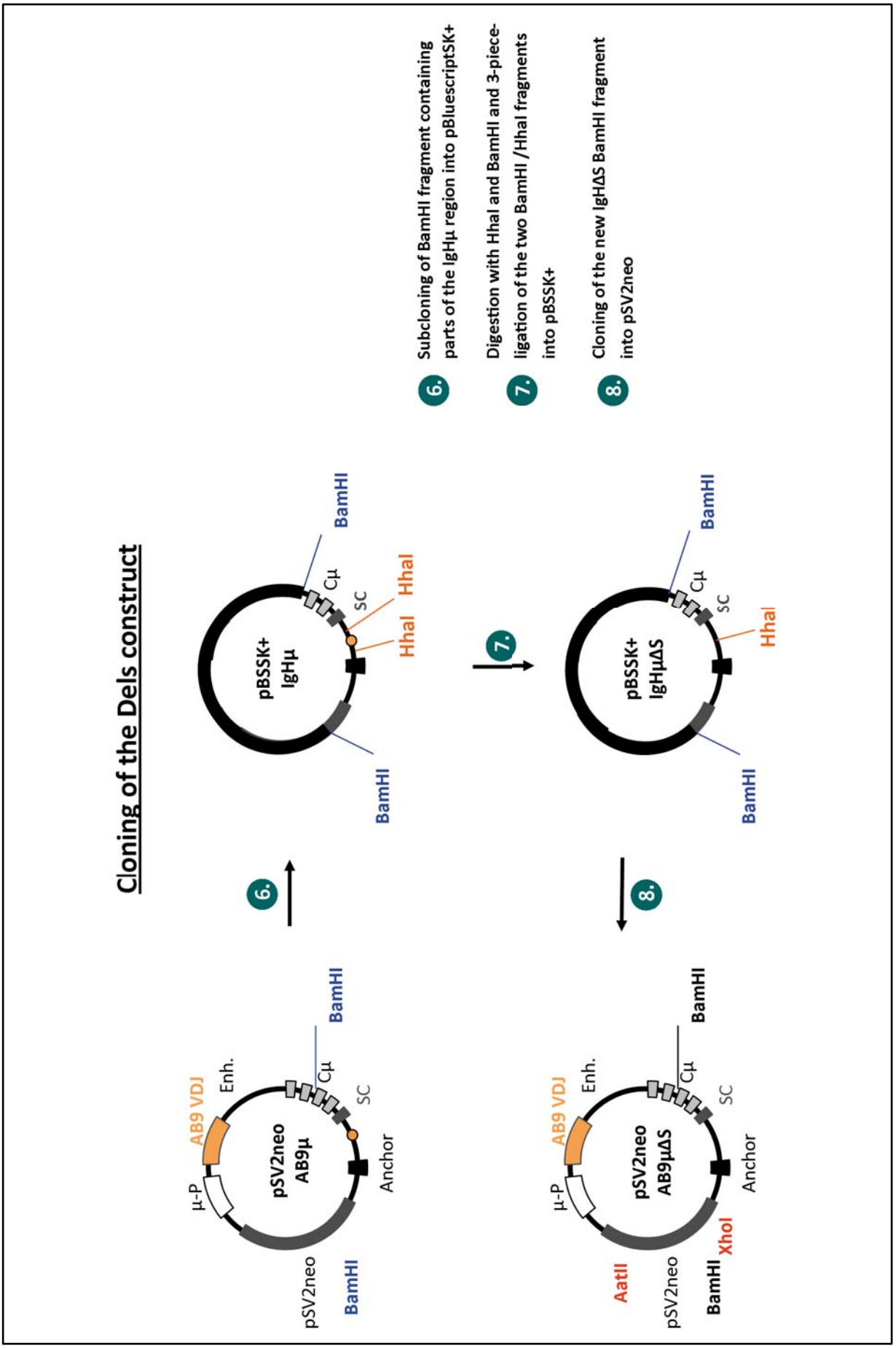

Fig. 7: Cloning strategy of the *DelS* vector

2. *15B3* mice

15B3 mice were used as control mice expressing transgenic IgMa antibodies that do not bind to Aβ. *15B3* specificity – at least in these tg mice – is unknown as it was shown that the *15B3* IgM antibody expressed by *15B3* mice did not exhibit binding to recombinant cellular prion protein (PrP^c).[165] These mice serve as ideal control for transgenic production of IgM antibodies.

3. *APPPS1* and *TgSwDI* mice

As animal models for Alzheimer's disease we were using 2 different transgenic mouse lines - heterozygous *APPPS1*[93] and Tg-SwDI[94] mice. *APPPS1* mice harbor the Swedish amyloid precursor protein (APP) mutation KM670/671NL in conjunction with the presenilin 1 mutation L166P. Swedish APP mutation lies within the β-secretase cutting site which shifts Aβ production towards amyloidogenic pathway. Presenilin mutations shift the Aβ40/Aβ42 ratio towards Aβ42 without increasing the total Aβ amount. In contrast, *TgSwDI* mice carry a triple mutated human APP with the Swedish mutation (KM670/671NL), the Dutch mutation E693Q and the Iowa mutation D694N. Both, the Dutch and the Iowa mutation, lead to amyloid deposition in the brain blood vessels and following severe cerebral amyloid angiopathy (CAA). *APPPS1* and *TgSwDI* mice have been generated on a B6 background; *APP23* mice were originally derived on a B6D2 background and were backcrossed to B6 mice for more than 15 generations. *APPPS1* or *TgSwDI* mice were crossed either to *AB9μ* and *DelS* mice or to *15B3* mice. Negative littermate controls (i.e. *APPPS1* mice not expressing transgenic B cells) were used as negative controls. Furthermore mice were sex and age matched.

All animals were kept under specific pathogen-free conditions on a 12 hour light/dark cycle, food and water was provided ad libitum. All animal experiments were performed in accordance to the national animal protection guidelines approved by the regional offices for health and social services in Berlin (ZH31, O 0132/09, G0154/08).

4. Genotyping

Mouse tail or ear biopsies were incubated for 30 minutes in 50-80 µl lysis buffer (25 mM NaOH, 0,2 mM EDTA; pH 12) in a thermomixer at 95°C. Afterwards equal amounts of 40 mM TrisHCL were added to obtain an optimal DNA storing solution. 1-2 µl were used for polymerase chain reaction (PCR).

PCR was used to genotype transgenic mice for the presence of Ab9, *DelS*, *15B3* and human APP with the primers listed in Table 2. The reactions were performed in a Thermocycler PCR machine. All amplifications were performed in a total reaction volume of 20 µl, containing template DNA, 25 pmol of each primer (purchased from MWG Biotech), and diluted RED Mastermix (Invitek). Standard PCR programs started with 2 minutes denaturation at 95°C, followed by 30 – 45 cycles consisting of denaturation at 95°C for 30 seconds, annealing at oligonucleotide-specific temperatures for 30 seconds and elongation at 72°C for 1 minute and a final elongation step at 72°C for 5 minutes.

Primer	Sequence 5'-3'	$T_{Annealing}$ (°C)
PaSeq 5'	CGGAGAGACCTATACCTGTGTTGTA	63
PaSeq 3'	ATCTGTTTCTGTGAGTGGTTGTGT	63
VDJ 5'	ACCACTCACCATGGGATGGAGC	63
VDJ 3'	AGACAGTGACCAGAGTCCCCTG	63
6H4 5'	TTT TTT ACC ATG GGA TGG AGC TGG ATC TTT	63
6H4 3'	AAA AAA GCC GGC ACT CAC CTG CAG AGA CAG TGA CCA G	63
PS1 5'	CAG GTG CTA TAA GGT CAT CC	58
PS1 3'	ATC ACA GCC AAG ATG AGC CA	58
APP CT 5'	GAA TTC CGA CAT GAC TCA GG	58
APP CT 3'	GTT CTG CTG CTG CAT CTT GGA CA	58

Table 2: Oligonucleotides used for genotyping

Afterwards the PCR samples were separated on a 1-2% (w/v) agarose gel (1 x TAE, 0.5 µg/ml ethidium bromide) at 120 mV.

Next we used SYBR Green I dye, a specific, double-stranded DNA binding dye, to detect our transgenic VDJ PCR product as it accumulates during PCR cycles. The same PCR settings were used for real time (RT-) PCR with SybrGreen to estimate transgenic copy numbers. Therefore the concentration of DNA was adjusted to 20 ng/µl. Then VDJ primers were added as well as Sybr Green instead of RED Mastermix. The samples were measured on 7900HT Real-Time PCR System (Applied Biosystems).

5. Flow Cytometric Analysis

Multi-colour flow cytometry has been used to identify cell populations expressing a given antigen. These cell populations were isolated from different tissues as described below. All antibodies used were purchased from BD bioscience, eBioscience or BioLegend. In each case, the amount of antibody used was based on the manufacturer's suggestion or titration experiments to optimize the signal/noise ratio. In all cases, the cells were evaluated using 4- to 5-color combinations. For compensation in 4- to 5-color analysis BD Compensation Beads (#552843 or #552844) were used.

5.1 Preparation of Cell suspensions from peripheral blood (PB), spleen and bone marrow (BM)

Cell suspensions obtained from peripheral blood (PB), spleen and bone marrow (BM) were prepared as follows: 6 drops of murine blood were collected in EDTA coated PBS filled tubes. For dissection of spleen and BM the mice were euthanized with CO_2. Spleens were removed; BM was isolated from tibia and femur by using an 18 gauge needle. Both, spleens and BM, were each passed through 70 µm nylon mesh cell strainers (Becton Dickinson, Franklin Lakes, NJ) to make a single cell suspension in DMEM supplemented with 2%FCS/10 mM Hepes.

After red cell lysis (150 mM NH_4Cl, 10 mM $KHCO_3$, 0,1 mM EDTA in ddH_2O, 5 min) the cell suspensions were incubated in 50-100 µl Fc-Block (1:200 in FACS Buffer (0.01% NaN_3, 1%FCS, 5 mM EDTA in PBS), 10 min) to block unspecific binding of the Fc-receptors on cells (CD16/CD32) via the Fc domain of the antibodies. The respective surface antibodies were added at their specific dilution and incubated for 20-30 min at 4°C in the dark. Following washing the cells were resuspended in 200 µl FACS buffer. The fluorescence cell properties

were measured with BD FACS Canto TM II and the data was analyzed with FlowJo 7.6 software and MS-Excel.

5.2 Flow Cytometric Analysis of transgenic B cells

Flow cytometry was used to test for the presence of transgenic B cells in BM, Spleen and PB. The identification of these transgenic B cells is based on the presence of surface-bound IgM allotypes described below[165]: B6 mice carry the IgMb allotype whereas Balb/c mice have an IgMa allotype. As the transgenic mice were bred on the B6 background the endogenous B cells are IgMb positive. The transgenic B cells however have the same allotype as Balb/c mice and thereby express IgMa. This enables the distinction between endogenous and transgenic B cells as follows:

Antibody	IgMa-Pe	IgMb-FITC	IgD-Alexa647	B220-V450
Dilution	1:200	1:100	1:100	1:200
Clone	DS-1	AF6-78	11-26c.2a	RA3-6B2

Table 3: FACS antibodies used for identification of tg B cells

5.3 Flow Cytometric Analysis of PB for immune cell composition

Blood immune cells were stained with fluorescently-labeled antibodies to CD4, CD8, B220, NK1.1, GR-1, CD11b and F480 to assure normal blood composition. This is important as several studies describe altered distribution of lymphocyte subsets in AD[4] which might indicate an impairment of peripheral immune function in AD[166]. Dilutions and fluorochrome conjugates used are listed below:

Antibody	CD4-Pe	CD8-FITC	B220-V450	NK1.1-APC	GR-1-PeCy7	CD11b-FITC	F480-Cy5
Dilution	1:400	1:600	1:200	1:100	1:400	1:400	1:200
Clone	GK1.5	53-6.7	RA3-6B2	PK136	RB6-8C5	M1/70	CI:A3-1

Table 4: FACS antibodies used for analysis of blood immune cells

5.4 Flow Cytometric Analysis of B cell development

BM in mouse contains B lineage cells at all stages of development, from earliest progenitors to mature B cells. We identified five B cell differentiation stages: pro–B cells, large pre–B cells type I and II and immature B cells as well as mature B cells. Spleen harbours both

recirculating and non-recirculating (residing) B cell subsets that can be distinguished immunophenotypically. By using an overlapping panel of antibodies, the different B cell populations can be identified and their relative distribution in BM, PB and Spleens can be enumerated.

The following panels of antibodies were used as a strategy for flow cytometric identification and enumeration of B cell subsets[167,168]:

Marker / Tissue	B220-V450	CD19-Pe-Cy7	CD43-APC	CD25-FITC	IgM-PerCP-Cy5.5	CD23-FITC	CD5-Pe	CD21-Cy5
BM	x	x	x	x	x			
PB	x	x			x	x	x	x
Spleen	x	x			x	x	x	x
Dilution	1:400	1:800	1:800	1:200	1:200	1:800	1:200	1:400
Clone	RA3-6B2	1D3	S7	7D4	R6-60.2	B3B4	53-7.3	7G6

Table 5: FACS antibodies used for analysis of B cell development

5.5 Flow cytometry-based B cell Proliferation Assay

Flow cytometry-based B cell proliferation assays with CFDA-SE (Carboxyfluorescein diacetate, succinimidyl ester, Invitrogen Molecular Probes (Carlsbad, CA, USA)) was performed to ensure normal functionality of transgenic B cells in presence of general stimuli[169] (anti-IgM (Jackson Immunoresearch (Baltimore, USA)), lipopolysaccharide (LPS) (Sigma Aldrich, #L 2630) as well as in presence of their antigen (Aβ).

Generally, CFDA-SE is a cell-permeable, fluorescent dye that is partitioned equally among daughter cells with each division. CFDA-SE is used in the current experimental setting to label splenic B cells for later detection of their proliferative behaviour via FACS. Therefore splenic cell suspensions of WT, *AB9μ* and *DelS* were prepared as described in 2. After red cell lysis, the cells were first washed with RPMI 1640 containing 1% Hepes (RH). The pellet was then resuspended in CFDA-SE, previously dissolved in pre-warmed RH at a concentration of 2.5 µM, and incubated for 10 minutes at 37 °C in the dark (all steps were performed in the dark, since direct light would interfere with the fluorescent characteristics of the dye). After labelling, the cells were washed twice with cold culture medium (RPMI-1640; 10%FCS; 50 µM β-MercaptoEtOH; 1% Penicillin/Streptavidin) and resuspended in culture medium

with an adjusted cell number of 2-4 Mio. cells/ml. The experiment was performed in 96-well plate. Three wells were plated out for each condition.

In the case of general stimuli the plates were pre-coated with 100µl stimuli containing complete mouse medium (1-10 µg/ml LPS, 4-40 µg/ml anti-IgM) for 1 hour. Afterwards 200 000 - 400 000 splenic cells in 100 µl were applied to the wells. In the case of Aβ stimulation of B cells we used CAD106 (Aβ1-6 peptides covalently conjugated to virus like particles (VLP) Qβ) from Novartis which carry around 350-550 Aβ peptides on their surface or 5-20 µg/ml of recombinant Aβ.

Finally, cell cultures were incubated at 37 °C and 5% CO2 for at least 72 hours. The proliferation rates were then measured via FACS. Cells were stained as described in 2.2. Surface antibodies used are listed below:

Antibody	B220-V450	IgMb-Pe	IgMa-Pe
Dilution	1:200	1:200	1:200
Clone	RA3-6B2	AF6-78	DS-1

Table 6: FACS antibodies used for B cell proliferation assay

6. Electrochemiluminescence linked immunoassay (ELISA) for anti-Aβ antibodies

Anti-Aβ antibody titers in sera of transgenic mice were measured by ELISA in the following way:

96-well plates were coated with 75 µl of 125-250 ng recombinant Aβ42 (Mobitec GmbH, #20276) over night at 4°C. Different concentrations (32.25-250 ng) and buffer conditions (PBS or H_2CO_3) for Aβ42 had been tested before screening. For screening 125 ng Aβ42 in H_2CO_3 were used. After washing (3x in PBS + 0,1% Tween20) the plates were blocked with 300 µl 5% BSA + 0,01% Tween in PBS (2 hours at RT) to inhibit residual binding capacity of the plate. Different blocking conditions had been tested before: Next to 5% BSA different concentrations of WT serum (1:40-1:160) were incubated before or after 5% BSA. Final blocking conditions used were 5% BSA. 50 µl of serial diluted serum (1:80-1:2560) and standard samples were incubated for 1 hour at RT. The plates were washed carefully to

remove unbound anti-Aβ antibodies and incubated with the HRP conjugated detection antibody (anti-IgMμ (1:1000), anti-IgG (1:1000), IgKappa (1:1000) (Rockland Immunochemicals, Gilbertsville, USA, #610-4312, #610-4310, #610-4307) anti-IgG,A,M (1:1000; Invitrogen, #61-6420) for 1 hour at RT. Unbound conjugates are washed out and tetramethylbenzidine (TMB; eBioscience, #60-4201-56) is added. As TMB is hydrolyzed by the bound HRP conjugate, a coloured product is generated. The amount of product generated is proportional to the amount of anti-Aβ antibodies in the sera. To terminate the peroxidase/TMB reaction 100 µl H_2SO_4 (2N) was added. Absorbance was read immediately at 450 nm with a TECAN® fluorescence plate reader (Tecan, Männedorf, Switzerland).

7. Histology of spleen, kidney and liver

To ensure normal histology of different organs in *DelS*, *AB9µ* and control (WT, *15B3*) mice, mouse spleen, kidney and liver were harvested, embedded in OCT compound embedding medium and frozen in liquid nitrogen. 7 µm sections were cut on cryostat, incubated and dried overnight at 4 ˚C, then fixed in acetone for 10 min and chloroform for 7 min. H&E staining was performed according to standard laboratory protocols. For antibody staining sections were blocked with PBS + 1:10 FCS, 5% BSA and 1:10 NGS serum at 25 ˚C for 30 min. Blocked sections were stained with primary antibodies overnight at 4 ˚C diluted in PBS (rat anti-mouse CD4 (1:500), mouse anti-mouse B220-biotin (1:300), rat anti-mouse CD11b (1:100)). After washing sections were stained with proper peroxidase coupled secondary antibodies and developed with DAB. Images were captured at x10 magnification with a Zeiss Axioplan microscope.

8. Vesicular stomatitis virus (VSV) Infection

VSV infection was used to confirm that the transgenic mice are able to cope with a viral infection despite reduction in B cell numbers. For immunizations with live virus $2x10^6$ p.f.u. of VSV were injected in 200 l of BSS i.v. into the tail vein[170]. Blood was taken every 4 days. The VSV neutralization assay was used to detect IgG- and IgM-titers: Shortly, 40-fold prediluted serum samples were diluted in log2 steps and mixed with equal volumes of virus containing 500 plaque-forming units ml-1. Mixtures were incubated 90' at 37°C with 5% CO2. 100 l of the mixtures were transferred onto Vero cell monolayers in 96-well plates and

incubated for 1 h at 37 °C. Monolayers were overlaid with 100µl of Dulbecco modified Eagle medium containing 1% methyl cellulose. After incubation for 24 h at 37 °C the overlay was removed and the monolayer was fixed and stained with 0.5% crystal violet dissolved in 5% formaldehyde, 50% ethanol, 0.8% NaCl. The antibody dilution reducing the number of plaques by 50% was taken as titer. (Performed in co-operation with Prof. Kalinke)

9. Immunization of *AB9µ* mice with Aβ42

AB9 mice were immunized twice with 100 µg Aβ42 – the antigen of the transgenic B cells – as described before.[104] Aβ peptide was freshly prepared from lyophilized powder for each set of injections. For immunizations, 2 mg Ab42 (human Aβ42; Bachem) was added to 0.9 ml deionized water and the mixture was vortexed to generate a relatively uniform suspension. 100 µl 10xPBS was added. The suspension was vortexed again and incubated overnight at 37 °C for use the next day. Aβ42 was emulsified 1:1 (v/v) with complete Freund's adjuvant (CFA; Thermo Scientific #77140) for the first immunization, followed by a boost in incomplete Freund's adjuvant (IFA; Thermo Scientific #77145) at 2 weeks. Serum samples and blood were taken on different timepoints: before immunization (d0), 13 days post immunisation (13 dpi), 27 dpi and 34 dpi and 43 dpi. The samples were used for Aβ antibody ELISA (see 4. ELISA) and IgM purification.

10. IgM purification

IgMs were affinity purified utilizing immobilised mannan binding protein (MBP).[171] Purification of IgM was temperature and calcium dependent. Binding was performed at 4 °C in a buffer that contained calcium chloride. Elution was achieved at room temperature in a buffer that contained EDTA in the absence of calcium ions. To avoid low IgM purification and to concentrate the samples buffer exchange (into 20 mM Tris, 1.25 M sodium chloride; pH 7.4/Pierce Concentrator; Thermo Scientific; #89920) and desalting (Dextran Desalting Column; Thermo Scientific; #43230) were performed prior to application of the samples to the column. All steps were conducted according to manufacturer's protocols (IgM purification Kit; Thermo Scientific; #44897): Shortly, the MBP column was washed with 5 ml of IgM preparation buffer (RT) and equilibrated with 20 ml of IgM binding buffer (4°C). Mouse IgM serum or supernatant solution (1 ml) prepared as described above was applied

to the column. After the sample entered the gel, 0.5 ml of IgM binding buffer was applied to the column to ensure complete loading of the sample into the gel. The column was allowed to incubate for 30 min at 4 °C and then was washed with 14 x 3 ml aliquots of IgM binding buffer. After washing, the column was removed from the cold room; 3 ml of elution buffer was added and allowed to incubate at room temperature for at least 1 h. After acclimation, the column was eluted with 0,5 - 3 ml aliquots of IgM elution buffer. Absorbance of all the fractions was measured at 280 nm. Peak eluted fractions ($A_{280\ nm}$ > 0.020) were pooled and concentration of IgM was determined using an $\varepsilon_{280\ nm}$ value of 1.18 mg^{-1} ml cm^{-1} [172].

11. Pump implantation

We directly delivered purified transgenic IgM antibodies (see 10. IgM purification) & control antibodies into the brain via an osmotic minipump. Twenty-four to 48 hours prior to surgery, osmotic pumps (Model 2004 for 4 wks, 0,25 µl/h; Alzet) were filled with a 1mg/ml solution of Ab9-IgG antibody/isotype in PBS or with a 0,25mg/ml solution of purified Ab9-IgM/isotype and primed in 37°C PBS. Mice were anesthetized using Isoflurane, treated with Rimadyl for pain relief (Carprofen, 5 mg/kg s.c.), placed on a warming pad, and secured on a modified stereotactic apparatus. The skin and the periosteum were opened and the pump was implanted under the skin of the back. The coordinates for the cannula implantation into the right lateral ventricle from bregma were AP: +0.1 mm, ML: +1.0 mm and DV: -2.5 mm. The cannula (Brain Infusion Kit III 1-3 mm, Charles River, Germany) was held in place by dental cement (Heraeus, Hanau, Germany). Following surgery, mice received Paracetamol (Ben-u-Ron) for three days. After 4 weeks the pump was removed by an incision at the back and replaced by a new one which also stayed in for 4 weeks.

12. Brain tissue preparation

APPPS1 mice were sacrificed at 120±2 as well as 250±2 days of age. *TgSwDI* mice were sacrificed at 6 month. Brains were removed and one hemisphere was immersion fixed in 4% buffered formaldehyde (PFA) for up to 1 day followed by either paraffin embedding or immersion in 30% sucrose for 1-2days for subsequent immunohistochemical and immunofluorescence analysis.

The other hemisphere was snap-frozen for measurement of Aβ levels using Western blot and Aβ ELISA analysis. Protein/RNA was extracted from homogenized tissue of the whole cerebral hemisphere.

13. Histology and stereomorphological analysis

Formalin fixed and paraffin-embedded brains were processed for immunohistochemical analysis and subsequent morphometric analysis as described previously[173]. A subset of the sections was stained with pan anti-Aβ antibody: Mouse anti-human Aβ antibody 4G8 (Covance, Princeton, NJ) or 6E10 (Covance, Princeton, NJ) were used as primary antibodies at a dilution of 1:2000 after blocking with 10% normal goat serum in PBS or PBS containing 0.3% Triton X-100. For analysis of APPS1 sections another subset was stained for fibrillar Aβ with Congo red which was done according to standard laboratory procedures.

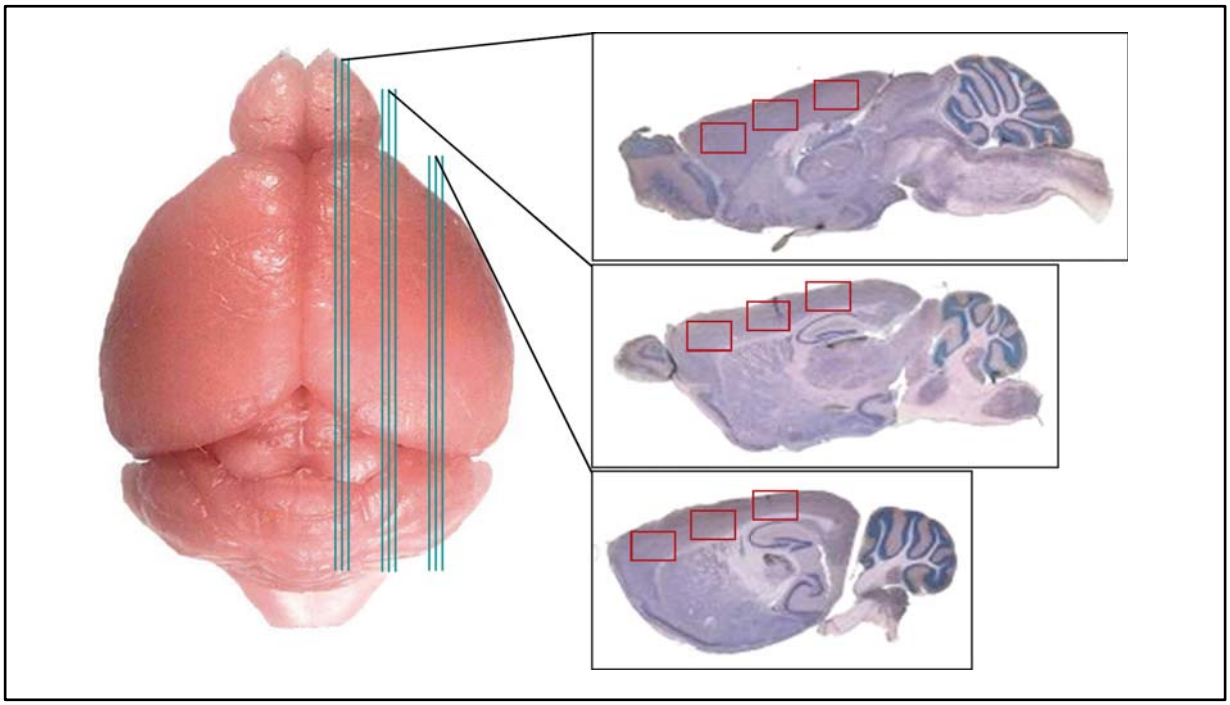

Fig. 8: Strategy for analysis of paraffin sections: 3 levels were analyzed for each mouse. Per level 3 sections were analyzed. On each section 3 regions were examined corresponding to the frontal, parietal and occipital cortex. In total, 27 pictures per brain were analyzed.

Paraffin-embedded brains were cut sagittally in 5µm thick sections. Immunohistochemical stainings were done using the Vectostain Elite ABC Kits (Vector Laboratories; Burlingame, CA) after deparaffinization in xylene and dehydrated in descencing alcohol series. Sections used for 4G8 staining were pretreated with 0.01 M citric acid. Aβ deposition and congophilic

amyloid were assessed by measuring the immunostained area of 3 cortical regions representing the frontal, parietal and occipital cortex (each 1.4 mm^2) on every 30^{th} systematically sampled 5-µm-thick Aβ-immunostained, Congo Red-stained or pentameric formyl thiophene acetic acid (PFTAA) stained section (Fig. 8). To reduce bias, all analyses were performed blind to genotype. The stereomorphologic analysis of 27 defined regions per mouse brain was performed with the aid of the Cell D software (Olympus, Tokyo, Japan) using the color filter and phase analysis tool. Congo Red-stained amyloid plaque can be quantified in presence or absence of the Cy3 filter. Both methods were compared at the 250 day analysis. In all groups on average 10 plaques more were counted with the Cy3 filter, but there was no difference among the groups.

Frozen floating sections were sliced as serial coronal 40 µm thick sections into cryoprotectant solution (30% ethylenglycol, 20% glycerol, 50 mm sodium phosphate buffer, pH 7.4) with a cryostat and immunostained according to previously published protocols.[2] Analysis was perfomed using the Area Fraction Fractionator method of StereoInvestigator (MBF Bioscience, Williston, VT) as described before.[174] Each section was viewed on an Olympus BX51 microscope with a computer-controlled motorized stage at low magnification (4×/0.32 N.A. Plan-Apochromat) and the regions were contoured onto a live computer image using StereoInvestigator software. Counting of individual plaques was performed at a higher magnification (10×/1.4 N.A. Plan-Apochromat), using an area fractionator grid to count plaque coverage. The counting frame was set to 90 x 90 µm, the scan grid 300 x 300 µm, and the Cavalieri grid spacing to 10 µm. Percent coverage counted from 8-10 sections was averaged to obtain a final estimate of plaque burden for each animal.

14. Plaque size determination

For the determination of plaque size distribution in 120 and 250 day old *APPPS1* mice 27 defined Aβ-immunostained section through the neocortex were imaged using Cell Sense software (Olympus, Tokyo, Japan) (Fig. 8).[173] Individual plaques were classified into different plaque size classes (50-500 µm, 500-1000 µm, 1000-1500 µm, 1500-2000 µm, 2000-2500 µm, 2500-3000 µm, 3000-6500 µm) Plaques smaller than 70 µm were excluded. In sections with high background false-positive detection was removed by hand.

15. Biochemical and molecular analysis of frozen hemispheres

15.1 Preparation of frozen sections for human Aβ ELISA and Western Blot

Frozen brain hemispheres were homogenized following published protocols[175] with slight modifications. Briefly, frozen cerebral hemispheres were homogenated in PBS/1% SDS including protease inhibitors (Roche, Cat. No.1836153) and centrifuged at 100.000g for 1 hour. The supernatant was collected as SDS-soluble Aβ fraction and the pellet was resuspended in 70% formic acid (FA). After incubation on ice and vortexing samples were centrifuged again for 1 hour at 100.000g. The supernatant was considered the insoluble fraction. Protein concentration of each fraction was determined using the Quantipro BCA Protein Assay Kit (Pierce #23227) according to the manufacturer protocol.

15.2 Human Aβ ELISA in brain homogenates and serum

Samples were diluted to fit the standard samples (Abeta Peptide 3-Plex) and were analysed on a MS6000 using MSD 96-well MultiSpot Human 6E10/ 4G8 Abeta Triplex Assay (Meso Scale Discovery, Gaithersburg, MD) according to manufacturer's instructions. Briefly, after blocking the MSD plate with 1% Blocker A Solution, 25 µl detection antibody solution and 25 µl sample or calibrator are added and incubated for 2 hours. After washing reading buffer is added and the plates are analysed.

15.3 Western Blot

Tris–tricine[176] SDS–polyacrylamide gel electrophoresis (PAGE) was performed to assess Aβ and APP levels following the procedure of Schagger and von Jagow[176]. Electrophoresis and blotting were carried out according to previously published protocols[92] using anti-Aβ 6E10 (1:1000, Covance, Princeton, USA) and anti-APPct (1:1000, Sigma-Aldrich, Schnelldorf, Germany) antibodies. As internal control monoclonal anti-β-Actin (1:5000, Abcam, Cambridge, UK) antibody was used. Anti-mouse and anti-rabbit HRP conjugated secondary antibodies were purchased from GE healthcare (1:10000, Munich, Germany). Equal quantity of total protein (20 µg/lane) was loaded on a 10-20% Tris–tricine (Novex, Invitrogen) or a Tris-bicine-urea polyacrylamide gel. Proteins were transferred onto nitrocellulose membrane

(Hybond, Amersham Biosciences) at 2.5 mA/cm^2 per gel by semi-dry blotting. Membranes were boiled for 5 min in PBS at 95°C and afterwards blocked in blocking buffer (TBS, 0.1% Tween-20 (v/v) and 5% (w/v) of skimmed milk) for 30 min. Membranes were incubated overnight at 4°C with appropriate dilutions of the primary antibodies and incubated for 1h at room temperature with secondary antibody. The immunoreactive complexes were visualized by chemiluminescence using ECL™ Western Blotting kit. GeneTool Software (Syngene, Cambridge, UK) was used to quantify the signal, and data were collected using Excel Software (Microsoft). Loading variations between Western blot lanes were normalized according to the β-Actin signal.

16. Statistical analysis

The statistical methodology used (i.e., the specific test to be used) to answer the question for significant differences in the data set depends on the underlying distribution of the measurements. It cannot be assumed that the data are normally distributed. Therefore normality tests are used to determine whether a data set is well-modeled by a normal distribution or not. To test for normality we have chosen the Shapiro-Wilk test as this test is quite sensitive even for small sample sizes ($n < 20$).[177] If the test resulted in a p-value greater than 0.05 it is assumed that the data are normally distributed. Hence the Student´s t-Test for pairwise comparison or ANOVA with Tukey's post hoc test[178] for comparison of more than 2 groups were used. Otherwise we used the nonparametric equivalent of the t test or ANOVA which are the Mann-Whitney U Test or the Kruskal and Wallis –Test, respectively. Both tests are based on ranks of the data sets. Level of significance was $p< 0.05$ if not otherwise specified. All analyses were performed with SPSS.

RESULTS

1. Generation of six transgenic founder lines with distinct transgene copy numbers

To generate a mouse model that selectively expresses anti-Aβ-IgM in the periphery to test the peripheral sink hypothesis of AD, we constructed a vector that expresses the Aβ specific heavy chain of AB9 under the control of the IgM-specific μ promoter (Fig. 9a, upper construct). As a second, more stringent model we created a vector in which the polyA site controlling the production of the secreted forms of the AB9μ heavy chain was deleted, resulting in α-Aβ-IgM antibodies which remained bound to B cells (Fig.9a, lower construct). In both constructs the heavy chain loci corresponding to other immune globulin (Ig) isotypes were removed. As a result, expression of these isotypes due to DNA rearrangement (referred to as class switching) was impeded. With the subsequent pronuclear injection of these vectors into C57BL/6 mice we generated two new transgenic (tg) mouse strains – *AB9μ* and *DelS* mice.

To verify the genotype of the tg founders two sets of PCR primers were designed (Fig. 9a, b). VDJ primers were specifically directed against the VDJ region of the transgene. PaSec primers detected the secretion sequence of the transgene and hence distinguished between both tg lines. We generated 8 founders in each lineage – in the AB9μ as well as the *DelS* lineage (2 died before genotyping). PCR analysis identified 6 positive AB9μ and 4 positive DelS founder lines (Fig. 9c). All positive *DelS* mice showed the smaller PCR product after PaSec amplification which verified the absence of the secretion sequence. Only 3 *AB9μ* lines (*AB9μ*-L2, L4, L7) and 3 *DelS* founder lines (*DelS*-L1, L2, L8) transmitted the transgene through the germline and were established as 6 tg lines.

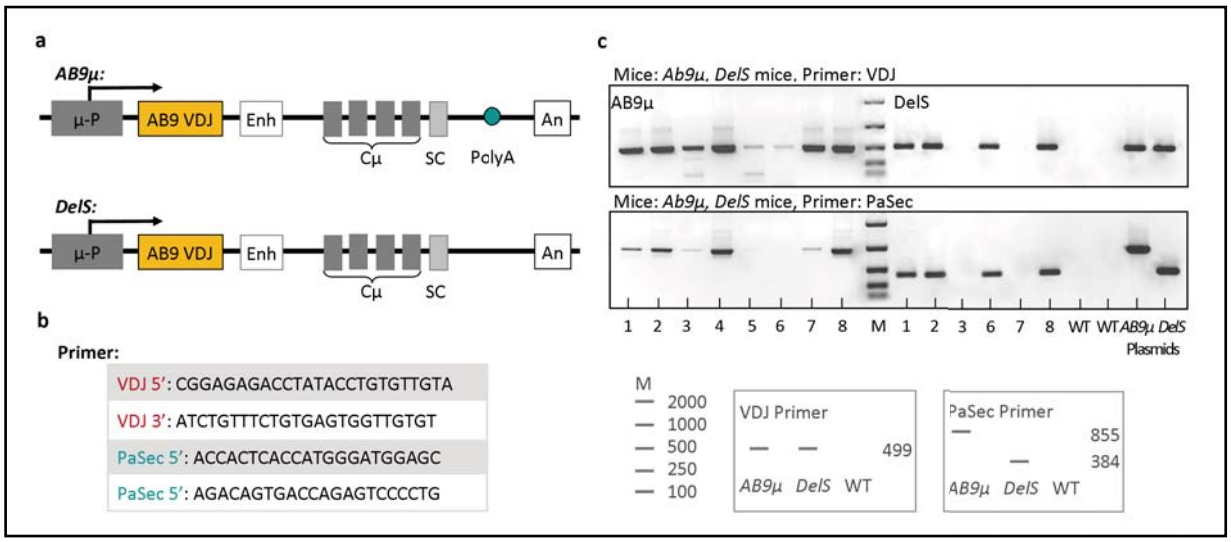

Fig. 9: Generation of *AB9µ* and *DelS* transgenic strains: a| Transgenic (tg) vectors pSV2neo*AB9µ*/*AB9µDelS* consisted of an IgM specific µ-promoter, the AB9 VDJ region for the heavy chain and the constant region of IgM (Cµ). In pSV2neo*AB9µDelS* the secretion sequence was removed (blue circle) b| Designed primers to identify tg founders (VDJ) and to distinguish *AB9µ* and *DelS* founders lines (PaSec) c| PCR amplification of *AB9µ* and *DelS* transgene using VDJ primers generated a 499 bp DNA fragment from genomic DNA of *AB9µ* and *DelS* tg mice but not from non-transgenic WT mice. PCR genotyping with PaSec primers produced an 855 bp DNA fragment for *AB9µ* tg mice and a 384 bp DNA fragment for *DelS* tg mice. Abbreviation: M, DNA size marker.

Next we estimated transgenic copy numbers in the different transgenic lines (Fig. 10) by quantitative PCR. Quantitative PCR revealed the first differences between the 6 tg lines. Most transgenic copy numbers we found in *AB9µ*-L4 and *DelS*-L2/8 (Fig. 10). All other lines showed far less transgenic copy numbers.

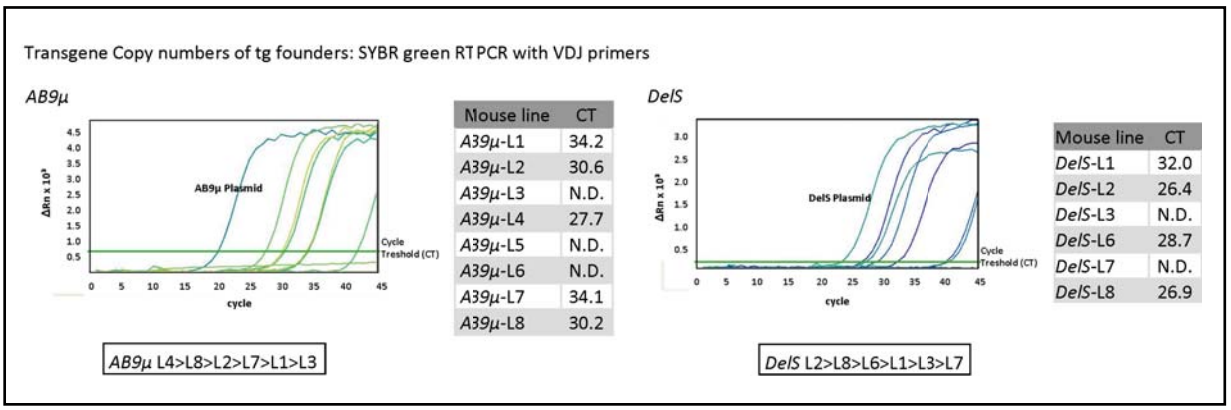

Fig. 10: SYBR Green analysis for transgenic copy numbers: Comparison of *AB9µ*-L1 to 8 confirmed absence of the transgene in 3 out of 8 lines. Most transgene copy numbers were found in *AB9µ*-L4. In the *DelS* tg lines 2 out of 6 mice did not express the transgene. Among the others *DelS*-L8 and L2 exhibited highest tg copy numbers.

The putative tg B cells of these lines were not purely tg as they contained endogenous light chains rearranged with the tg heavy chains. This generated a polyclonal response which in general confers advantages on the immune system as it increases the probability of reacting against the antigen (in this case Aβ) by attacking different epitopes. However, it also increases the chance of developing antibodies to self-antigens.[179-181] To further address the functionality of the different transgenes and exclude unwanted side effects – such as the influence of random integration, tg copy numbers or autoimmunity – we subjected *AB9µ*, *DelS* and control lines to a series of experiments (arranged by the chapters that follow)

- Flow cytometric analysis of B cells with allotype-specific anti-IgM antibodies
- Flow cytometric analysis of B cell development and subtypes in spleen and bone marrow
- Flow cytometric immune cell profile of blood with CD8, CD4, B220, NK1.1, Gr-1 and CD11b
- Histological assessment of spleen, kidney and liver for pathological changes
- ELISA for anti-Aβ antibodies in serum
- B cell proliferation in tg mice
- Analysis of immune response towards infection with the Vesicular stomatitis virus
- Antibody purification from cell culture supernatants and serum of *AB9µ* mice

2. Immunological and histological characterisation of *AB9µ* and *DelS* mice

2.1 Flow cytometric analysis of B cells with allotype-specific anti-IgM antibodies

Expression of tg anti-Aβ surface IgM was tested by flow cytometric analysis of B cells. To distinguish tg from endogenous B cells we took advantage of the expressed IgM allotype – while the C57BL/6 recipient mice express the IgM^b heavy chain (Fig. 11, second row), the *AB9µ*/*DelS* transgenes harbour the IgM^a allotype. The latter allotype is normally expressed in Balb/c mice (Fig. 11, first row) which served as positive IgM^a control for the tg mice.

Flow cytometric analysis of blood cells with allotype-specific anti-IgM antibodies revealed that all six tg lines (*DelS* and *AB9µ*) expressed tg surface IgM of the IgM^a allotype (Fig. 11, third and fourth row/ Table 7). However, there was considerable variability between the tg lines (*AB9µ* and *DelS*) in the numbers and proportion of B cells expressing transgene-encoded IgM (Fig. 11/ Table 7). With regard to this variability we could identify two distinct phenotypes (Fig. 11, *AB9µ*-L4I and *DelS*-L8) which are illustrated by *AB9µ*-L4I and *DelS*-L8. *AB9µ*-L4I had normal total B cell frequency (39.7% ± 1.5) comparable to C57BL/6 and Balb/c mice (Fig. 11, last column), high frequency of endogenous IgM^b positive B cells (88.9%) as well as chimeric B cells carrying both IgM allotypes (Fig. 11). Apart from *AB9µ*-L4I no other mouse line displayed this first phenotype with chimeric B cells. In contrast *DelS*-L8 – and all other tg lines (*AB9µ*-L2,4II,7 and *DelS*-L1,2,8) – exhibited the second phenotype having reduced total B cell frequency (16.2% ± 1.1) with low frequency of endogenous IgM^b positive B cells (7.3% ± 1) and no chimeric B cells (Table 7). Furthermore it is important to state that, consistent with the quantitative PCR data, *AB9µ*-L4I and *Dels*-L8 had the most tg B cells, 7140 and 13690 B cells per 10^5 Lymphocytes, respectively (Table 7).

The occurrence of chimeric B cells as well as variable numbers of endogenous and tg B cells in immune globulin tg mice is a common phenomenon. It is caused by the varying, but not absolute inhibition of the endogenous immune globulin gene rearrangement and expression induced by the transgene – referred to as incomplete allelic exclusion.[182] Allelic exclusion under normal circumstances ensures clonal specificity of a B cell. Variable incomplete allelic exclusion (range 7.3-27.8% endogenous IgM^b positive B cells) was observed in all tg lines of the second phenotype (Fig. 11, Table 7). In line with these observations, *15B3* mice which served as control mice expressing a transgenic µ heavy chain with unknown specificity demonstrated similar expression of tg B cells and allelic exclusion, which has already been described before.[165] *AB9µ*-L4I was the only line showing no allelic exclusion as it had 90% endogenous IgM^b positive B cells.

Next to variable allelic exclusion the second phenotype displayed another obvious feature which needs to be analysed further. This is the marked reduction of total B cells in peripheral blood (range 4.9-16.2% compared to 47.3% in C57BL/6).

Interestingly, *AB9μ*-L4I and L4II originated from the same founder line, namely *AB9μ*-L4 which was split into two separate stable lines with contrary phenotypes. This might be due to mutations leading to germ line mosaicism.

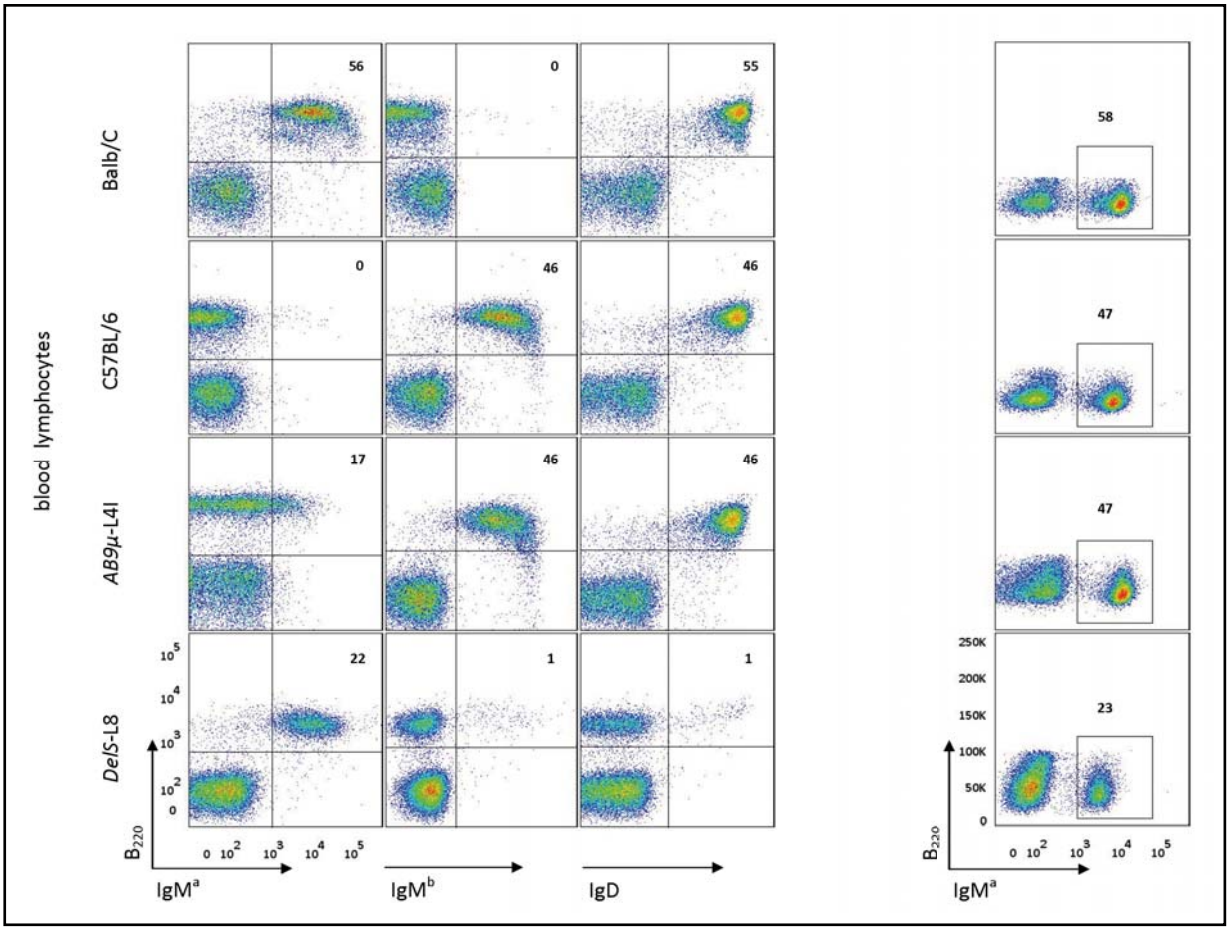

Fig. 11: Flow cytometric analysis of blood B cells in *AB9μ*-L4I, *DelS*-L8 and control mice: Flow cytometry profiles of anti-IgM^a- and anti-IgM^b-stained blood cells from BALB/c, C57BL/6, *AB9μ*-L4I and *DelS*-L8 mice (gated on lymphocytes) demonstrated differential expression of endogenous and transgenic B cells. B_{220} staining further revealed reduction in B cells. The additional marker IgD was used to evaluate allelic exclusion. Whereas a high degree of allelic exclusion took place in *Dels*-L8, no allelic exclusion was found in *AB9μ*-L4I. Values in panels represent percentages.

Transgenic line	B cell frequency [%]	IgM^{a+} B cells (tg B cells) [%]	IgM^{b+} B cells [%]	IgD^{+} B cells [%]	number of tg B cells in 10^5 LC
WT	47.32 ± 1.61	—	94.08 ± 0.47	94.56 ± 0.62	—
***AB9µ*-L2**	4.85 ± 0.47	22.10 ± 3.49	27.82 ± 3.72	23.9 ± 2.95	663.09 ± 5.36
***AB9µ*-L4I**	**39.73 ± 1.54**	**13.68 ± 1.13**	**88.96 ± 1.21**	**92.11 ± 0.57**	**7141.84 ± 44.77**
***AB9µ*-L4II**	3.56 ± 0.53	17.97 ± 2.90	44.20 ± 5.68	34.96 ± 7.38	1040.2 ± 9.83
***AB9µ*-L7**	6.38 ± 0.49	29.23 ± 1.84	25.15 ± 2.87	19.89 ± 2.67	1410.59 ± 17.08
***DelS*-L1**	4.90 ± 0.41	52.21 ± 1.53	20.47 ± 1.72	19.41 ± 1.69	2559.8 ± 6.36
***DelS*-L2**	14.28 ± 0.94	57.58 ± 1.68	20.36 ± 1.37	20.18 ± 1.69	8221.38 ± 15.71
***DelS*-L8**	**16.19 ± 1.12**	**84.52 ± 1.46**	**7.32 ± 0.99**	**5.72 ± 0.91**	**13687.2 ± 16.28**

Table 7: Frequency of B cells in the lymphocyte population of the different tg lines in blood: After gating on the lymphocyte gate the frequency of B cells in the lymphocyte population was recorded. To estimate total tg B cell numbers the total number within 10^5 lymphocytes was calculated for each line. Most B cell numbers were found in *DelS*-L8. The values given represent the mean ± SEM from ten to forty individual mice analysed.

2.2 Flow cytometric analysis of B cell development and subtypes in spleen and bone marrow

In adult mice, B lymphopoiesis occurs in the bone marrow (BM) in a series of steps that are definable by changes in cell surface expression of a variety of molecules, starting with the expression of B220. From the pre-pro B cells stage, B cells develop into pro B cells ($B220^+CD19^+CD25^-CD43^+IgM^-$), followed by pre B cells I ($B220^+CD19^+CD25^-CD43^-IgM^-$) and pre B cells II ($B220^+CD19^+CD25^+$), then to immature B cells ($B220^+CD19^+CD25^-CD43^-IgM^+$) which express functional cell surface IgM. These immature (transitional) B cells migrate to the periphery and populate the spleen in which we can find recirculating and resident B cells that can be distinguished immunophenotypically.

Within the peripheral B cell pool we saw a marked reduction in the frequency of peripheral B cells in most tg *DelS* and *AB9µ* lines (apart from *AB9µ*-L4I) (Fig. 11, last column). To determine the origin of this reduction we carried out flow cytometric analyses of B cell development and subtypes in spleen and bone marrow (BM). Similar to blood, the frequencies of splenic B cells were also reduced (Fig. 11), and we found a reduction in the fractions of follicular recirculating B cells, accompanied by a proportional increase in the frequencies of marginal zone (MZ) and transitional B cells (Fig. 13 and Table 9). These deviations from the normal frequencies suggested an impairment of B cell development in the tg animals that became more apparent when B cell development in the BM was analyzed

by flow cytometry. Staining of the cells for B220, CD19, IgM, CD25, and CD43 revealed a marked reduction of immature B cells in the BM – identified by expression of IgM compared to mature B cells – in all *AB9µ* and *DelS* tg lines except for *AB9µ*-L4I and control mice (C57BL/J) (Fig. 12/ Table 8). In contrast, no reduction was observed in pre or pro B cells – the B cell stages arising before immature B cells (Fig. 12/ Table 8). Accordingly, a partial disruption at the transition from pre/pro B cells to immature B cells (Fig. 12 and Table 8) was noted. Previous publications describing similar observations however failed to detect important qualitative differences in immature B cells by functional and flow cytometric analyses.[183,184]

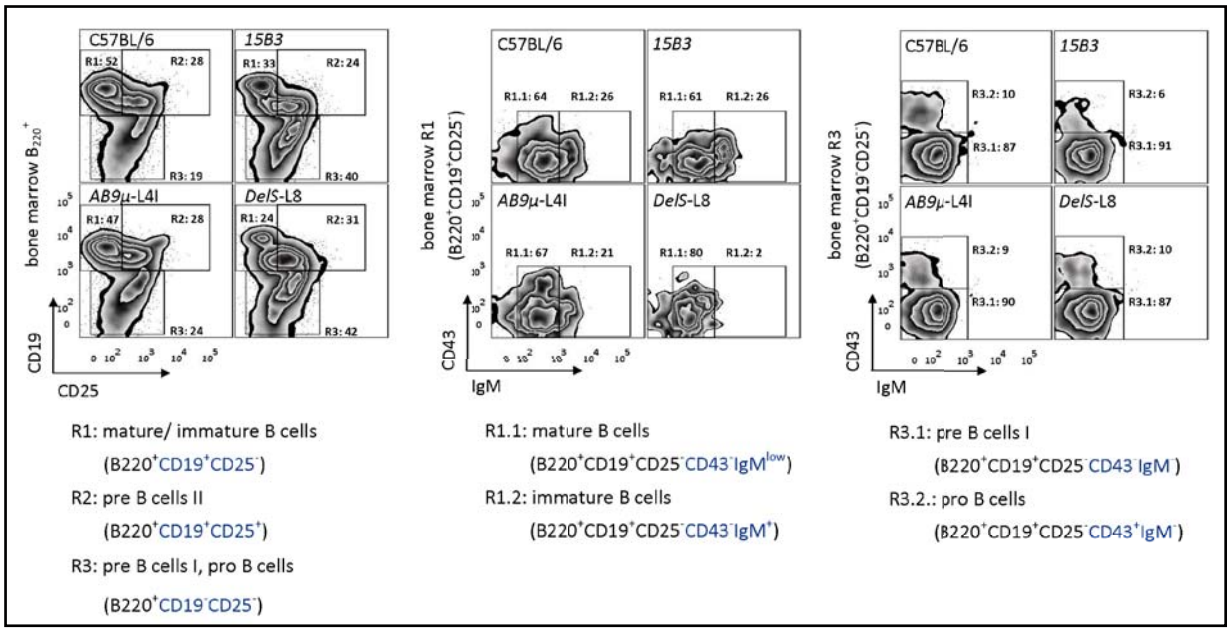

Fig. 12: Flow cytometric analysis of B cell development in the BM of *AB9µ*, *DelS*, *15B3* and WT mice: B_{220}^{+} cells were displayed and gated based on expression levels of surface CD19 and CD25. A two-fold decrease was observed in mature/immature B cells which can be attributed to a reduction in immature B cells as shown in the second panel. The last panel shows the distribution of pro–B cell ($CD43^{+}CD25^{-}IgM^{-}$) versus pre–B cell ($CD43^{-}CD25^{-}IgM^{-}$) populations within $CD19^{+}B220^{+}$ BM cells. No change in pro and pre B cell was observed. Numbers represent the percentage of cells within the designated gates.

Transgenic line	Pro B cells	Pre B cells I	Pre B cells II	Immature B cells [%]	Mature B cells [%]
WT (C57BL/J)	9.6	87.1	27.8	**26.2**	64.4
15B3	6.0	91.4	24.1	**26.5**	61.3
***AB9μ*-L2**	10.7	86.9	21.3	**4.9**	70.0
***AB9μ*-L4I**	9.1	89.6	28.1	**21.2**	67.0
***AB9μ*-L4II**	9.2	89.7	26.0	**7.9**	72.4
***AB9μ*-L7**	9.0	89.7	37.5	**4.5**	72.7
***DelS*-L1**	7.4	91.5	34.9	**2.2**	72.8
***DelS*-L2**	8.1	89.9	30.9	**6.7**	73.4
***DelS*-L8**	9.6	87.1	31.2	**2.2**	79.5

Table 8: B cell populations in the BM for all tg lines measured by flow cytometry: After gating on the B220+ cells the frequency of immature/mature, pro/pre B cells I and pre B cells II was recorded by staining against CD19 and CD25. Immature/mature B cells, pro B cells/ pre B cells I were further gated for CD43 and IgM to gain insight into the reduced cell population. The frequency for each of these single cell populations according to the above shown gating strategy is displayed here. All lines showed a reduction in the immature B cell pool apart from *AB9μ*-L4I, *15B3* and WT mice. All other cell populations remained unchanged. The values represent the percentage seen for each line.

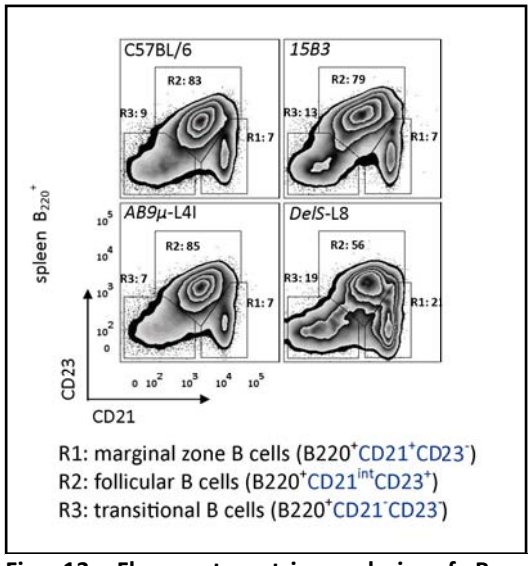

Fig. 13: Flow cytometric analysis of B cell development in the spleen of *AB9μ*, *DelS*, *15B3* and WT mice: B_{220}^{+} cells were displayed and gated based on expression levels of surface CD23 and CD21. A reduced number of follicular B cells was observed. Numbers represent the percentage of cells within the designated gates.

Transgenic line	MZ B cells	FO B cells	T B cells
WT (C57BL/J)	7.4	82.8	9.4
15B3	6.9	79.2	13.2
***AB9μ*-L2**	18.7	44.8	35.1
***AB9μ*-L4I**	6.9	85.3	7.2
***AB9μ*-L4II**	16.2	52.1	29.0
***AB9μ*-L7**	15.6	52.4	30.1
***DelS*-L1**	28.2	40.8	28.8
***DelS*-L2**	17.5	55.4	24.6
***DelS*-L8**	21.7	56.8	19.8

Table 9: B cell subtypes in the spleen for all tg lines measured by flow cytometry: It was gated as shown in Fig.16. A reduction in follicular B cells was observed for all tg lines except for *AB9μ*-L4I, *15B3* mice and nontransgenic littermates. The values represent the percentage seen for each line. Abbreviations: FO-follicular, MZ-marginal zone, T-transitional

In summary, the decline in the peripheral B cell pool was due to a compromised B cell generation in BM with a partial developmental block at the pro/pre B cell to immature B cell transition.

2.3 Flow cytometric immune cell profile of blood with CD8, CD4, B220, NK1.1, Gr-1 and CD11b

A growing number of studies in AD have reported alterations in systemic immune responses including changes in lymphocyte and macrophage distribution and activation or abnormal cytokine production.[3-5] Studies in animal models of AD support the notion that immune cells infiltrate the brain and may modulate the disease.[185,186] As we introduced tg B cells into the immune system of mice it is conceivable that this might alter the frequency of other immune cells – especially as a compensatory effect for the diminished B cell compartment in the tg mice (*DelS*-L1,2,8 and *AB9µ*-L2,4II,7). To exclude possible effects on other peripheral immune cells in the blood, we examined *AB9µ, DelS* and control mice for the distribution of subpopulations of leukocytes (lymphocytes, granulocytes, and monocytes) and lymphocyte subtypes (helper and cytotoxic T lymphocytes and NK cells) in blood by flow cytometric analysis with CD4, CD8, Gr-1, CD11b and NK1.1. Frequencies of these non-B cell leukocytes were proportionately increased (in *DelS*-L1,2,8 and *AB9µ*-L2,4II,7), reflecting the aforementioned reduction in the B cell compartment. Additionally, the ratio of CD4+ to CD8+ cells was not affected. Thus, in contrast to the B cell compartment, other immune cells such as T cells, NK cells, and granulocytes in blood of all tg mice studied were not affected by the transgene, as judged by flow cytometry (Table 10 and Fig. 14). Especially, we demonstrated that the CD4/CD8 ratio was unaltered which is important as alterations are associated with progressive multifocal leukoencephalopathy or Hodgkin lymphoma (HL).[187-189]

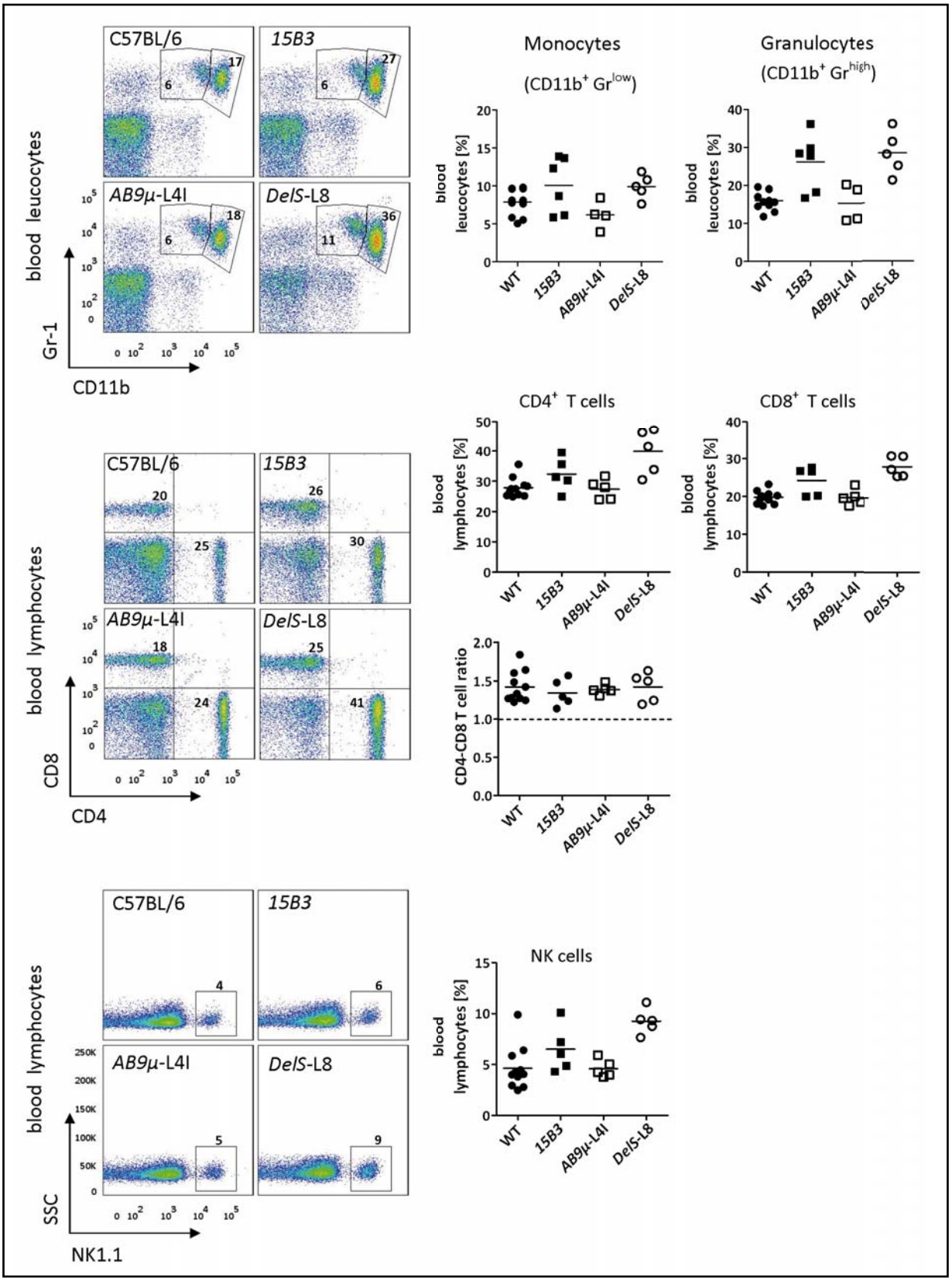

Fig. 14: **Flow cytometric analysis of blood immune cells in *AB9μ*-L4I, *DelS*-L8 and control mice**: Upper panel| Flow cytometry profiles of leukocytes from C57BL/6, 15B3, *AB9μ*-L4I and *DelS*-L8 mice stained for Gr-1 and CD11b did not show an up regulation of granulocytes or monocytes. Middle panel| Stainings of lymphocytes for CD4 and CD8 did not demonstrate any differences between tg and WT mice either. Lower panel| NK cell are not changed in tg mice compared to WT mice. Values in figures represent percentages.

Transgenic line	$CD8^+$ T cells [%]	$CD4^+$ T cells [%]	CD4/CD8 T cell ratio	NK cells [%]	Granulocytes [%]	Monocytes [%]
WT (C57BL/6)	19.75 ± 0.51	27.89 ± 0.97	1.42 ± 0.06	4.63 ± 0.64	16.01 ± 0.76	7.89 ± 0.53
15B3	24.22 ± 1.69	32.38 ± 2.46	1.34 ± 0.08	6.50 ± 1.03	24.18 ± 2.78	9.65 ± 1.76
***AB9µ*-L2**	28.48 ± 1.22	42.20 ± 2.13	1.50 ± 0.12	12.72 ± 0.95	36.70 ± 1.86	12.22 ± 0.75
***AB9µ*-L4I**	**19.70 ± 0.93**	**27.38 ± 1.47**	**1.39 ± 0.03**	**4.59 ± 0.39**	**15.35 ± 2.21**	**6.18 ± 0.82**
***AB9µ*-L4II**	27.14 ± 0.34	44.88 ± 1.48	1.66 ± 0.07	9.77 ± 1.58	28.46 ± 1.44	11.72 ± 0.56
***AB9µ*-L7**	26.37 ± 0.74	42.96 ± 1.39	1.64 ± 0.09	9.53 ± 0.71	36.22 ± 1.58	11.44 ± 0.66
***DelS*-L1**	29.26 ± 0.75	37.42 ± 1.14	1.28 ± 0.05	10.52 ± 0.65	29.33 ± 4.59	13.45 ± 1.01
***DelS*-L2**	28.38 ± 0.77	35.03 ± 0.72	1.24 ± 0.04	9.21 ± 0.62	23.80 ± 2.38	13.00 ± 0.93
***DelS*-L8**	**27.92 ± 1.20**	**39.86 ± 3.32**	**1.42 ± 0.09**	**9.25 ± 0.56**	**28.50 ± 2.55**	**9.68 ± 0.76**

Table 10: Frequencies of peripheral immune cells in *AB9µ*, *DelS* and control mice: Flow cytometric analysis of peripheral immune cells with CD4, CD8, B220, Gr-1, CD11b, NK1.1 only showed a relative increase in peripheral immune cells which was inversely proportional to the decrease in B cells observed in each line (Fig). Values represent mean ± SEM of 5-10 mice per line.

2.4 Histological assessment of spleen, kidney and liver for pathological changes

Tg mice harbouring *AB9µ* or *DelS* transgenes were further examined for morphological alterations due to transgene expression and observed changes in the B cell compartment. Mice from all tg lines developed normally, were fertile, and did not show any obvious abnormalities. Histological examination can furthermore differentiate among pathological changes and signs of autoimmunity at the microscopic level. Putative autoimmunity could arise from the polyclonality of the tg antibodies which leads to wider range of antibody-specificities increasing the chance of autoreactive antibodies to self-antigens. To investigate this possibility, histological examination of kidney, liver and spleen was conducted to report on putative qualitative differences in the tg mice. None of the organs showed inflammatory infiltrates or obvious pathological alterations in H&E stained sections (Fig. 15 and Fig. 16). However, *DelS* spleen architecture was found to be altered: Splenic follicles appeared reduced in size and less well defined demonstrated by a representative example that illustrates the difference in size (Fig. 16).

Additionally, spleen sections were stained with CD4, B220, and CD11b to visualize the presence of B cells (B220), CD4+ T cell as well as macrophages and dendritic cells (CD11b). The B cell staining confirmed the reduction in B cell numbers in the spleen as it was already

observed by means of FACS analysis (Fig. 11). There was no obvious difference in the number or location of macrophages or CD4+ T cells in tg compared to WT mice.

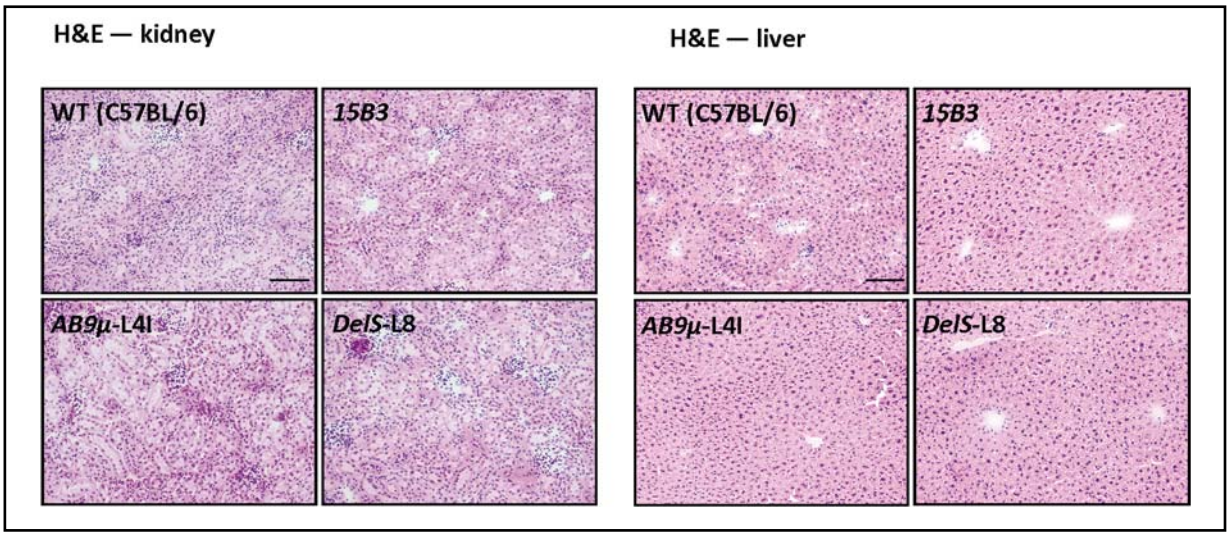

Fig. 15: Analysis of putative pathological changes in kidney and liver of *AB9μ* and *DelS* mice: H&E stainings of kidney and liver sections from *AB9μ*, *DelS*, *15B3*, and WT mice. Glomeruli and tubules in kidneys did not display pathological alterations, nor did hepatocytes in the liver. Bar = 200µm

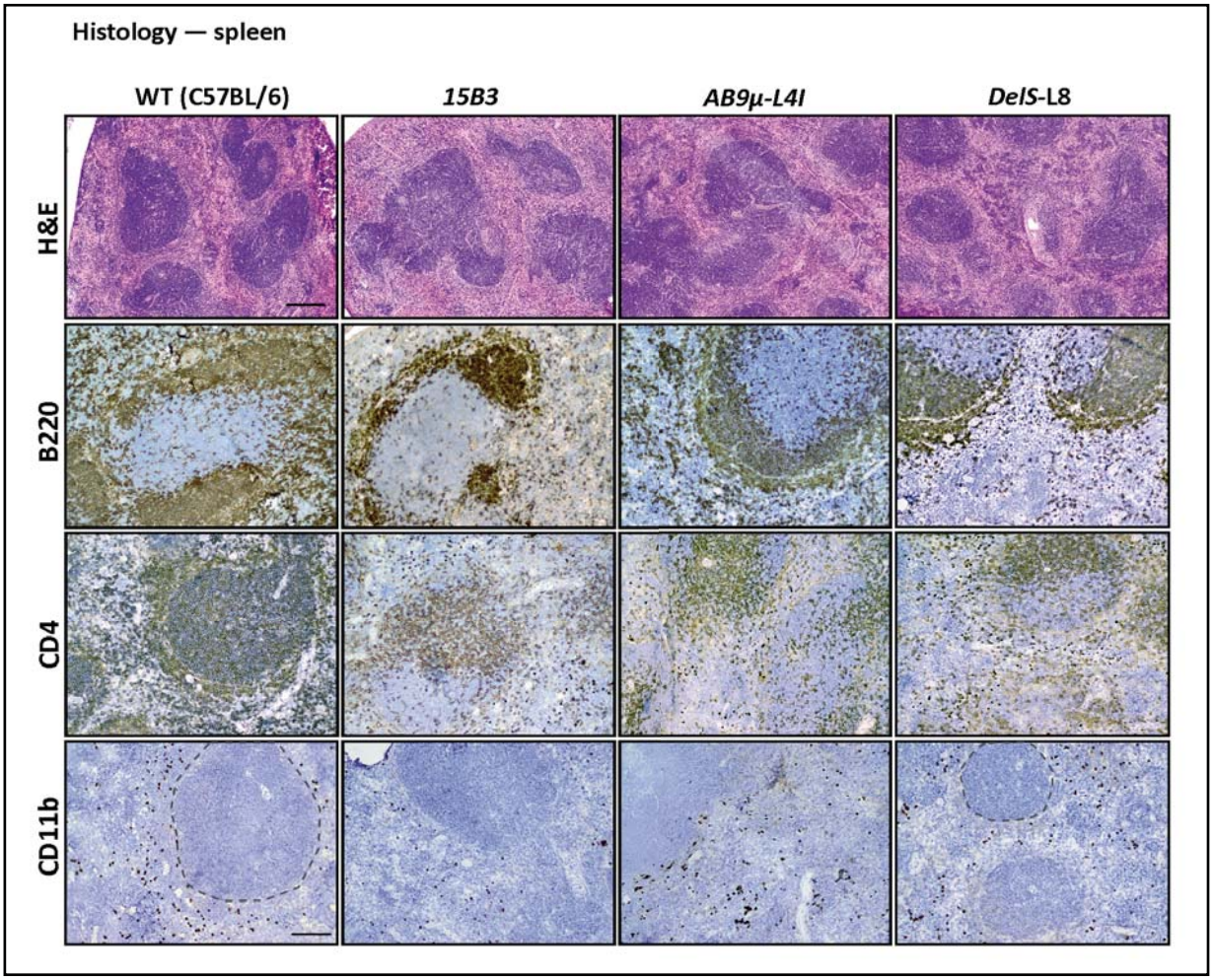

Fig. 16: Lymphoid follicles in spleens of *AB9μ* and *DelS* mice: Histological spleen sections stained with H&E, B220, CD4 and CD11b. Lymphoid follicles appeared smaller in *DelS* mice shown by the outline in the lower panel (CD11b staining). B220 staining revealed a reduced number of splenic B cells. No difference in CD4+ and CD11b+ cells could be observed. Upper scale bar = 100µm, lower scale bar = 200µm

In summary, these data show that transgene expression followed by a reduction in the peripheral and splenic B cell pool did not alter morphological structure and histoarchitecture of kidney, liver and spleen.

2.5 ELISA for anti-Aβ antibodies in serum

We showed that all the tg lines produced IgM^a positive B cells to various degrees. Also it was possible to show by PCR that *DelS* mice were missing the secretion sequence. Whether this absence of the secretion sequence led to cell surface-bound IgM^a which cannot be released into the blood – and whether *AB9μ* mice on the contrary released anti-Aβ-IgM^a antibodies – remained to be proven. To test this, we designed an anti-Aβ42 specific ELISA in which antibodies recognizing Aβ42 can be detected. To establish a reliable and specific method to identify Aβ-IgM^a antibodies, we tested different coating concentrations of Aβ42, different Aβ42 coating buffers and blocking conditions (see method section). This was important to avoid non-Aβ specific antibody binding which increases the background but still remain high sensitivity and specificity.

With the optimized ELISA we were able to prove that all *AB9μ* lines (Fig. 17, blue lines) produced anti-Aβ-IgM antibodies to different extents, with *AB9μ*-L2 having the highest titer at 70 days (Fig. 17, upper two panels and lower left panel). Furthermore, none of the *DelS* lines (Fig. 17, green lines) elicited an Aβ specific antibody response nor did the control mice (WT, *15B3*) (Fig. 17, upper two panels and lower left panel). Considering the possibility that transgenic anti-Aβ-IgM antibodies might class switch to IgG by usage of an alternative IgG locus, we used different detection antibodies (Fig. 17). Whereas antibodies detecting all isotypes (Fig. 17, anti-IgG, A, M and Igkappa) and especially IgM specific antibodies (Fig. 17, upper right panel) showed the same anti-Aβ response in the *AB9μ* lines, the anti-IgG detection antibody failed to show a response (Fig. 17, lower right panel), indicating that *AB9μ* B cells did not class switch to another isotype and only released anti-Aβ-IgM antibodies. Anti-Aβ-IgM concentration in *AB9μ* mice ranged from 1.5 to 2.5 μg/ml (Fig. 17, bottom panel)

To investigate whether aging and subsequent B cell senescence influence the peripheral anti-Aβ titers, we also inspected the anti-Aβ response at an age of 500 days. This is especially

important as AD is an age-related disease and thus titers should be high also in old mice. Aged mice showed an even more pronounced titer against Aβ (Fig. 18), indicating a humoral response of transgenic B cells to the murine antigen Aβ. Also, at that age we could not detect Aβ specific IgG antibodies (Fig. 18, lower left panel). Anti-Aβ-IgM response at that age ranged from 2 to 5 µg/ml (Fig. 18, lower right panel).

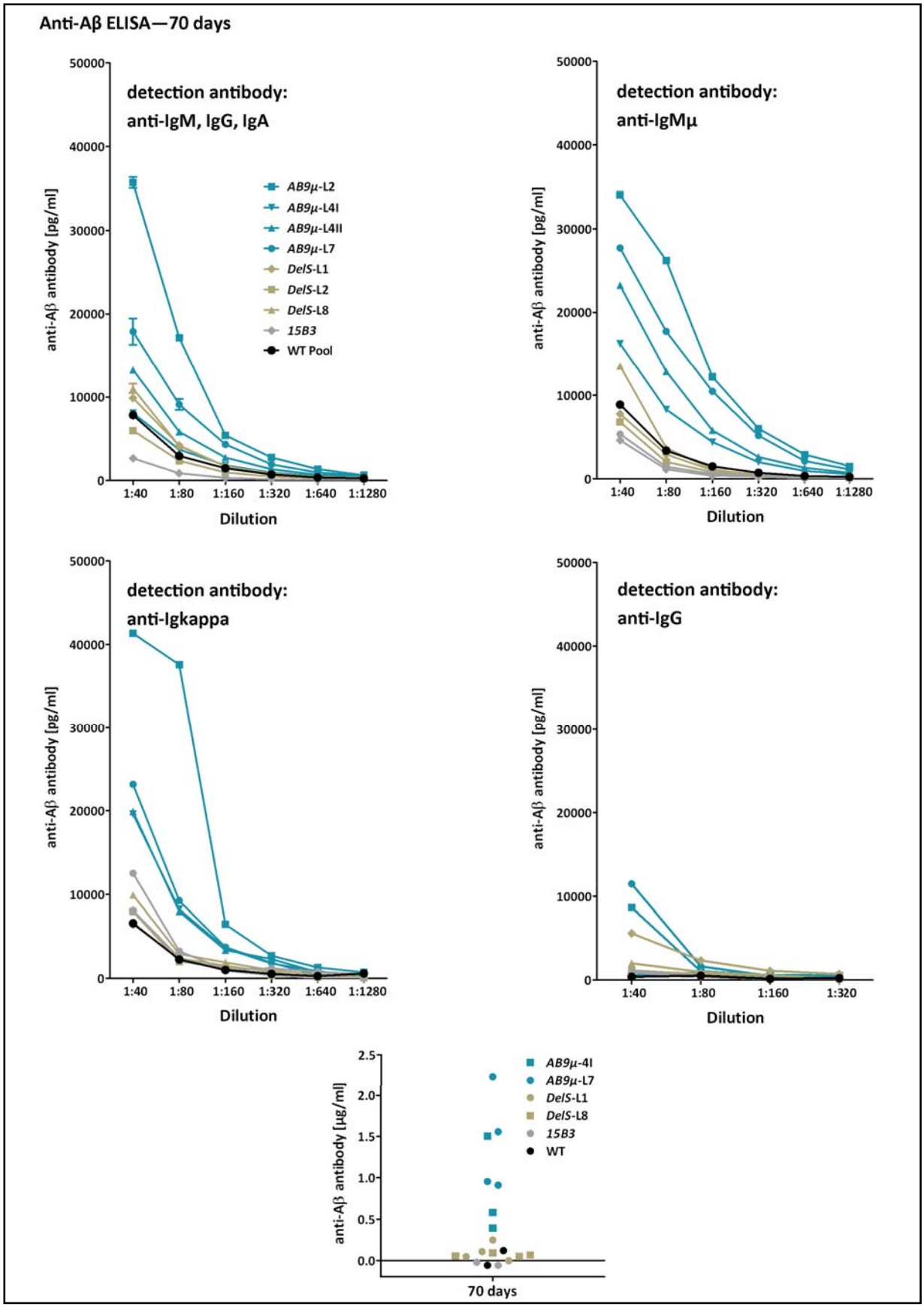

Fig. 17: Aβ specific ELISA with sera of *AB9μ*, *DelS*, *15B3* and WT mice at 70 days: ELISA showing anti-Aβ titers in sera of *AB9μ* mice (blue lines), but not of *DelS* mice (green lines), nor of *15B3* mice (grey lines) or of non-tg littermates (black lines). Immunoreactivity of *AB9μ* mice was only detectable with anti-IgM, anti-IgG+A+M, but not with anti-IgG secondary antibodies. Representative figures show two to four mice per line with SEM

(cannot be seen due to small variation). The summary (bottom panel) shows that all *AB9µ* lines exhibit an anti-Aβ response above background (black line). Values were calculated from anti-IgM detection (dilution 1:160).

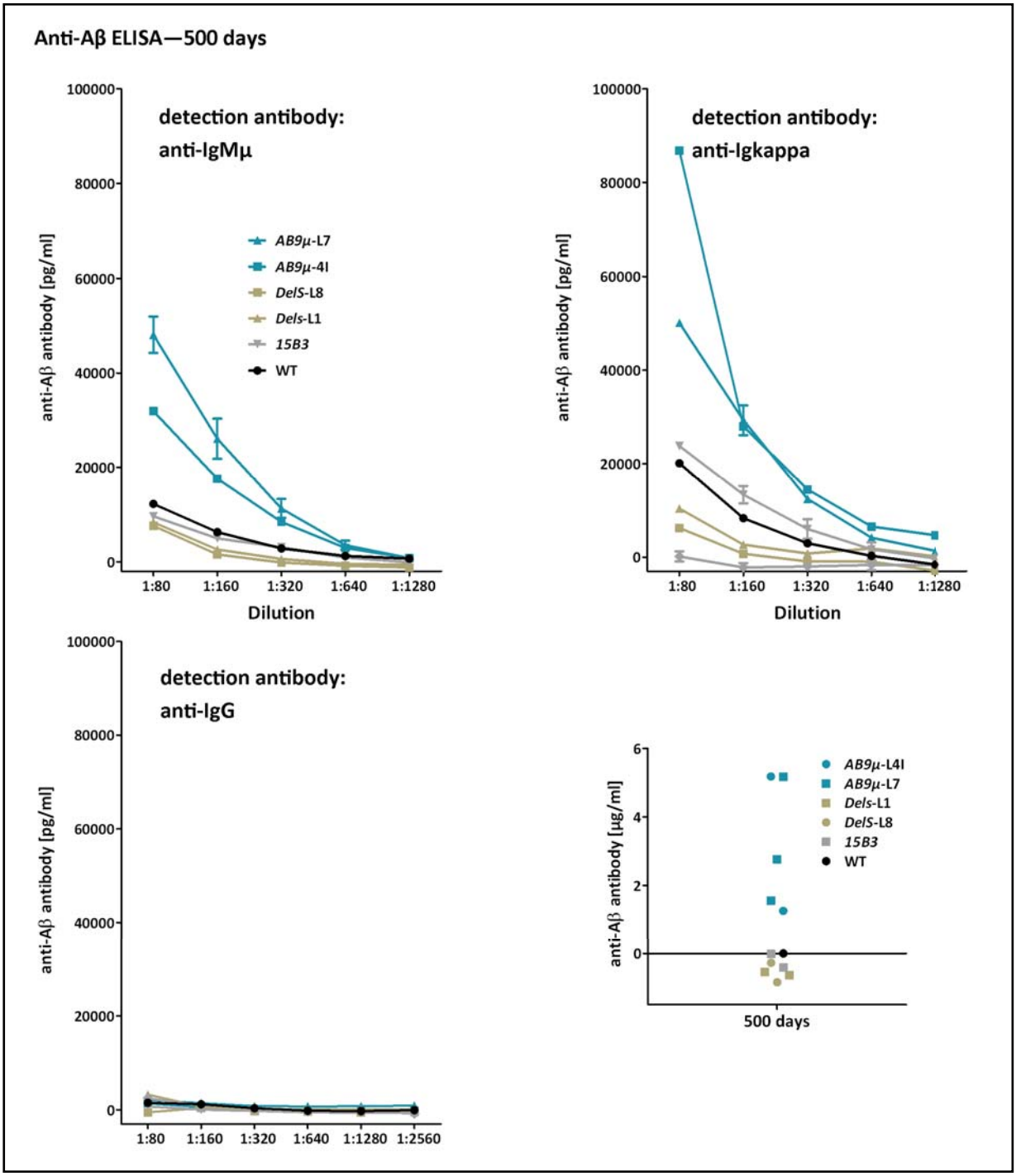

Fig. 18: Aβ specific ELISA with sera of *AB9µ*, *DelS*, *15B3* and WT mice at 500 days: ELISA showing anti-Aβ response in sera of *AB9µ* mice (blue lines), but not of *DelS* mice (green lines), nor of *15B3* mice (grey lines) or of nontransgenic littermates (black lines) at 500 days of age. Immunoreactivity of *AB9µ* mice was only detectable with anti-IgM, anti-IgG+A+M, but not with anti-IgG secondary antibodies. Representative figures show two to four mice per line. The summary (right side) shows that all *AB9µ* lines show an anti-Aβ response above background (black line). Values were calculated from anti-IgM detection (dilution 1:160).

2.6 B cell proliferation in *AB9μ* and *DelS* mice

Antigen exposure activates a profound functional metamorphosis in resting B lymphocytes leading to proliferation and differentiation into antibody-secreting plasma cells. We next examined B cell function in *AB9μ*, *DelS*, *15B3* and WT mice. First we assessed the proliferative potential of splenocytes from tg and control mice in response to LPS with the use of CFDA-SE which is distributed between daughter cells upon division. Splenocytes in *AB9μ, DelS* and *15B3* showed a normal proliferative response to LPS (Fig. 19a, b). Normal proliferation of tg B cells was also observed upon stimulation through the BCR with anti-IgM F(ab')2 (α-IgM) (Fig. 19a,b). However, tg B cells did not proliferate upon exposure to Aβ – their cognate antigen – which might be due to several reasons (see Discussion). Aβ was presented in two different ways – as the recombinant Aβ42 version or as highly organized repetitive Aβ1-6 peptides covalently conjugated to virus like particles (VLP) Qβ (CAD106) to optimize antigen presentation (Fig. 19b).

To conclusively prove that tg B cells were indeed proliferating within the pool of endogenous and tg B cells after LPS and α-IgM stimulation, we stained proliferated B cells with the allotype marker IgM^a and subjected the supernatants of the cell culture to anti-Aβ ELISA analyses. Both, *DelS* and *AB9μ* tg B cells proliferated in the presence of LPS and α-IgM as assessed by IgM^a staining (Fig. 19c). Furthermore, Aβ-specific ELISA demonstrated that only *AB9μ* lines secrete anti-Aβ antibodies in response to both stimuli (Fig. 19d). Accordingly, tg B cells of *AB9μ* mice have been differentiated into antibody-secreting plasma cells.

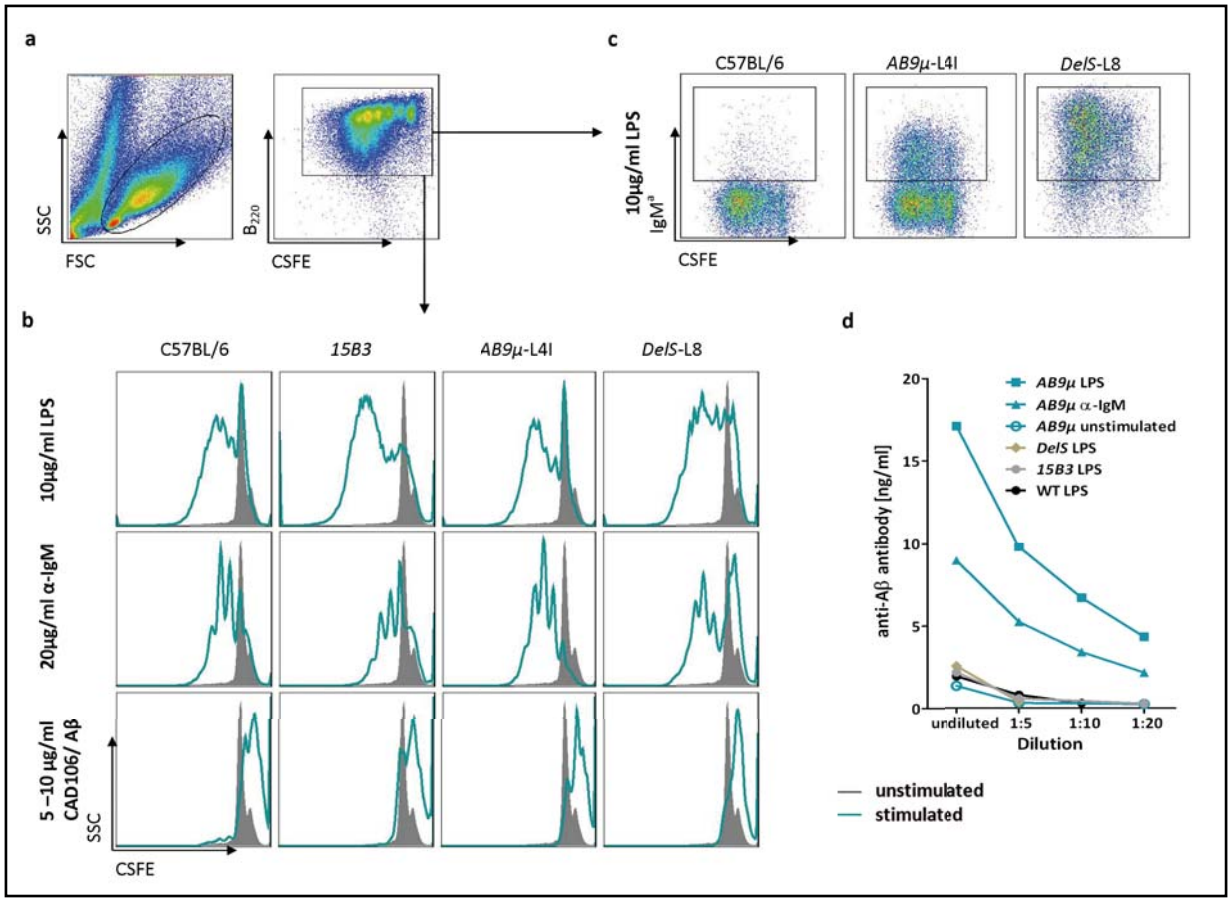

Fig. 19: B cell proliferation assay of *AB9μ*-L4I, *DelS*-L8, *15B3* and WT mice in response to different stimuli: a| Gating strategy for all mice b| Histograms of proliferating B cells in response to 10 µg/ml LPS, 20 µg/ml α-IgM or 5-10 µg/ml CAD106 or Aβ. Tg B cells proliferated in response to LPS and α-IgM comparably to WT mice, but not in response to Aβ or CAD106. c| Among the proliferating B cells some were positive for IgM^a in *Dels*-L8 and *AB9μ*-L4I, however not in WT mice demonstrating proliferation of tg B cells. d| ELISA of cell culture supernatants furthermore showed an anti-Aβ-antibody response to LPS and anti-IgM in *AB9μ*-L4I but not *DelS*-L8, *15B3* or WT mice.

2.7 Analysis of immune response towards infection with the vesicular stomatitis virus (VSV)

We used VSV to answer the question whether tg mice displaying a decrease in B cell frequencies might have a compromised antiviral response. For this, we used *AB9μ*-L7 and *DelS*-L8. In general, VSV is a cytopathic rhabdovirus that resembles rabies in humans and is used to model acutely cytopathic viruses in mice. It is rapidly controlled by a strong, early, initially T-cell-independent, neutralizing IgM response that switches to a T-cell-dependent IgG response after 4–6 days.[190] Altered B cell physiology, development, or histoarchitecture and cellular composition of germinal centers might impair such antiviral responses. Accordingly, B-cell-deficient mice that are infected with VSV die in 5–10 days.[191,192]

AB9µ mice mounted IgM and IgG responses to VSV with similar kinetics as WT mice, however with slightly reduced titers (Fig. 20). *DelS* mice, on the contrary, showed an impaired induction of T cell dependent neutralizing IgG response – the titer kinetics were slower with one mouse showing a neutralizing IgG response starting at day 12 (Fig. 20). This could be due to the fact that the number of endogenous B cells in *DelS*-L8 was extremely and thus antibody response might be delayed. Nevertheless, all the mice survived the VSV infection and showed T cell dependent and T cell independent antibody responses. Therefore, expression of transgenic µ chains did not alter the immune system in a way that would suppress B cell responses although a reduction of B cell counts was seen in peripheral blood, spleen and BM.

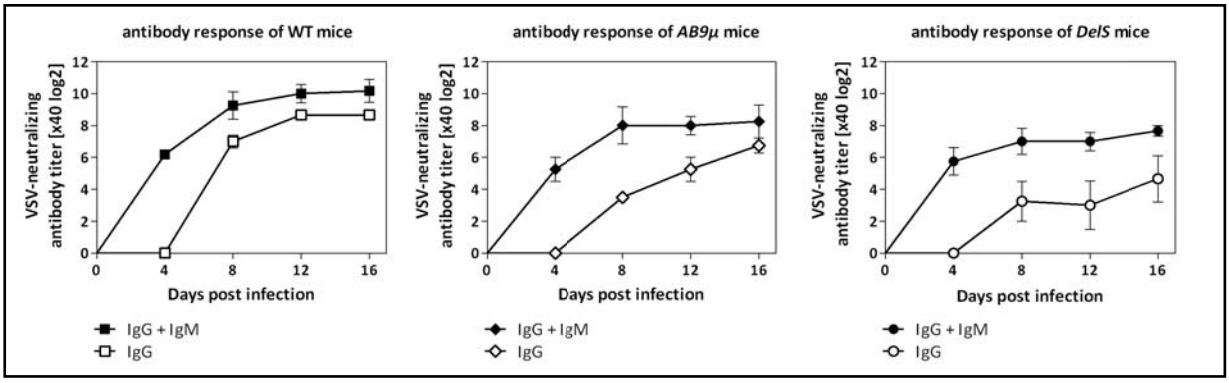

Fig. 20: Neutralizing antibody response to VSV infection in *AB9µ*, *DelS* and WT mice: All mice mounted an anti-VSV antibody response with *DelS* mice showing slowed response kinetics and both *AB9µ* and *DelS* mice having slightly reduced titers. Especially the T cell dependent IgG response occurring after 4-6 days of infection was slowed down in *DelS* mice.

2.8 Antibody purification from cell culture supernatants and serum of *AB9µ* mice

Purification of antibodies is an important tool for therapeutic and diagnostic applications. However, most IgM purification methods lack purity of the preparation or may damage the isolated product. Therefore we used affinity purification utilizing immobilised mannan binding protein (MBP), which has been shown to yield greater than 95% purity.[171] To purify antibodies from mice we pursued two strategies:

In the first approach we immunised *AB9µ* tg mice with Aβ, the antigen of the tg B cells. This approach also activates endogenous B cells making endogenous B cells secrete endogenous Aβ-specific IgM antibodies (Fig. 21a). The purification of endogenous anti-Aβ IgMs was circumvented by a second immunisation step with Aβ – after which B cells should class

switch to IgG antibodies. Due to the absence of the other Ig loci in our transgene, the tg *AB9µ* B cells cannot class switch and thus persist with IgM expression. Accordingly, after the second immunisation only tg AB9µ B cells should produce anti-IgM antibodies, whereas endogenous B cells are expected to switch to IgG. In line with this prediction, we confirmed that 28 days post first immunisation (dpi) – which is 14 days after the second immunisation – there was a sudden increase in Aβ specific IgG antibodies (Fig. 21a, second graph, see arrows) accompanied by a decline in the anti-Aβ IgM response at 34 dpi (Fig. 21a, first graph, see arrows). Operating under the assumption that this decline was based on the circumstance that most of the endogenous anti-Aβ antibodies switched to IgG, we purified sera of seven *AB9µ*-L4I mice at 34 dpi (Fig. 21a, orange line).

In the second purification approach we employed LPS as stimulation agent in proliferation assays. LPS stimulation leads to switching of the expressed isotype directly from IgM to IgG.[193-195] Thus, we expected that endogenous B cells should produce IgG and tg *AB9µ* B cells IgM antibodies. We showed that only Aβ specific IgM (Fig. 21b, left graph) and not IgG (Fig. 21b, right graph) were produced.

After purification we checked by Western Blot whether only IgM, or also IgG was present in the purified samples from cell culture and serum (Fig. 21c, Western Blot). Only the purified samples from cell culture contained pure IgM antibodies (Fig. 21c, third lane of Western Blot) whereas samples from serum showed contamination with IgG (Fig. 21c, last lane of Western Blot). Consequently, only samples from cell culture were used for further analyses. These samples showed production of Aβ-specific IgM antibodies in ELISA (Fig. 21c, middle figure) which had up to 52% chimeric $IgM^{a\&b}$ phenotype (Fig. 21c, right figure) shown by flow cytometry.

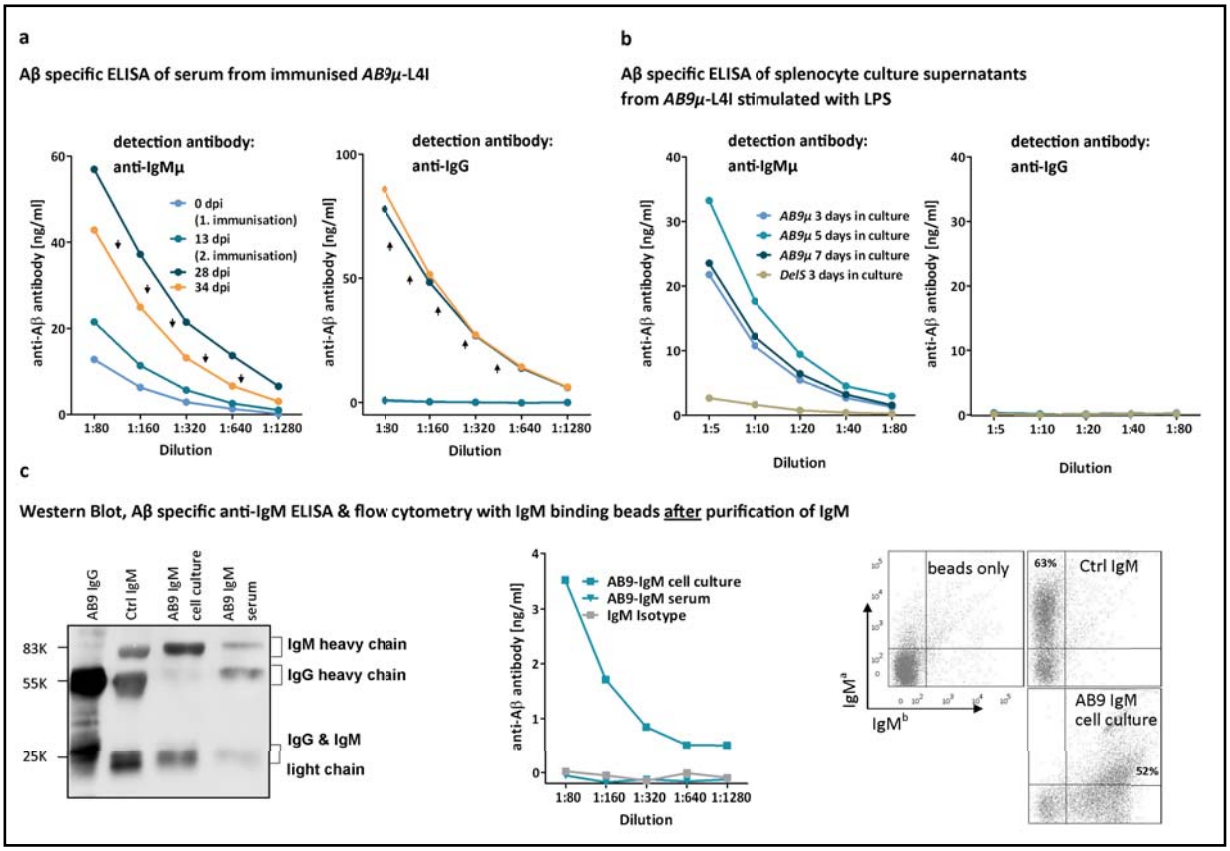

Fig. 21: Purification of anti-Aβ-IgM antibodies from *AB9μ*-L4I: a| To purify antibodies from serum of *AB9μ*-L4I we immunised 7 mice twice(day 0 and 14 days post first immunization) with Aβ to induce class switching of endogenous B cells to IgG. Starting at 28 days we saw an increase in Aβ-specific IgG expression followed by a decrease in anti-Aβ IgM expression. b| Transgenic B cells stimulated with LPS produced Aβ-specific IgM but not IgG. c| After purification we tested the purified antibodies from cell culture and serum on the western blot to detect IgG and IgM. Only the cell culture supernatant showed a pure IgM antibody. In their capacity to bind to Aβ in an ELISA only the purified *AB9μ* from cell culture showed binding to Aβ. *AB9μ* purified from cell culture was further tested by FACS with the help of IgM binding beads and $IgM^{a\&b}$ staining demonstrated a chimeric antibody consisting of $IgM^{a\&b}$.

3. Selection of the best transgenic lines for AD experiments

The second aim of this thesis was to inspect whether the peripheral sink hypothesis of immunotherapy was true. In order to pursue this aim, it was especially important to pick the best tg *AB9µ* and *DelS* lines. In this final section we summarized all results which were needed for the choice (Table 11). The first criteria and parameters for this selection were fulfilled by all generated tg mice – 4 *AB9µ* and 3 *DelS* lines – meaning all lines contained tg B cells and all *AB9µ* mice elicited anti-Aβ-antibody titers. Furthermore it was important to obviate possible adverse effects resulting from the transgene. Such adverse effects could arise from tg copy numbers, tg integration site or the polyclonality of the tg mice. Also concerning this parameter all mice demonstrated if at all only minor changes in B cell development which however were comparable to the *15B3* control mice. Next, we characterized the tg mice in more detail to find out which lines had the most tg B cells in *AB9µ* and *DelS* mice and appropriate anti-Aβ antibody titers in the *AB9µ* mice. Based on this we selected *AB9µ*-L4I and *DelS*-L8 as the predominant lines. *AB9µ*-L4I was chosen despite the relatively low titer, because in all other parameters this line was most similar to WT mice (Table 11). Especially with respect to B cell frequencies, this line most closely resembled WT mice. This is especially important as we cannot exclude that a reduction in B cells might have an effect on AD. *DelS*-L8 was selected because it was in all parameters the optimal line among the non-Aβ-antibody secreting lines. Nevertheless, all other *AB9µ* lines were also crossed to *APPPS1* mice to not miss potential effects of these lines. Furthermore *DelS*-L1 was crossed to *APPPS1* mice as a second non- Aβ-antibody secreting line, specifically to control for effects of partial B cell deficiency.

Transgenic line	Transgenic copy numbers	B cell frequency	Number of tg B cells	Anti-Aβ titer	Blood immune cell profile & histology	B cell development	B cell proliferation	Purification of Anti-Aβ antibodies
WT (C57BL/6)	none	+++	nd	nd	+++	+++	+++	nd
15B3	-	++	++	nd	+++	++	-	nd
***AB9µ*-L2**	++	+	+	+++	+++	+	-	-
***AB9µ*-L4I**	+++	+++	++	+	+++	+++	+++	++
***AB9µ*-L4II**	+++	+	+	+	+++	+	-	-
***AB9µ*-L7**	+	+	+	++	+++	+	+++	-

Transgenic line	Transgenic copy numbers	B cell frequency	Number of tg B cells	Anti-Aβ titer	Blood immune cell profile & histology	B cell development	B cell proliferation	Purification of Anti-Aβ antibodies
***DelS*-L1**	+	+	+	nd	+++	+	-	nd
***DelS*-L2**	+++	++	++	nd	+++	+	-	nd
***DelS*-L8**	+++	++	+++	nd	+++	++	+++	nd

Table 11: Summary of the results in all experiments performed to characterize the tg mice: +++ = not altered or high occurrence; ++ = slightly altered/low occurrence; + = altered a lot/ very low occurrence; nd = not defined; - = not done

4. Effect of peripheral anti-Aβ IgM on AD-like pathology in AD mouse models

Several studies have shown that anti-Aβ antibodies can lower plaque burden in AD mouse models (see introductory section 5. immunotherapy). In line with these studies, Levites and colleagues showed that AB9-IgG is one of the most effective anti-Aβ antibodies in long-term peripheral immunization studies.[164] Nevertheless, how the mechanism of immunotherapy works remains unclear.

We investigated whether unambiguous presence of anti-Aβ antibodies in the periphery lowers cerebral Aβ levels in vivo. To this end, *AB9μ*, *DelS* and *15B3* mice were crossed to two AD mouse models. As mentioned in section 1.9 the predominant lines analyzed were *AB9μ*-L4I and *DelS*-L8. However, all other *AB9μ* mice were also crossed to *APPPS1* mice for the first experiment. For all subsequent paragraphs, the nomenclature mentioned (*AB9μ*/ *DelS*) always refers to *AB9μ*-L4I and *DelS*-L8 unless otherwise explicitly mentioned.

4.1 Effect of peripheral restriction of Aβ antibodies on plaque pathology of *APPPS1* mice at 120d

The first AD model used was the *APPPS1* mice, which develop rapid and robust plaque pathology with cerebral amyloidosis starting at 6 weeks. These mice coexpress the Swedish APP K670N/M671L mutation and the L166P mutation in presenilin. In the first experiment, 120-day-old mice were analyzed. According to Hefendehl and colleagues who performed multiphoton *in vivo* imaging to study Aβ plaque formation in the brains of *APPPS1* mice, the highest rate of new plaque formation occurs at this timepoint.[196] We sought to investigate

whether antibodies in the periphery might delay plaque formation. As plaque growth appears to be constant over time[196] we also recorded plaque size to check whether peripheral anti-Aβ antibodies might interfere with plaque growth.

We used quantitative image analysis to determine amyloid burden. Data were assessed for normality using the Shapiro-Wilk test. Parameters that were not normally distributed (Shapiro-Wilk p-value <0.05) were subjected to Kruskal-Wallis test with a subsequent Mann-Whitney U test for pairwise comparison and an adjusted p-value (p-value divided by the number of comparisons (Bonferroni adjustment), otherwise one-way ANOVA followed by Tukey's post-hoc test was used. Relative to control mice (*15B3-APPPS1* and *APPPS1*), Aβ specific IgM antibodies and B cells in the periphery did not reduce histological total amyloid plaque burden at 120 days (Fig. 22a). Consistent with these findings there was no significant change in the number of plaques between the control mice and the *AB9μ* and *DelS* mice (Fig. 23 a). This was also true for all other *AB9μ* lines (L2, L4II, L7) crossed to *APPPS1* and for *DelS*-L1 (Fig. 23). Congophilic amyloid plaque staining, representing core plaques, showed similar results – no significant reduction in compact core plaques in the *AB9μ* lines or *DelS* lines (Fig. 24).

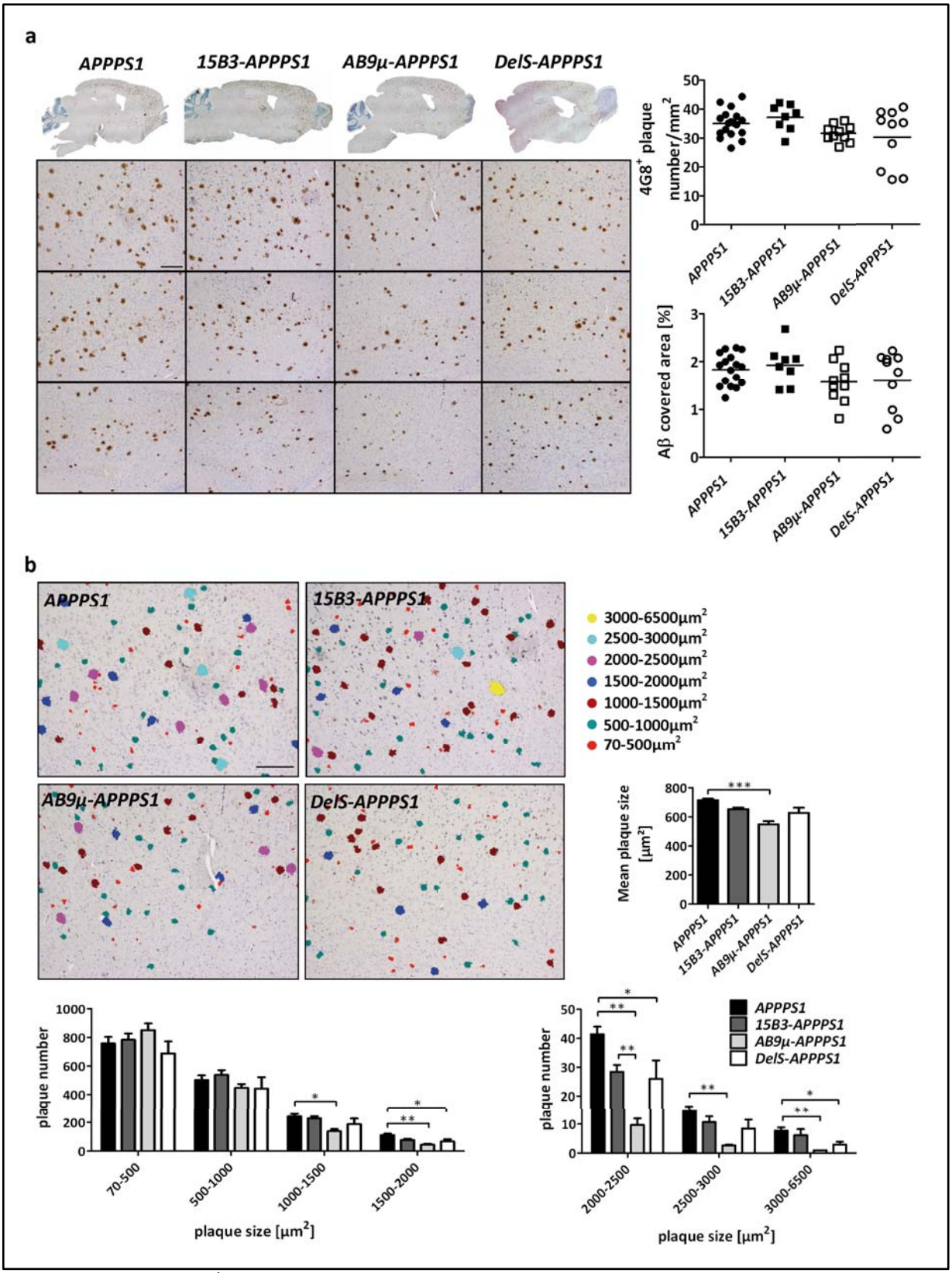

Fig. 22: Histological 4G8$^+$ plaque analysis of 120 day old mice: a| Representative sections of frontal, parietal and occipital cortex for *AB9µ-*, *DelS-APPPS1* and control mice, as well as overview sections are displayed. Some mice showed a trend towards a reduction in the plaque number in *AB9µ*-L4I and *DelS*-L8, albeit no significant reduction in Aβ covered area nor in plaque number was observed. b| Color-coded sections represent the frontal image of each line shown in Fig.22a. Plaque size distribution analysis (mean ± SEM) displayed a reduction in medium-sized and large plaques of *AB9µ* mice and a significant reduction in medium-sized plaques of *DelS* mice. Due to non-Gaussian distribution (Shapiro-Wilk test<0.05) in the values of the large-sized plaque

groups (2000-6500µm²) Kruskal-Wallis test followed by Mann-Whitney U-test (p-value<0.125) was performed. ANOVA and Tukey's post-hoc test were conducted for all other groups. scale bars=200µm

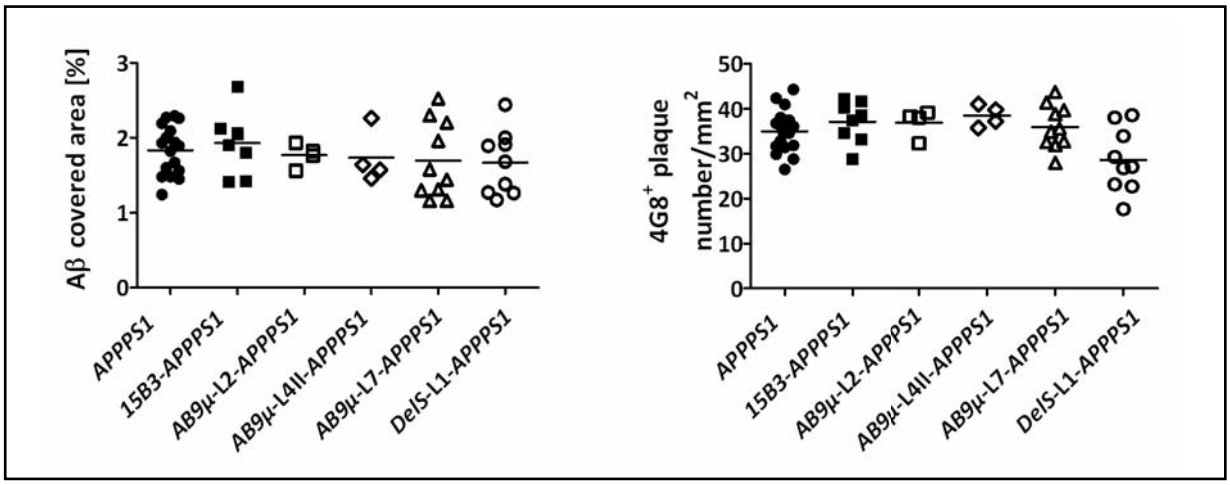

Fig. 23: Histological plaque analysis of 120 day old mice: Shown are *DelS*-L1 and all *AB9µ* lines (L2, L4II, L7) except for *AB9µ*-L4I (see Fig.22) crossed to *APPPS1* in comparison to control mice (*15B3-APPPS1* and *APPPS1* mice). None of the *AB9µ*/*DelS* harboring *APPPS1* mice showed a significant reduction in plaque load and plaque number.

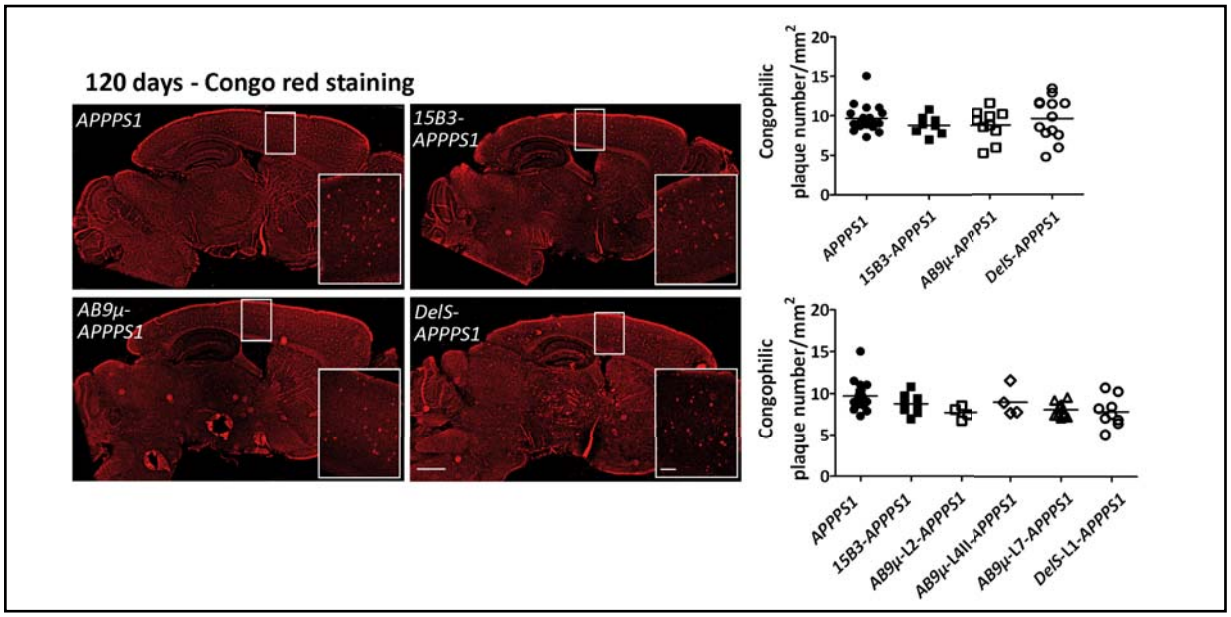

Fig. 24: Histological analysis of Congophilic plaques in 120 day old mice: Representative overview (scale bar overview = 1000 µm) brain tissue section as well as higher magnification images (scale bar = 200µm) are shown. No difference could be observed in the analysis of congophilic core plaques.

However when scrutinizing the results in more detail it appeared that some of the mice in the *AB9µ* group as well as in the *DelS* group had an abated plaque number. Quantification according to plaque size revealed a selective reduction of medium-sized and large 4G8$^+$ Aβ plaques (plaque area, 1000–6500 µm²) in the *AB9µ* mice and to some extent also in *DelS* mice (1500-2500 µm², 3000-6500 µm²) (Shapiro-Wilk test (for 2000-6500 µm²) <0.05,

Kruskal-Wallis test followed by Mann-Whitney U-test (p=0.0125), n=6, p<0.007; one-way ANOVA, Tukey's post-hoc test, n=6, p<0.041). Although the number of large plaques (2000-6500 µm²) in *AB9µ-APPPS1* mice was reduced to 77-87% of *APPPS1* mice (Fig. 22b), this reduction did not translate into significant amelioration of the Aβ covered area or total plaque number. However, large plaques contributed relatively little to the total plaque number (7-40 plaques) at that early time point which explains this discrepancy. In terms of mean plaque size the reduction in medium and large plaques resulted in a reduced mean plaque size in AB9µ-APPPS1 mice (24% reduction)

4.2 Effect of peripheral restriction of Aβ antibodies on biochemical Aβ analysis of *APPPS1* mice at 120d

Next to histological analysis of plaque deposition it also is essential to obtain data on the amount and rate at which various forms of Aβ are deposited. In this study, we obtained these data using an analytic paradigm that combines sequential extraction of brains, enzyme-linked immunoassay (ELISA) to determine Aβ42 and Aβ40 levels and immunoblots to quantify total Aβ levels in the brain. Sequential brain extraction with SDS followed by formic acid (FA) was done because it is well established that much of the Aβ deposited as amyloid in AD brain is resistant to SDS extraction and requires FA for solubilization.[197] In general, Aβ in the SDS fraction represents soluble Aβ and Aβ deposited in diffuse plaques, whereas Aβ extracted in the FA fraction includes Aβ deposited in fibrillar compact plaques.

ELISA measurements and immunoblots further confirmed the Aβ pathological results with no significant differences in total Aβ, Aβ40 and Aβ42 in the soluble SDS fraction and insoluble FA fraction between control mice and *AB9µ* as well as *DelS-APPPS1* mice (Fig. 25). However, similar to the reduction of the plaque number in some mice, we also observed reduced Aβ levels in the immunoblot analysis in some of the *Dels*- and *AB9µ-APPPS1* mice (Fig. 25a). This however did not reach significant difference. Furthermore we could not observe a reduction in APP levels indicating that the transgene expression in *Dels*- and *AB9µ-APPPS1* mice did not affect the expression of the precursor protein of Aβ.

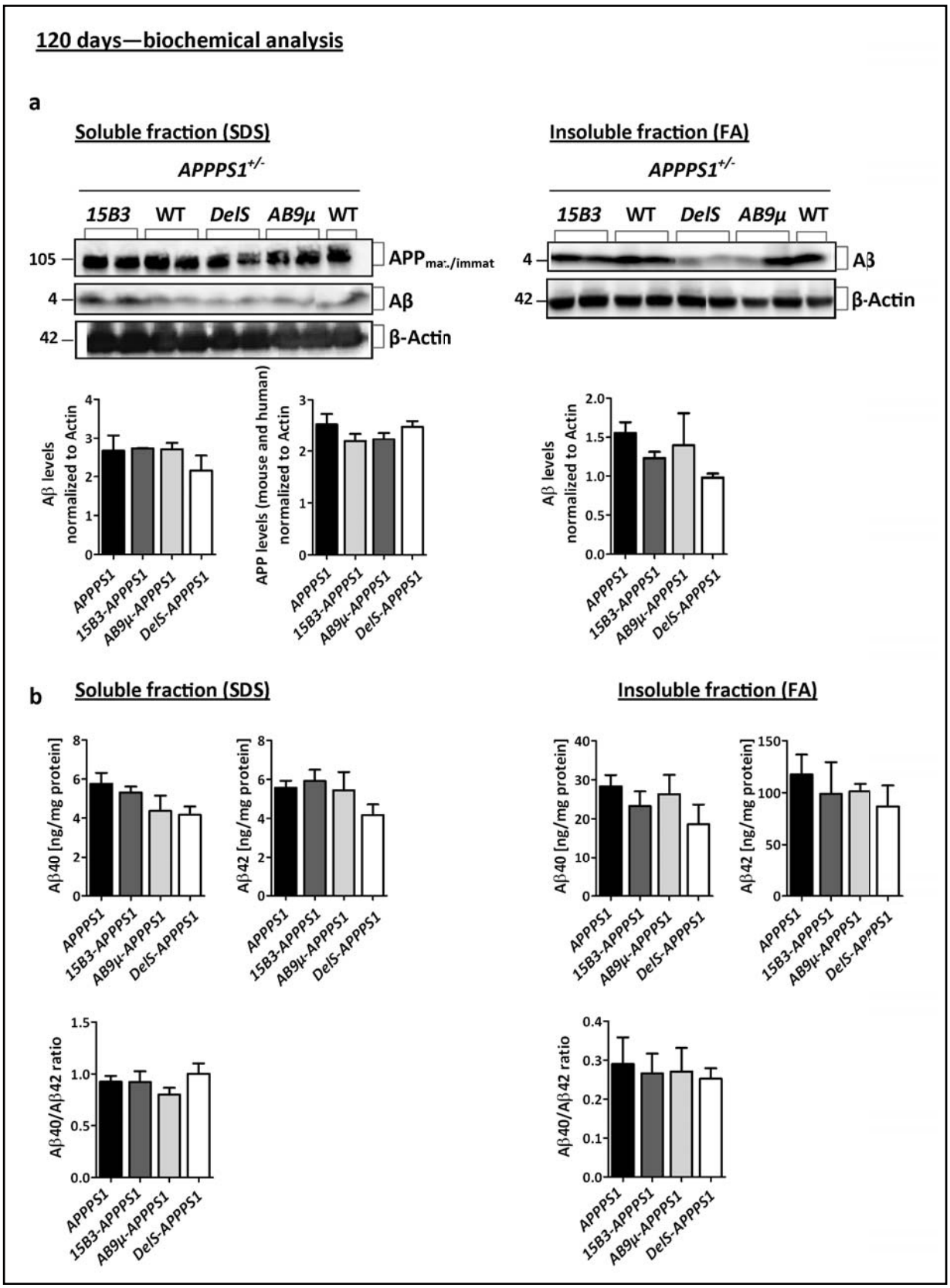

Fig. 25: Biochemical quantification of Aβ in brain homogenates of 120 day old mice: Values represent mean ± SEM a| Representative Western Blot of soluble (SDS) and insoluble fractions (FA). Presence of anti-Aβ *AB9µ* antibodies in the periphery decreased the levels of total Aβ in some of the *AB9µ*- and *DelS-APPPS1* mice compared to controls. This decrease failed to reach significance. b| Aβ specific ELISA analysis by Mesoscale did not show any significant changes in Aβ40 and Aβ42.

4.3 Effect of peripheral restriction of Aβ antibodies on plaque pathology of *APPPS1* mice at 250d

In the second experiment, *AB9μ* and *DelS* mice crossed to *APPPS1* mice were examined at the age of 250 days. As described by Hefendehl and colleagues, there is nearly no new plaques formation at this time point.[196] Hence, plaque growth dominates plaque size which gradually shifts from smaller plaques at four months to larger plaques at eight months. We wanted to evaluate the potential of peripherally restricted anti-Aβ antibodies to impact on amyloid pathology at this late time point in which nearly no new plaques are born and a constant plaque growth is observed.

The experimental read out was the same as in section 4.1. Total Aβ (4G8) plaque load was 28% lower in the cortex of *AB9μ-APPPS1* mice compared to *APPPS1* mice (ANOVA followed by Tukey's post-hoc test, n=8-9, p=0.0003) (Fig. 26a). The 14% reduction in total Aβ plaque load in *DelS-APPPS1* mice was close to significant (ANOVA followed by Tukey's post-hoc test, n=8-10, p=0.058). This effect was also reflected in a significant reduction in plaque number by 15% in *AB9μ-APPPS1* mice and by 10% in *DelS-APPPS1* mice (Shapiro-Wilk test <0.05, Kruskal-Wallis test followed by Mann-Whitney U-test (p=0.016) n=8-10, p<0.009) (Fig. 26a). Quantification according to plaque size demonstrated a reduction of total large Aβ plaques (2500-6500μm², reduction = 35-51%), as well as of small plaques (70-1500μm², reduction <13%) in mice having an *AB9μ* background (one-way ANOVA followed by Tukey's post-hoc test, n=6, p<0.04) (Fig. 26b). As both large and small plaques were reduced mean plaque size did not change at 250 days. *DelS*-APPS1 mice only displayed a significant reduction in small plaques (500-1500μm²), however not in the smallest plaques, although it was close to significant (as also for the large plaques).

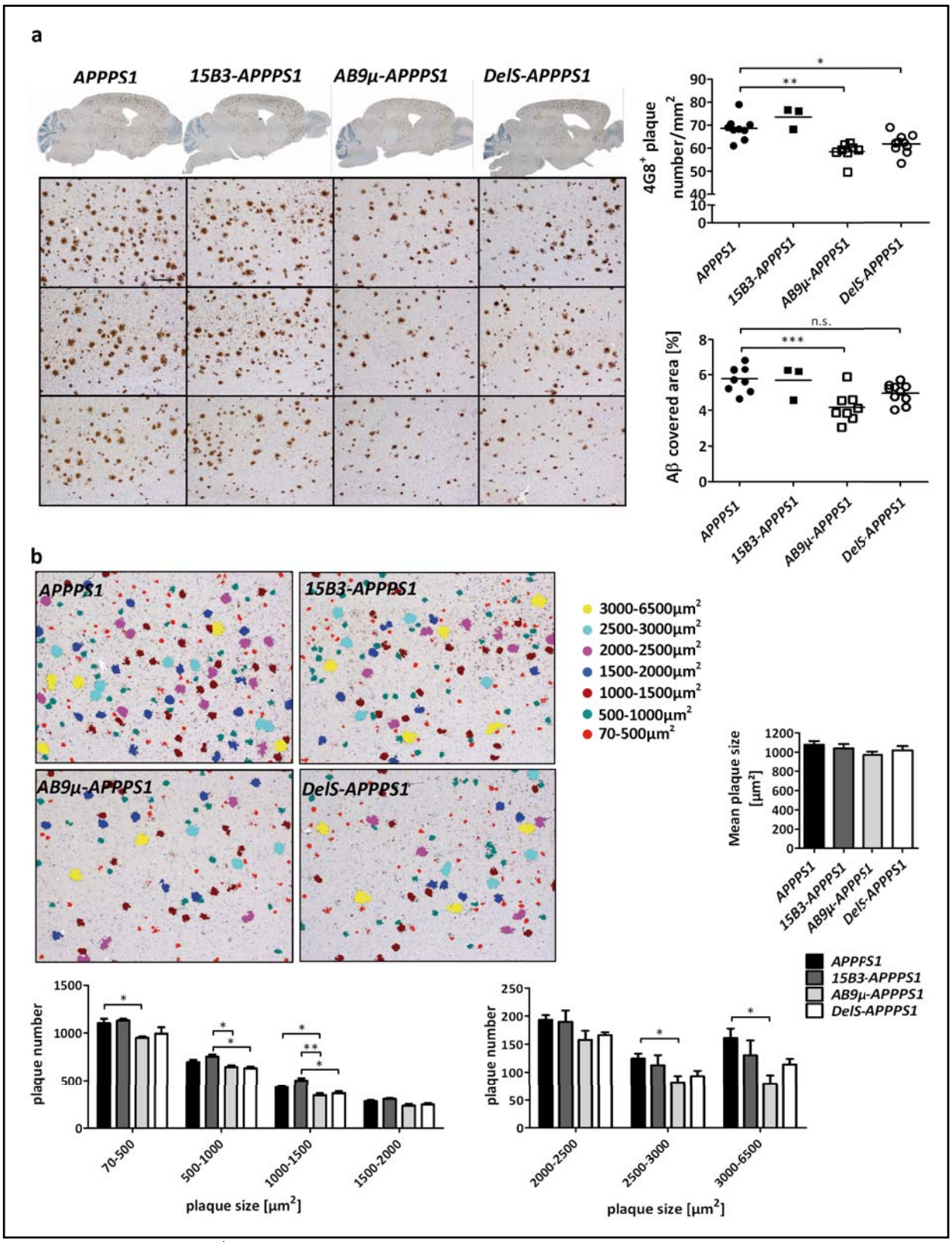

Fig. 26: Histological 4G8^{+} plaque analysis of 250-day old mice: a| Representative 4G8 stained sections of frontal, parietal and occipital cortex for *AB9µ-*, *DelS-APPPS1* and control mice, as well as overview sections are displayed. There was a significant reduction in total Aβ covered area for *AB9µ-APPPS1* mice. *DelS-APPPS1* mice trended to have a reduction in this read-out. Both, *AB9µ-* and Dels-*APPPS1* mice, showed a significant reduction in plaque number. b| Color-coded sections represent the frontal image of each line shown in Fig.26a. Plaque size distribution analysis (mean ± SEM) displayed a significant reduction in small and large plaques of *AB9µ* and in part also in *DelS-APPPS1* mice. scale bar = 200µm

Thus far, the immunohistochemical staining with 4G8 only looked at total Aβ plaques comprised of parenchymal diffuse (preamyloid) plaques and compact-core plaques of fibrillar amyloid nature. To further address the plaque type, paraffin sections were stained with the conventional amyloidotrophic dye Congo red recognizing compact amyloid plaques, and PFTAA, a highly sensitive dye, binding to diffuse and compact amyloid plaques[198] (as a complementary dye to the 4G8 staining). We only found a significant reduction of 29% in the PFTAA staining, which next to core plaques mainly detects diffuse plaques (one-way ANOVA, Tukey's post hoc test, n=4-8, p=0.014), whereas we could not observe a significant reduction in congophilic fibrillar plaques (Fig. 27). Congo red stain was counted with and without the Cy3 filter to precisely dissect the findings (Fig. 27). We did not observe a difference in compact plaque deposition.

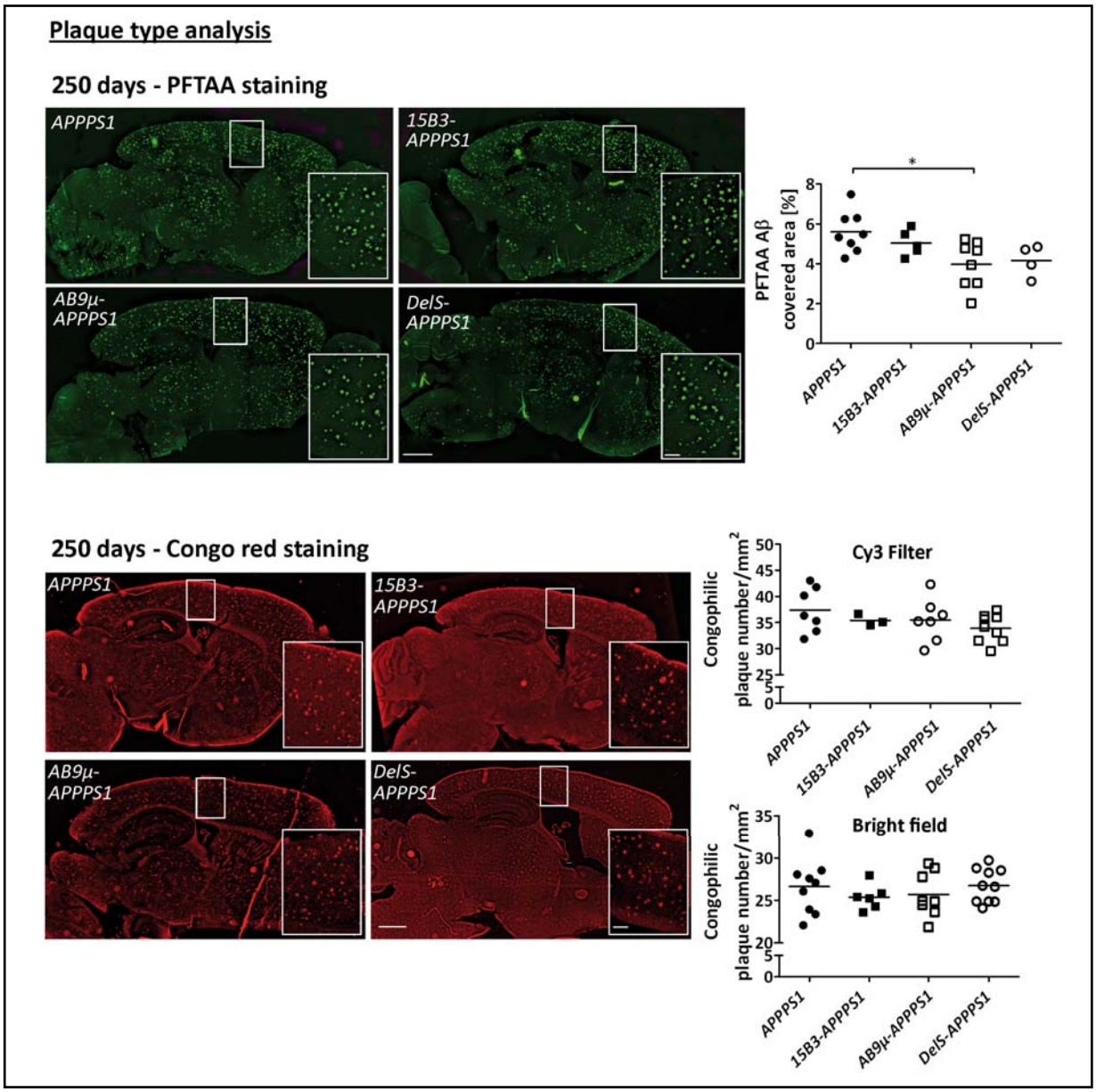

Fig. 27: Analysis of plaque types in 250-day old mice: Upper panel| PFTAA stains diffuse and compact plaques similar to 4G8. A significant reduction was observed also for PFTAA staining in *AB9µ-APPPS1* mice, but not in *DelS-APPPS1* mice. Lower panel| Congo red is a specific amyloid dye only binding to fibrillar compact plaques. Here we could not find any significant difference between the groups. scale bar overview = 1000µm, scalebar high magnification = 200µm

4.4 Effect of peripheral restriction of Aβ antibodies on biochemical Aβ analysis of *APPPS1* mice at 250d

The experimental read out was the same as in section 4.2. Consistent with the Aβ pathology results, *AB9µ-APPPS1* and *DelS-APPPS1* had less Aβ40 (23% in both groups) and Aβ42 (17% in *AB9µ-*, 11% in *DelS-APPPS1*) in the soluble SDS fraction (one-way ANOVA, Tukey's post hoc test, n=5-6, $p<0.036$) although total Aβ levels detected by western blot analysis failed to show differences (Fig. 28a, b). To further pursue the analysis of distinct Aβ pools we also

analyzed the FA fraction of brain homogenates. In keeping with the histochemical data, the FA fraction showed a difference regarding total Aβ and Aβ42, however these differences failed to reach significance (Fig. 28b). Due to the reduction in Aβ42 the Aβ40/Aβ42 ratio was increased in *AB9μ*- and *DelS-APPPS1* mice, yet this alteration was not significant.

APP is mainly cleaved by three proteolytic enzymes: α, β, and γ-secretases. Sequential cleavage by β- and γ-secretases generates Aβ (amyloidogenic processing of APP), while sequential cleavage by α- and β-secretases precludes generation of Aβ (nonamyloidogenic processing of APP).[199] To examine whether mitigated Aβ pathology and decreased Aβ production by peripheral anti-Aβ antibodies were related to changes in APP expression and its amyloidogenic processing, APP proteolytic products present in the brain homogenates were analyzed by immunoblotting using two selective antibodies. We did not find significant differences in APP expression between *AB9μ*- and *DelS-APPPS1* compared to control mice (Fig. 28a). Furthermore, the APP derivates, CTFβ and CTFα, did not differ significantly between the groups (Fig. 28a). These data suggest that transgenic peripheral antibodies have no significant influence on expression and proteolytic processing of APP and secretase activities.

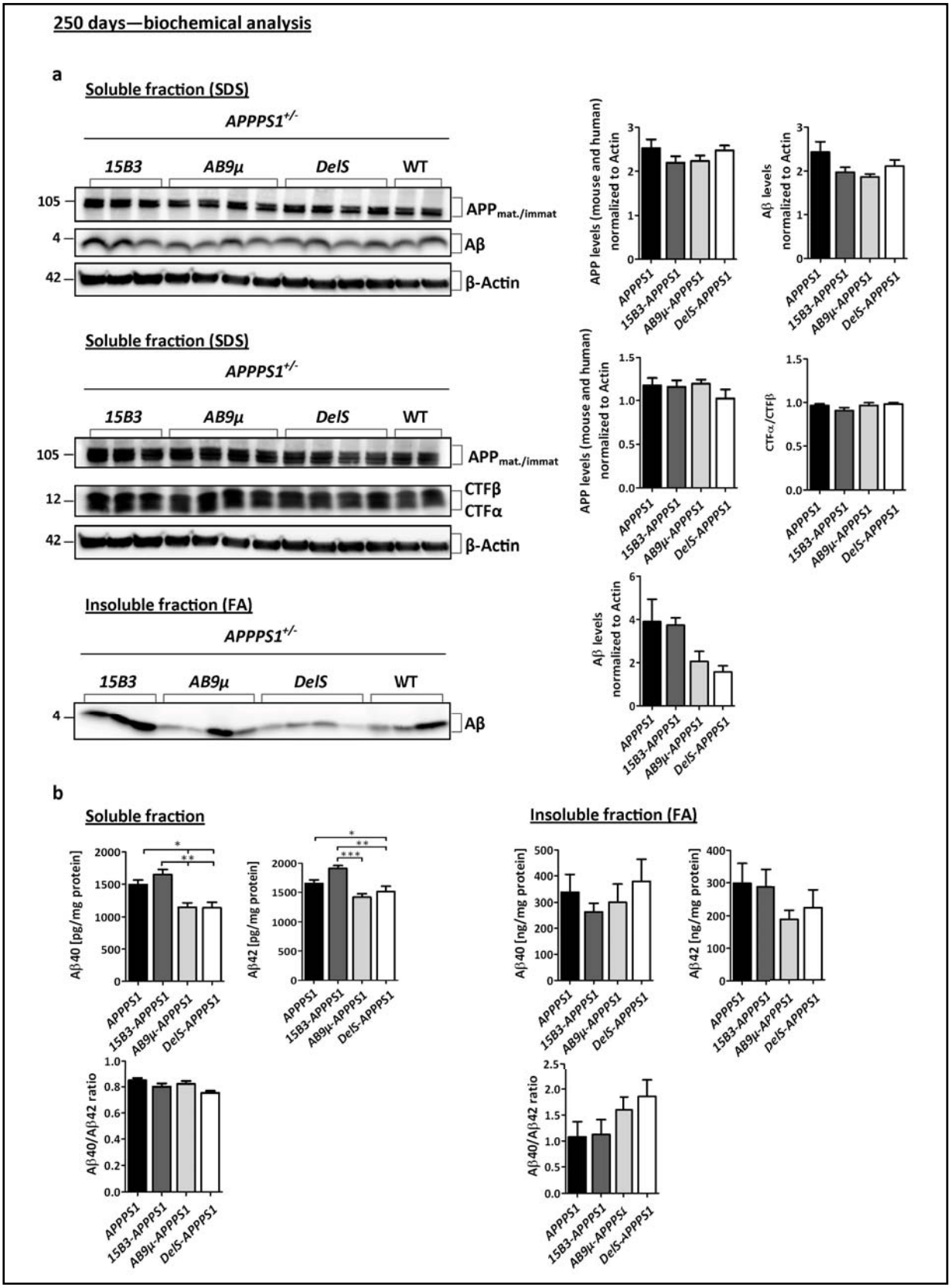

Fig. 28: Biochemical quantification of Aβ and APP proteolytic processing in brain homogenates of 250-day old mice: a| Western blot analyses were performed to detect the APP expression, APP proteolytic derivatives and Aβ in brain homogenates of 250-day old animals using antibodies directed to C-terminal APP and N-terminal APP. APP expression and its proteolytic derivates CTFβ and CTFα were unchanged. Total Aβ levels were only changed in the FA fraction for both *AB9µ*- and *DelS-APPPS1* mice. b| Aβ-specific ELISA to dissect Aβ40 and Aβ42 more closely revealed a prominent reduction in Aβ42 in the FA fraction, however not in Aβ40 which increases Aβ40/Aβ42 ratio to a more beneficial ratio.

4.5 Analysis of serum Aβ levels in *APPPS1* mice at 250 days

The last crucial issue to address concerning the peripheral sink hypothesis was the question of whether Aβ was increased in blood. This is a key aspect of this hypothesis, as it proposes a shift of Aβ equilibrium from brain to circulation – and as immunization with anti-Aβ antibodies has already been shown to induce a rapid and marked increase in plasma Aβ which also correlated with amyloid burden.[108,135] Since we created the first model in which only an Aβ-specific IgM response is elicited which is assumed to only act as a peripheral sink, and since we have seen that this causes a reduction in Aβ burden, we now had to establish that Aβ was indeed drained into the blood. To assess this issue, we performed an Aβ-specific ELISA for Aβ40 and Aβ42 and correlated the results with total Aβ covered area (4G8). Serum Aβ42 levels significantly increased about 73% in *AB9μ-APPPS1* mice compared to *APPPS1* mice (one-way ANOVA with Tukey's post hoc test, n=8-9, p=0.0003) (Fig. 29). There was no significant change in Aβ40 levels in the *AB9μ*- however in the *DelS-APPPS1* mice. This increase accounted for 43% in Dels-*APPPS1* mice compared to *APPPS1* mice (one-way ANOVA with Tukey's post hoc test, n=8-9, p=0.05) (Fig. 29). In addition, we also observed a highly significant correlation between serum Aβ42 levels and total Aβ burden (4G8) when we took into account all groups (Fig. 29). No correlation was found between serum Aβ40 and total Aβ burden (4G8) (Pearson correlation, p=0.0002). Accordingly, Aβ42 increased in the circulation while total Aβ plaque burden decreased in the brain (Fig. 29).

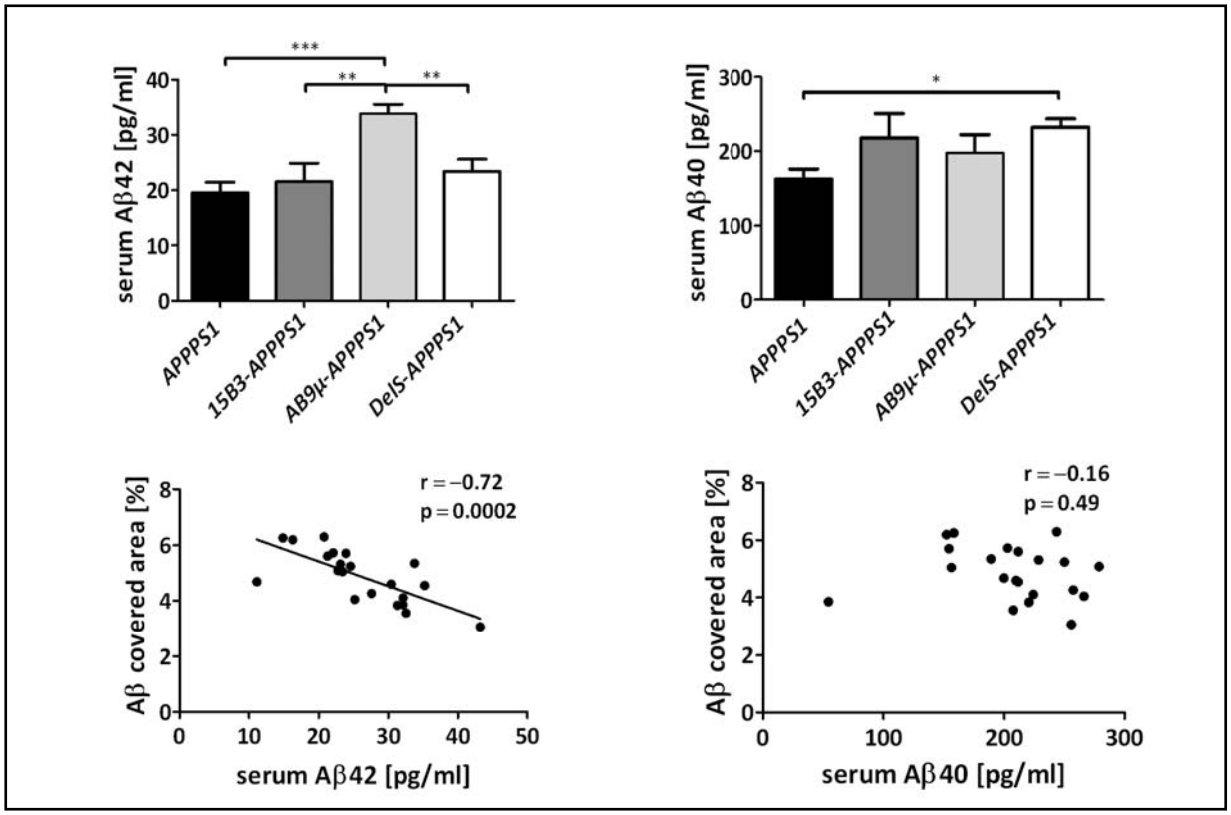

Fig. 29: Serum Aβ levels and their correlation with varying amounts of Aβ deposition: We observed a marked increase in serum Aβ42 levels in *AB9μ* mice crossed to *APPPS1* mice. This increase was accompanied by a decrease in total Aβ plaque load. Total Aβ plaque load of all analyzed groups highly correlated with serum Aβ42 levels detected in these mice. Aβ40 levels were significantly increased in *DelS-APPPS1* mice. However Aβ40 levels did not correlate with Aβ plaque burden. Correlation performed was a linear Pearson correlation.

4.6 Icv injection of AB9-IgM or AB9-IgG antibodies into the brain of *APPPS1* mice

We assumed that IgM antibodies cannot enter the brain as they are too large – indeed they are 6 times larger than IgG and only 0.1% of IgG access the brain after intravenous injection.[200,201] To evaluate the effects of this antibody in the brain purified AB9-IgM antibodies were transiently infused (0.25µl/hour) into the CSF of 60-day old *APPPS1* mice for a time span of two months. AB9-IgG antibodies served as a positive control, whereas control (ctrl) IgM and ctrl IgG were used as negative controls. Infusion of AB9-IgM into the brains of *APPPS1* mice did not reduce total Aβ plaque load at 120 days of age (Fig. 30a). Following the same infusion protocol for AB9-IgG and control IgG, a 22% reduction in Aβ plaque load determined by 4G8 staining was observed (Mann-Whitney U-test, n=5, p=0.0079) (Fig. 30a). In both treatment protocols we did not observe any difference in the congophilic plaque area (Fig. 30b). Interestingly, when measuring anti-Aβ antibody titers in serum we only could detect AB9-IgG but not AB9-IgM indicating that AB9 IgM did not cross the blood-brain barrier into the blood (Fig. 30c).

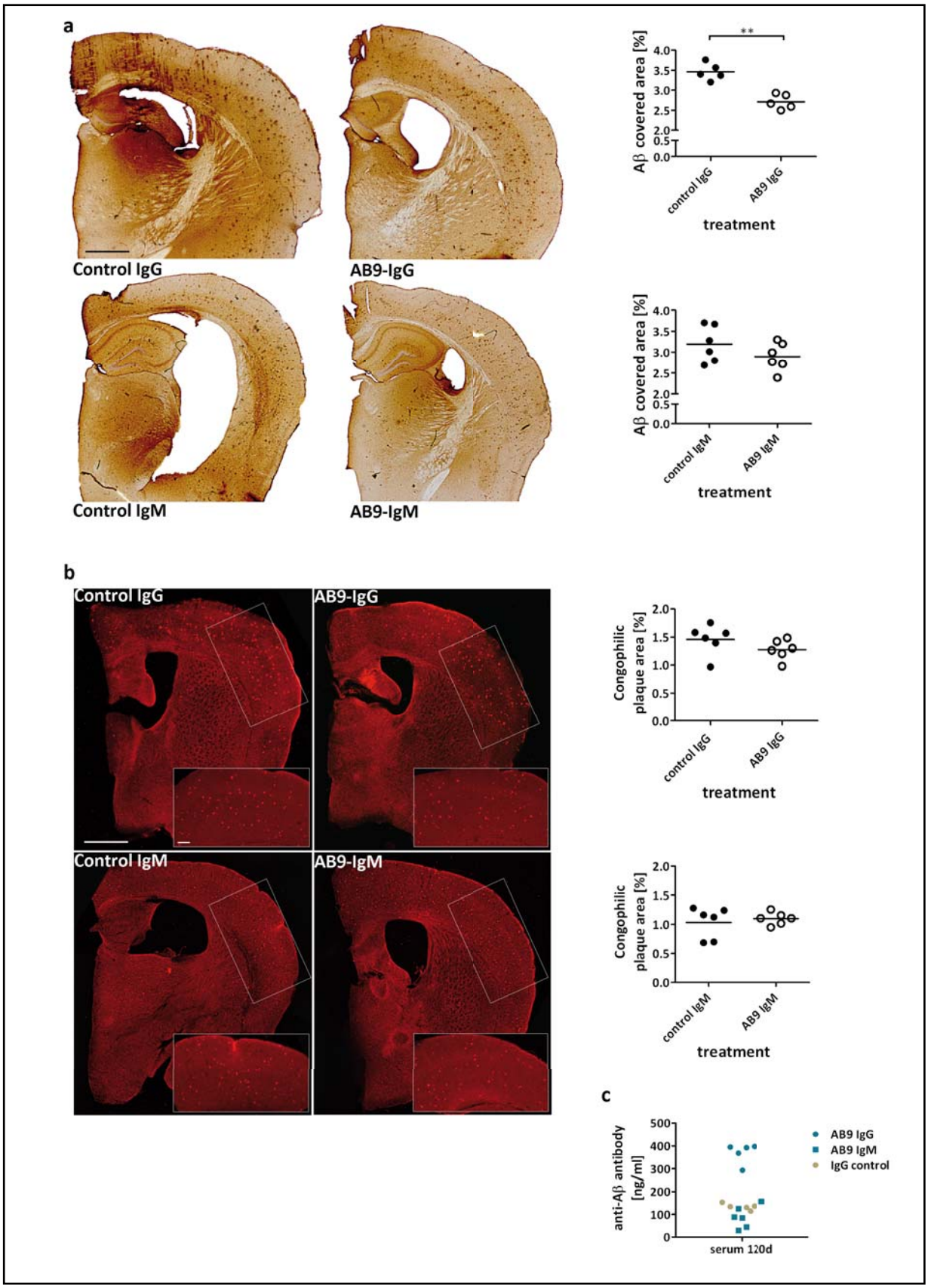

Fig. 30: Stereological plaque analysis from *APPPS1* mice treated icv with AB9-IgG, AB9-IgM or ctrl antibodies: a| Representative sections of 4G8 stained section are shown. Icv administration of AB9-IgG for two months starting at 6 weeks of age reduced plaque load about 22% in 120-day old mice. The same administration protocol for AB9-IgM did not alter the plaque load at 120d. b| Representative Congo red stained sections are displayed. No difference in congophilic plaque number was observed for neither AB9-IgG treatment nor for

AB9-IgM treatment. c| Analysis of Aβ specific antibodies in serum at 120 days revealed that only AB9-IgG leaked out of the brain into the blood. scale bar overview = 1000µm, scalebar high magnification = 200µm

4.7 Effect of peripheral restriction of Aβ antibodies on plaque pathology of *TgSwDI* mice at 180d

TgSwDI mice carry three different mutations within the APP gene – the Swedish K670N/M671L mutation, the Dutch E22Q and the Iowa D23N mutation. The last two mutations reside within residues 21–23 of Aβ which leads to loss of negative charges and a gain of pathogenicity in Aβ. This may directly correlate with the accumulation of Aβ in the brain, particularly around the cerebral vasculature.

To test the efficacy of peripheral Aβ specific antibodies in a second AD mouse model we chose *TgSwDI* mice as they develop perivascular/vascular Aβ deposits in conjunction with numerous largely diffuse, plaque-like structures in the cortex and the hippocampus starting at 3 months of age. We crossed *TgSwDI* mice to *DelS*, *AB9µ* and *15B3* mice and analyzed plaque pathology. We detected an unreported difference between male and female mice, with female mice displaying an elevated plaque load (Fig. 31a). However, we did not observe differences in cortical and hippocampal plaque load and plaque number between the groups (Fig. 31a).

4.8 Effect of peripheral restriction of Aβ antibodies on biochemical Aβ analysis of *TgSwDI* mice at 180d

As *APPPS1* mice demonstrated a reduction mainly in soluble Aβ42 and to some extent also in insoluble Aβ42 after peripheral restriction of Aβ antibodies, it was essential to also examine *TgSwDI* mice for Aβ40 and Aβ42 in SDS and FA brain fractions. This was exceedingly interesting as the predominant Aβ species in these mice is the shorter Aβ40 peptide and not the Aβ42 peptide. In keeping with the histological data we did not find a significant reduction in Aβ40 and Aβ42 in the soluble SDS and insoluble FA fraction of *AB9µ-*/*DelS-TgSwDI* brain homogenates. However Aβ42 levels tended to be diminished again in the SDS fraction of *AB9µ-TgSwDI* brains (Fig. 31b). Although *15B3-APPPS1* seemed to display higher concentrations of Aβ40 and Aβ42 in the FA fraction, this elevation failed to reach significance (Fig. 31b).

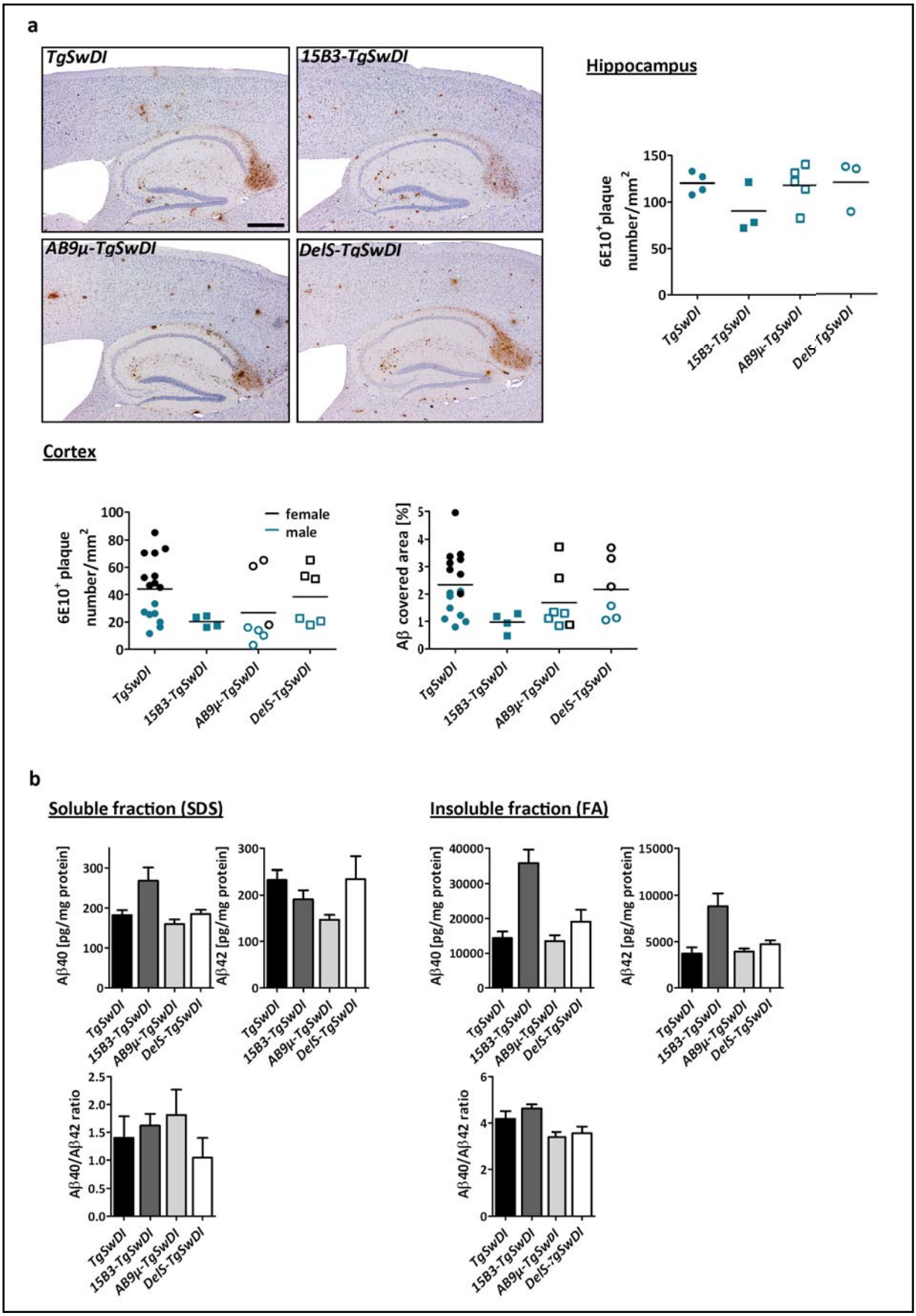

Fig. 31: Histological 6E10^{+} plaque analysis and biochemical anaylsis of 180-day old *TgSwDI* crossed mice: a| Representative 6E10 stained sections for *AB9µ-*, *DelS-TgSwDI* and control mice. There was no reduction in total Aβ covered area for *AB9µ-* and *DelS-TgSwDI* mice. b| Biochemical analysis also revealed no differences in Aβ40 and Aβ42, although Aβ42 trended to be reduced. scale bar = 500µm

DISCUSSION

Immunotherapy targeting Aβ is a promising approach to combat AD as a disease-modifying strategy. Drawbacks in AD vaccination stressed the importance of understanding Aβ clearance mechanisms to refine therapeutic antibodies and efficiently combine these with further therapeutics. There have been several possible mechanisms postulated to explain how antibody-directed abatement of Aβ could work (Fig. 3) – initiation of microglial phagocytosis, catalytic dissolution of Aβ and enhancing net clearance of Aβ across the BBB by shifting the dynamic Aβ equilibrium between blood versus the CNS. The latter was called peripheral sink hypothesis and was object of the present study. This study was undertaken with the goal to gain further insight and better understanding of the mechanistic mode of action of immunotherapy in AD.

1. Characterization of the *AB9μ* and *DelS* tg lines

Co-workers of the Department of Neuropathology created tg mice that elicit an Aβ specific antibody response. This response is either restrained to the B cell membrane, which means antibodies cannot be secreted (*DelS*), or is allowed to be released as IgM antibodies (*AB9μ*). Since IgM antibodies are expected not to cross the BBB, both approaches act only in the periphery, and were so designed to test the peripheral sink hypothesis of Aβ immunotherapy. We generated 3 founders of the *AB9μ* construct and 3 founders of the *DelS* construct. Before testing the peripheral sink hypothesis in *AB9μ/DelS* mice, it was necessary to characterize them in order to exclude potential unwanted adverse effects on AD. There were several possible confounders that sought to be experimentally addressed or excluded. The random nature of transgene integration poses several potential problems: (a) the transgene may be expressed poorly or inappropriately; (b) an essential gene may be disrupted, or another gene activated. Furthermore, the generated antibody response in the mice was polyclonal, comprising antibodies against several Aβ epitopes, thus increasing the diversity and specificity to Aβ, leading to an increased likelihood of rapid elimination of the desired antigens. However polyclonal response can be accompanied by the problem of limited reaction to self-antigens due to cross-reactivity. To address this we looked at the histopathology of different organs, the immune cell profile in the blood and anti-Aβ antibody

titers. Finally, the B cell pool in most of the tg lines was diminished – an outcome which could adversely affect the immune system and its functionality. To determine the origin of this we examined B cell development and B cell subtypes in spleen and bone marrow. Basic B cell and immune system function were further addressed by *in vitro* B cell proliferation and an *in vivo* VSV (vesicular stomatitis virus) infection study.

Due to polyclonality and random transgene integration, the different *AB9μ* lines had diverse anti-Aβ antibody titers, but importantly none of the lines exhibited an IgG specific antibody response, demonstrating that indeed only Aβ specific IgM antibodies were produced that could not class switch to IgG. In contrast, *DelS* mice did not exhibit an anti-Aβ antibody response in the serum confirming the lack of the tg polyA site which is required for antibody release. Furthermore all histopathologically examined organs showed no gross alterations without, and the peripheral immune cell profile was unaltered.

To distinguish the tg from endogenous B cells we took advantage of the expressed IgM allotype. Whereas tg B cells carried an IgM^a allotype, endogenous B cells carried an IgM^b allotype. Both, *AB9μ* and *DelS* lines expressed IgM^a on the surface of some of their B cells indicating a potent transgene expression. However considerable variability exists between the tg lines (*DelS* and *AB9μ*) in the number and proportion of transgene-encoded IgM. In some tg lines, the majority of B lymphocytes expressed a transgene-encoded antigen-receptor specificity. In these lines, namely *AB9μ*-L2, L4II, L7 and all *DelS* lines, the numbers of B cells in the spleen and the blood were considerably lower than in non-tg littermates (4-16%, compared to 47% in WT littermates). By contrast, *AB9μ*-L4I exhibited normal numbers of splenic or blood B cells, and most of the B cells present expressed endogenous Ig chains with or without transgene-encoded chains. As a consequence, *AB9μ*-L4I line carried dual-expressing (chimeric) B cells, having both endogenous and transgene-encoded heavy chains at the cell surface. In addition, they secreted mixed IgM molecules containing both transgenic and endogenous μ heavy chains. In all tg lines except for *AB9μ*-L4I a striking functional consequence of the expression of functional IgM-transgenes was the partial inhibition of endogenous Ig-gene rearrangement and expression, a common phenomenon also in other Ig-tg mice.[202-205] This feedback inhibition, called allelic exclusion of Ig-genes in B cells, is brought about by a regulated mechanism, triggered by expression and assembly of

membrane-bound IgM.[202,204,206-209] This is in contrast to *AB9μ*-L4I in which this phenomenon of allelic exclusion was absent, and even led to the creation of double-expressing chimeric B cells. The mechanisms underlying these observations are unclear. Some authors speculate that allelic exclusion is mediated by a more complex mechanism than the presence or absence of membrane μ heavy chains.[210] Others found evidence that the extent of allelic exclusion is related to the level of expression of the transgene, since in homozygous mice fewer B cells express the endogenous heavy chain.[211] In contrast, another study noted a relationship between transgene copy number and reduced numbers of transgene-expressing B cells due to adverse effect of high copy number or heavy-chain toxicity.[212] Accordingly the observed variability may have a number of causes including variable regulation of transgene expression, transgene expression after endogenous heavy chain recombination or transgene copy number. In *DelS* and *AB9μ* mice it is unlikely that high tg copy numbers decreased tg expression as *AB9μ*-L4I had the highest number of transgenic B cells. It is rather likely that the tg μ-heavy chain is expressed after endogenous recombination.

Due to these observed differences in peripheral B cell numbers it was necessary to carry out analyses of B-cell development. Within the B cell lineage, a marked reduction in the number of immature B cells in the BM was noted in those tg mice with functionally rearranged μ-heavy chain genes, which also displayed reduced numbers of peripheral B cells (all lines except for *AB9μ*-L4I). In other reported immune globulin (Ig) tg mice, such a reduction was mainly restricted to the pre-B cell population.[183,184,211,213-215] Pre B cells arise out of pro B cells after successful rearrangement of the heavy chain VDJ region. This rearrangement leads to the assembly of intact μ heavy chains forming a pre B cell receptor (pBCR) together with the surrogate light chain λ5.[216] The pBCR is an important checkpoint in B cell development. Developmental blocks at the pre-B cell stage are generally due to an inability of μ-chains to form a signal-competent pre-BCR which can be induced by mutant heavy chains or lack of λ5[216,217], and lead to a reduction in the pre B cell pool but not necessarily in the peripheral immature/mature B cell pool. In the next step, pre B cells carry out light chain rearrangements to form an intact surface IgM and are further classified as immature B cells. This step, although not highly regulated, seemed to be disrupted in our mice as we saw a decline in immature B cells. At this tolerance checkpoint, B cells are tested for autoreactivity and most autoreactive B cells are removed (clonal deletion) from the nascent repertoire

before the surface IgM-positive immature B cell stage is induced. This elimination is mediated through strong BCR binding to self-antigens. There are two mechanisms by which this could have led to a reduction in the B cell pool: (a) strong binding to murine Aβ; or (b) polyclonal tg B cells were reactive to other self-antigens. Furthermore tg pre-B cells show an accelerated differentiation to non-dividing stages of B cell maturation due to more rapid and synchronous expression of tg μ chains.[212] Crossing *DelS* and *AB9μ* to *APP-KO* mice – in which no murine Aβ is present – would clarify whether murine Aβ caused the elimination of tg B cells.

Taken together, B cell development in μ-tg mice (*DelS* and *AB9μ*) seems to be obstructed at the pre- to immature B cell level in the BM. This would mean that the generation of newly arising B cells is clearly compromised or even blocked. Nevertheless, the peripheral B cell pool stayed constant over time, and the mature B cell pool in the BM was similar to WT and *AB9μ*-L4I. As a consequence it is possible that during the life of the animal long-lived B cells are accumulating, which could be explained by prolonged average life spans for the tg B cells as compared to those of WT mice. This is indeed suggested by BrdU chase experiments, in which the decay of cells having incorporated BrdU was determined.[218] Furthermore it is well established that the average half-life of B cells is dramatically prolonged when B cell generation in the BM is blocked.[219] These observations resemble findings in aged mice in which (a) production of B cells in BM declines with age[220-223] and (b) peripheral B cells have a much longer life span than their counterparts in young mice[224], explaining how total B cell numbers can be maintained despite decreased generation of new B cells. In aged mice it seems plausible that the peripheral B cell pool gets dominated by B cells that have encountered antigen stimulation, resulting in their long-term survival. Based on that, it is likely that the already defined antigen specificity of tg *AB9μ* and *DelS* mice renders the B cells long-lived

Transgenic expression of IgM antibodies against Aβ did not fully abrogate endogenous B cell generation as all tg mice (*DelS* and *AB9μ*) exhibited a small proportion of non-tg B cells. In line with this, *AB9μ* and *DelS* mice responded to the T cell -independent as well as T cell-dependent infection with vesicular stomatitis viridae (VSV). As already stated, B cell-deficient mice are expected to die with 5-10 days after infection.[191,192] None of *AB9μ* and *DelS* mice

died, although antibody responses were delayed. This clearly indicates that these mice can cope with infections and that the changes in the B cell pool did not abate the general function of the immune system.

We also tested B cell functionality *in vitro* in a B cell proliferation assay. Here, too, we did not find a reduction in B cell proliferation in response to non-specific stimuli such as LPS and anti-IgM. However, B cells lacked response to their antigen Aβ presented in different ways. This lack of response could be explained in two ways: First, recombinant proteins or peptides often differ structurally and have different post-translational modifications than their natural counterparts[225-227], which might lead to an altered conformation that shows lower binding affinity to the tg B cells, so that they cannot be activated. Second, although CAD106 was designed to optimize antigen presentation to B cells due to the repetitive structure of the VLP and the organized arrangement of the Aβ1-6 peptides, it might not be sufficient to activate the polyclonal tg B cell pool. Normally, AB9-IgG is directed against Aβ1-16; *AB9μ* is polyclonal and might be directed against more epitopes with different affinities. Hence, the presented epitope might be too narrow to activate the B cells, or only a small proportion of the B cells recognize this epitope.

Summarizing the characterization of the two tg models (*AB9μ* and *DelS*) developed, we were able to generate mice harboring B cells which recognize Aβ. These mice produce either pentameric anti-Aβ IgM antibodies as well as B cell-bound anti-Aβ antibodies (*AB9μ* mice) or only B cell-bound antibodies (*DelS* mice). Neither B cells nor IgM antibodies are expected to enter the brain during the course of Alzheimer's disease.[2] Thus we restricted anti-Aβ antibodies to the periphery. *AB9μ* and *DelS* mice were lacking severe alterations in the immune system, which is insofar crucial as a growing number of publications report that changes of the systemic immune system influence AD pathology[3-5], which could blur putative specific changes of the transgenes introduced by us (*AB9μ* and *DelS*) in *APPPS1* mice. Furthermore all minor changes in the immune system observed were also present in the control mice, namely *15B3* mice in which the same IgM transgene with a CDR (Complementarity Determining Region) of unknown specificity is expressed. This was essential for the selection process of the *DelS* and *AB9μ* lines which were finally chosen to examine whether the peripheral sink hypothesis of immunotherapy in AD is true. In general,

all lines were appropriate concerning these two parameters (Aβ specificity and alterations in the immune system). However we decided to focus on *AB9μ*-L4I and *DelS*-L8 for all AD-related investigations for two reasons. First, these lines had the most tg Aβ binding B cells of all lines tested. Second, these mice had the least reduction in the peripheral B cell pool. This reduction was the only change in the tg mice of which had the potential to confound the analysis of the plaque load in AD mice. To control for the possible effects of this reduction, we also included *DelS*-L1 in the first analysis. This *DelS* line had the lowest frequency of total peripheral B cells (4.9% ± 0.4). Accordingly this line served as reference modeling the reduction of B cells (which is close to B cell deficiency).

2. Effect of peripheral anti-Aβ antibodies on *APPPS1* mice

The formation and deposition of amyloid plaques composed of aggregated Aβ peptides is an hallmark feature of AD. Biomarker-based temporal staging of AD suggests that biomarkers of Aβ deposition become abnormal before neurodegeneration and clinical symptoms occur. Accordingly, immunotherapeutic strategies addressing Aβ seem to be powerful tools to combat AD. It is established that anti-Aβ immunotherapies efficiently clear brain Aβ plaques in amyloid-bearing mice and delay plaque formation when administered in presymptomatic animals.[101] Yet, the mechanism by which this therapy acts is unclear. Our main object was to *in vivo* proof or falsify one of the many proposed mechanisms how Aβ immunotheraspy works – the peripheral sink hypothesis. This hypothesis claims that Aβ-antibodies create a peripheral Aβ sink in the blood causing an elevated efflux of Aβ from the brain to the blood, or by hindering Aβ transport to the brain. We addressed this topic by crossing *AB9μ* and *DelS* mice to *APPPS1* mice and analyzed them at two different time points. First, 120 day old APPPS1 mice were analyzed as Hefendehl and colleagues demonstrated that the highest rate of new plaque formation occurs at this timepoint.[196] At 120 days of age peripheral Aβ antibodies showed neither a significant reduction in plaque size nor in plaque covered area. However, at this early stage of the disease we did observe a significant abatement of large- and medium sized plaques, whereas small *de novo* generated plaques were not diminished, and even tended to be increased in *AB9μ-APPPS1* mice. This reduction entailed an attenuated mean plaque size. Other immunization studies with second-generation vaccines mainly reported a reduction in small and medium-sized plaques.[142,228] In one of these studies the authors speculated that the observed effects were likely related to peripheral clearance

of Aβ.[142] Accordingly these studies - in contrast to the present data at 120 days - indicate that immunotherapy has a larger effect on small *de novo* generated plaques and does not remove or diminish older large plaques. However, the AD mouse models used in these studies (*APP23*, *Tg2576*) exhibit much slower rates of plaque production than *APPPS1* mice with the first plaques appearing at 6 month of age.[229,230] Furthermore, the Aβ antibody titer in our mice was lower compared to the titers in these mentioned studies (35 µg/ml). The present results indicate that peripheral anti-Aβ antibodies possibly cannot prevent plaque formation, but may attenuate plaque growth at this stage of the disease, in which the built-up of Aβ burden in *APPPS1* mice is known to be stronger than at later time points.

It is furthermore noteworthy to mention that we did not observe a significant plaque reduction in *DelS*-L1-*APPPS1* mice, the reference control mice modeling a partial B cell deficiency. This was exceedingly important as unpublished data from our group (Wilke G., Prokop S., Heppner FL.) with *APPPS1* mice crossed to *JHT* mice which lack mature B cells showed a significant reduction in plaque burden at 120 days. Accordingly we can conclude that the peripheral reduction in the B cell pool did not obscure the effect of peripheral IgM antibodies.

Between 5 and 7 month of age new plaque development declines until subsequently no novel plaques are generated.[196] Thereafter existing plaques only grow constantly over time.[196] We therefore analyzed *APPPS1* mice crossed to *AB9µ* and *DelS* mice at 250 days - a time point at which existing plaques are supposed to only grow in size. Notably here, we observed a significant reduction in plaque number in both *AB9µ*- (15%) and *DelS-APPPS1* (10%) mice (Fig. 26a). Furthermore, *AB9µ-APPPS1* mice illustrated a significant mitigation (28%) in plaque covered area (Fig. 26a). Analysis of plaque size distribution further demonstrated a reduction in large as well as small plaques in *AB9µ-APPPS1* mice (Fig. 26b). As mentioned above, reduction in small plaques after vaccination has been observed before, most notably also in a study in which Aβ clearance was proposed to be due to peripheral IgM antibodies.[142] Especially when comparing the increase in the number of small plaques from 120 days to 250 days the difference between *AB9µ-APPPS1* and *APPPS1* mice became even clearer. Whereas in *APPPS1* the small plaque number increased about 45% during that time span, in *AB9µ-APPPS1* this increase was reduced to 14%. It is conceivable that small plaques

were newly formed deposits[196] and that peripheral anti-Aβ immunotherapy has an effect on *de novo* generation of plaques at late time points of the disease. This can be interpreted in two different ways: First, it might be that peripheral antibodies slow down or prevent plaque formation at the stage of kinetically moderate *de novo* plaque generation. Second, the antibody might have cleared some small pre-existing plaques during the time in which *de novo* generation of plaques is not occurring.

The above mentioned reduction in Aβ deposition was limited to diffuse plaques as shown by 4G8 and PFTAA staining (Fig. 26 and Fig. 27). We also tested the ability of peripheral antibodies to specifically reduce compact amyloid deposits in *APPPS1* mice. As noted previously Congo red staining labels compact fibrillar amyloid plaques, but not diffuse Aβ. Peripheral anti Aβ antibodies did not affect compact plaques. This observation is consistent with previous findings, in which diffuse amyloid was affected to a larger extent than compact amyloid after immunotherapy.[163,228,231]

Biochemical measurements of Aβ concentrations in the brain confirmed that the reduction in amyloid burden resulted from an attenuation of soluble (SDS-dissociable) Aβ levels in diffuse deposits as peripheral anti-Aβ antibodies significantly reduced Aβ42 (23%) and Aβ40 (17%) in the soluble SDS brain fractions compared with control groups (Fig. 28). No significant reductions were observed for insoluble (FA-requiring) Aβ40 and Aβ42, although Aβ42 levels trended towards a decrease in the insoluble FA brain fraction, which, in turn, increased the Aβ40/Aβ42 ratio. Surprisingly, peripherally restricted immunotherapy reduced Aβ42 more strongly than Aβ40 even though the respective antibody does not discriminate between either isoform. Consistent with these findings are the above mentioned results on a reduction in diffuse amyloid deposits mainly consisting of Aβ42. Furthermore, this might be of benefit for Aβ associated with cerebral microvessels (CAA) as it is dominated by insoluble (FA-requiring) Aβ40. Of note, vascular amyloid promotes CAA-associated vascular lesions which have been reported to induce hemorrhages in the course of Aβ immunotherapy.[124,125,128,232,233] Hemorrhages were associated both with elevation[124,125,128] or reduction of vascular amyloid[233]. Interestingly, it has been proposed that peripheral anti Aβ antibodies might aggravate CAA due to a redistribution of solubilized parenchymal Aβ.[127,234] However, administration of antibodies in humans and mice that are thought to work as

peripheral sinks (e.g. m266, solaneuzumab) had no effect on the vascular pathology.[125,235] Also our findings, in which predominantly Aβ42 was reduced and no effect Aβ40 was observed, suggest that peripheral clearance did not impact vascular Aβ. To prove or disprove this point, CAA and subsequent cerebral microhaemorrhages would have to be quantified in *AB9μ-* and *DelS-APPPS1* mice. However, consistent with the observation that high levels of Aβ40 determines the amount of vascular amyloid, vascular amyloid is almost undetectable in *APPPS1* mice, which predominantly have an Aβ42 driven amyloidosis.[93] Consequently, analysis of vascular amyloid in these mice was not undertaken. An alternative mechanism for the observed elevation in CAA after immunotherapy is the binding of anti-Aβ antibodies to brain amyloid at the brain vasculature forming a seed enhancing CAA, triggering inflammation in these vessels and subsequently inducing microhaemorrhages and vasogenic edema.[124,125,236] In this case anti-Aβ antibodies acting only in the periphery would be advantageous as they do not cross the BBB to bin intracerebral Aβ.

In order to exclude that the observed changes in amyloid burden are caused by unspecific genetic interaction of the transgene and/or by interfering with APP processing, we also examined the APP processing apparatus. Peripheral Aβ-specific antibodies did not alter the steady-state level of APP or its metabolites CTFα and CTFβ.

The above results focus only on the central reduction of diffuse amyloid-β deposits. In order to establish that the observed reduction in the Aβ pathology was due to the sink created by the presence of tg Aβ antibodies in the blood we set out to demonstrate presence of Aβ in the blood. Consistent with the biochemical data, we observed a significant increase of Aβ42 in serum of 250 day old *AB9μ-APPPS1* mice, whereas *DelS-APPPS1* mice displayed elevated Aβ40 plasma levels. As expected, plaque burden and Aβ42 serum levels closely correlated in an inverse fashion, further suggesting that the relief in Aβ burden was most likely due to the presence of anti-Aβ antibodies in the periphery.

In summary, we observed a reduction of Aβ plaque load at 250 days with Aβ42 being the prevalent Aβ species reduced. At 120 days, we only observed alterations in plaque size distribution which might be due to the fast kinetics of *de novo* plaque generation at this rather early time point which overrules putative anti-Aβ antibody-mediated effects. The

noted reduction of Aβ burden at 250 days was limited to diffuse plaques and did not involve compact core plaques. This is also reflected by the biochemical data for different Aβ species – there was no reduction in insoluble core plaque associated Aβ, whilst we found a reduction of soluble diffuse plaque associated Aβ. Notably, alterations in insoluble Aβ40 were not observed, arguing against an increase of vasculotropic Aβ. Furthermore these effects were not due to an interaction of the transgene as APP processing was not altered. One key finding providing further evidence for the peripheral sink paradigm is the increase in serum Aβ42 in *AB9μ-APPPS1* mice which is in accordance with the predominant reduction in Aβ42 in the brain of these mice (Fig. 29).

A comparison of *AB9μ*-and *DelS-APPPS1* mice points to *AB9μ* mice being more efficient in affecting the Aβ burden, especially by sequestering Aβ42 in the blood of *APPPS1* mice. This difference might be caused by the mentioned polyclonality of the tg *AB9μ* and *DelS* mice. Each of the mouse lines represents an individual and unique situation with respect to the anti-Aβ antibody repertoire, irrespective of the fact of harboring membrane bound and /or soluble antibodies. It is possible that *AB9μ*-L4I, the line of choice in my experiments, may have a higher Aβ specificity and affinity than *DelS*-L8, or harbors more antibodies binding the N-terminal region of Aβ, which have been shown to increase Aβ clearance across the BBB, whereas C-terminal antibodies have no influence.[237] Given that *DelS*-mice have only B cell membrane-bound antibodies and no additional antibody in the serum, their anti-Aβ antibody "titer" is also lower than in *AB9μ* mice. In general, the titers in our mice were not exceedingly high (1.5-4μg/ml) when compared to conventional passive or active immunization strategies (in which antibody responses around 12-240 μg/ml[143,228,238] are generated, or 500μg antibody are injected weekly[163,231], respectively). Moreover, the tg mice elicit a constant production of anti-Aβ antibodies, whereas immunization creates a boost with a sudden increase of respective antibodies. Despite this low titer we were able to demonstrate an improvement in Aβ pathology in *APPPS1* mice – at least at late time points. We certainly cannot exclude that an increased IgM titer in the periphery would benefit plaque depletion even more and earlier. This could be achieved by passively administering Aβ specific IgM antibodies.

3. Effect of peripheral anti Aβ antibodies on *TgSwDI* mice

To further examine the relative efficacy of peripheral anti-Aβ antibodies in altering Aβ accumulation, we crossed *AB9µ, DelS* and control mice to *TgSwDI* mice. This transgenic model has a later onset of Aβ deposition compared to *APPPS1* mice, both as compact amyloid fibrils and in more diffuse plaques. Furthermore, compared with *APPPS1* mice, the relative level of Aβ40 is much higher than that of Aβ42. Thus, in *TgSwDI* mice the predominant species deposited is Aβ40. In contrast Aβ42, as in most cases of AD, is the predominant species deposited in *APPPS1* mice. At 3 months of age, *TgSwDI* mice develop amyloid pathology with both vascular and parenchymal Aβ due to high Aβ40 expression. This allowed us to investigate the peripheral Aβ-specific antibody response in a mouse model dominated by Aβ40 production. At 180 days of age we analyzed *TgSwDI* mice crossed to *AB9µ* and *DelS*, and noted that male and female mice differed greatly in plaque deposition. Furthermore, we could not find any difference in cerebral and hippocampal plaque deposition, nor any alteration in brain Aβ42 and Aβ40 even though Aβ42 – as in *AB9µ* mice crossed to *APPPS1* mice – tended to be reduced in the SDS brain fraction of *AB9µ-TgSwDI* mice, again indicating that Aβ42 in the soluble fraction is affected more than Aβ40. Moreover, the analysis of Aβ peptides revealed that Aβ42 was equally abundant as Aβ40 in the SDS fraction, whereas in the FA fraction four times more Aβ40 was detected. In contrast, *APPPS1* mice have up to 4 times more Aβ42 in the FA fraction. This is consistent with the deposition of Aβ in the brain that predominates in these two AD mouse models: *APPPS1* mice have lots of parenchymal plaques classified by diffuse plaques (SDS-soluble Aβ42 and Aβ40) and compact core plaques (insoluble Aβ42). *TgSwDI* mice have many diffuse plaques as well, but additionally have vessel-associated compact core plaques due to high amounts of Aβ40 in the FA fraction. One caveat in these mice – presumably explaining the lack of a reduction of Aβ burden upon providing anti Aβ antibodies – is that the Dutch/Iowa mutant Aβ peptides might exhibit low efficiency for LRP-1-mediated transport across the blood-brain barrier due reduced affinity to LRP-1.[94] Furthermore, it is conceivable that the polyclonal anti-Aβ antibodies of *AB9µ* mice also exhibit lower affinity to the Dutch/Iowa Aβ, which is mutated at position Aβ22 and Aβ23 and for this reason cannot efficiently bind to Aβ. It has been previously shown that *TgSwDI* mice show no altered plaque load after peripheral vaccination, but only when antibodies are injected directly into the brain, which provides further support for the peripheral sink hypothesis.[239] Thus, the data obtained in *TgSwDI* mice

are – in contrast to the data obtained in *APPPS1* mice – not fully conclusive as *TgSwDI* mice – for the reasons mentioned – do not serve as an ideal tool for the herein proposed question.

Taken together thus far, these results support the notion that peripheral sink clearance in *APPPS1* mice contributes to the amelioration in plaque burden, whilst *TgSwDI* mice are rather "resistant" to peripheral clearance of Aβ due to the APP mutation they are harboring.

4. Effects of short-term icv administration of anti-Aβ antibodies on *APPPS1* mice

As reported above, the effect of peripheral anti-Aβ antibodies was rather small at early time points (120 days). At 120 days we are at the peak of *de novo* plaque generation in APPPS1 mice which declines thereafter. Therefore, we wondered whether direct application of anti-Aβ antibodies to the CSF might ameliorate Aβ pathology already at that early time point. For this, we administered AB9-IgG, purified AB9-IgM and control antibodies using a mini-osmotic pump into the brains of *APPPS1* mice for 60 days starting at the age of 60 days. The antibodies were administered at a flow rate of 0.25 µg/hour, which in turn is 0.25 µg for AB9-IgG and 0.05 µg for AB9-IgM (which was administered in a fivefold decreased concentration due to its 10 antigen binding sites compared to two binding sites of the IgG molecule). As we have a volume of 35 µl of mouse CSF [240], we achieved an initial antibody concentration in the CSF of around 7 µg/ml or 1.4 µg/ml, respectively. With a CSF turnover rate of about 18 µl/hour this initial concentration decreases to about 50% to 3.5 µg/ml and 0.7 µg/ml, respectively, within this first hour. The attenuated increase every hour of 3.5 (0.7)/ 2^{hour-1} allows stabilization of the initial concentration at around 7 (1.4) µg/ml after 10 hours of administration. Accordingly, IgM concentrations were thought to be comparable to a constant serum concentration of around 1.5-4 µg/ml.

Although concentrations were similar in serum and brain of *APPPS1* mice centrally applied AB9-IgM antibodies did not exhibit an alteration in plaque load (Fig. 30a). In contrast, we observed a significant amelioration in Aβ pathology in the AB9-IgG treated group, which had a concentration comparable to AB9-IgM (fivefold more than AB9-IgM) (Fig. 30b). Furthermore AB9-IgG antibodies were able to leave the brain and enter the blood stream (0.5µg/ml in serum) whereas IgM antibodies do not (Fig. 30c), since IgM molecules are likely

to be too large to be transported out of the brain. This observation makes it conceivable that IgM, in turn, cannot enter the brain.

This suggests that anti-AB9-IgG antibodies appear to be more efficient than AB9-IgM antibodies in ameliorating Aβ pathology due to several possible reasons. It might be that IgM is unable to penetrate significantly into tissue owing to its size and therefore does not reach the Aβ plaques. Furthermore the pentameric structure of the IgM molecule makes it especially effective in activating the complement system, whereas it is not reported to execute other downstream functions such as opsonization and Fcγ-R mediated activations. Whether activation of the complement system has adverse[241-245] or favorable effects[246,247] remains unclear. Yet, it is interesting that complement activation is weaker in transgenic mice than in AD patients[248], a difference that could explain the side effect observed after the first clinical trial. Recently, a group observed that some but not all anti-Aβ monoclonal IgM antibodies can cross the blood brain barrier in spite of their large molecular weight.[201] Our study demonstrated that – even if that is the case – IgM antibodies are less likely to produce the same effect due to the fact that IgM effector functions might not be sufficient to reduce plaque load locally. Also, this does not exclude that IgM antibodies cannot penetrate that far into the tissue.

One possible explanation for the above mentioned results is that anti-Aβ antibodies in the brain possess a stronger and faster capability of reducing plaques. This interpretation is supported by the observation that only 0.5 µg/ml AB9-IgG antibody left the brain and entered the blood stream. As tg *AB9µ-APPPS1* did not show an abatement in plaque pathology although these mice had higher concentration of AB9-IgM (1.5-4 µg/ml) in the blood stream for an even longer time span than the icv treated mice, it can be assumed that 0.5µg/ml AB9-IgG in the blood does not exert a measureable peripheral effect. Possible mechanisms other than the peripheral sink hypothesis could explain the central effect. Some results argue that amyloid opsonization and Fcγ-R mediated phagocytosis by microglia is the major mechanism by which Aβ is removed from the brain[115,133,249-251]. Other experiments, using a single focal intracranial delivery approach, suggested that the activation of microglia can facilitate the removal of Aβ plaques in the brain, but may not be essential[133,251,252] indicating microglia-independent mechanisms. Such mechanisms may involve the disruption

of plaques by the antibody itself followed by disaggregation of the β-sheet conformation of Aβ and subsequent removal[249]. As described in the introduction several data argue against the Fcγ-R mediated mechanism for plaque removal.[253,254] Other studies proposed that centrally applied antibodies may form a sink in the ventricular space of the brain, reducing parenchymal deposits.[112] Our results argue against this theory as AB9-IgM antibodies did not reduce Aβ plaques after injection into the ventricular space, whilst they presumably acted as a sink in blood (Fig. 28 and Fig. 29). Unpublished results from our lab, in which a nearly complete abrogation of vaccination efficiency occurred when the microglia compartment was ablated (Eom G. Prokop S., Heppner FH.) favor the microglia dependent mechanism of immunotherapy.

Admittedly, the vaccine mechanism might be highly dependent on the immunization strategy and adjuvants[107,255] and especially the antibody isotypes[109,250], which exert different functions. Our results also indicate such an isotype dependence as central AB9-IgM was not able to promote the same effect as AB9-IgG - an IgG2a isotype being particularly prone to Fcγ-R activation[256,257] and operating mainly in the body tissues. In general, IgG isotypes have variable effector functions such as antigen neutralization, antigen opsonization and subsequent phagocytosis by recruited cells as well as recruitment of complement. The activation of all these inflammatory mechanisms in the CNS might not be of benefit, and might induce the mentioned side effects such as vasogenic edema and microhaemorrhages in an already inflamed milieu. Especially notable are the putative adverse effects of opsonization of vascular amyloid or complement activation.

In sum, these findings indicate a faster clearance of Aβ when antibodies enter the brain which seems to be isotype-dependent. However, the potential side effects of antibody entrance to the CNS must be considered.

CONCLUSION

The design of passive immunotherapy with specially tailored antibodies, which lack activation of complement and over activation of microglial cells, could greatly reduce some mentioned side effects of Aβ immunotherapy. Another potentially safe and promising strategy would be the design of antibodies acting as peripheral sink, namely IgM antibodies. These antibodies cannot enter the brain, which avoids formation of APP-antibody immune complexes on neurons or of Aβ-antibody immune complexes in the vessels. Consequently, they should not induce adverse events such as neuronal membrane attack and inflammatory responses. With respect to microhemorrhages, the cause is not yet entirely clear as solaneuzumab (anti-Aβ antibody) entry into the brain was reported, which lead to intracerebral soluble Aβ sequestration.[112,258] Hence, this IgG antibody does not only act in the periphery, as was assumed. Accordingly it is not clear whether peripherally acting antibodies impact on vessel-associated amyloid. The designed peripheral IgM antibody should be directed against the N-terminal region of Aβ as it has been shown recently that these antibodies increase Aβ clearance across the BBB by preventing Aβ from interacting with the RAGE, whereas antibodies binding to the C-terminus of Aβ do not influence the BBB clearance of Aβ.[237] Moreover, N-terminal specific antibodies have been shown to be more efficient at reducing plaque burden in AD transgenic mice than C-terminal antibodies.[108,109,259] In addition to conventional monotherapy with antibodies, a combination therapy should also be considered. One example would be the combination of IgM treatment with therapeutics blocking RAGE or enhancing LRP-1 function, receptors which are possibly involved in the transport of Aβ into and out of the brain (see introduction). One clinical trial with RAGE antagonists was already initiated by Pfizer in 2006, however this was halted in 2011 due to unwanted side effects.[260] Despite these setbacks in RAGE-based therapies for AD, a new generation of compounds that regulate RAGE activity hold promise for an efficacious strategy.[261,262] A combination therapy with chitin, which stimulates perivascular macrophage turnover and promoted Aβ clearance along the perivascular space would be another alternative.[157] However caution has to be taken as stimulated perivascular macrophages mainly reduce vascular Aβ.

OUTLOOK

Our findings indicate that long term treatment with peripherally acting antibodies – at least to some extent – delay or even clear amyloid plaque deposition. Further careful studies are required in AD animal models to prove these data and ensure the safety and efficacy of chronic treatments. First of all, a third AD mouse model which has been shown to be immunizable should be crossed to *AB9µ* and *DelS* mice. We have already crossed mice to *APP23* mice, which have been shown to be susceptible to immunotherapy.[124] These mice carry the Swedish APP mutation driven by the murine Thy-1 promoter. *APP23* mice show first rare deposits at 6 months of age.[229] Deposits increase with age in size and number and eventually occupy a substantial area of the neocortex and hippocampus in 24-month-old mice. Hence, in contrast to *APPPS1* mice, *APP23* mice show slower kinetics of plaque production. Furthermore these mice also develop vascular amyloid and microhemorrhages which can be quantified to investigate effect of peripheral anti-Aβ antibody treatment on cerebral amyloid angiopathy (CAA) and associated pathology. Next to pathological assessment of *APP23* mice crossed to *AB9µ* mice could be tested for behavioral improvement as described before.[263,264] Also *APPPS1* mice could be behaviorally tested, as we have established several behavioral tests for these mice, such as fear-conditioning, barnes-maze and object recognition. Another possible read-out is to assess putative changes in long-term potentiation (LTP) which also has been shown to be impaired in *APPPS1* mice starting at 8 month.[265] Such functional parameters can be improved in *AB9µ-APPPS1* mice despite the rather small reduction in Aβ burden observed in 250 day old *AB9µ-APPPS1*.

To test whether higher concentrations of anti-Aβ IgM antibodies could attenuate Aβ pathology earlier and more effectively, monoclonal AB9-IgM antibodies could be produced and injected into AD mouse models. Furthermore, combination therapies should be carried out, for example with the new generation of RAGE antagonists. Also the effect of clodronate-mediated depletion and/or chitin-mediated stimulation of perivascular macrophages on immunotherapy could be further investigated.

Anti-Aβ antibodies acting in the periphery such as IgM also might be indirectly dependent on microglia. Microglia might solubilize Aβ being captured in plaques, which subsequently could

be transported across the BBB. To address this hypothesis, *AB9μ-APPPS1* and control mice could be crossed to *CD11b-HSVTK* mice[266] in which microglia can be depleted. Thus the effect of peripheral vaccination in absence of microglia could be investigated.

To pinpoint the mechanism of peripheral clearance in more detail we could further dissect transport mechanisms across the BBB by using antibodies against LRP-1 and other receptors associated with Aβ transport.[148] Blocking different transport systems in the presence of peripheral anti-Aβ antibodies could help to identify the predominant pathway by which Aβ is transported out of the brain in presence of peripheral anti-Aβ antibodies. Enhancing the function of the responsible transport molecules could open new avenues for combinational therapies with peripheral anti-Aβ vaccination.

A final interesting question which remains to be answered is what happens to the Aβ-antibody immune complexes in the blood. What are the downstream mechanisms resolving and degrading these complexes? The first degradation pathway is the standard pathway by which immune complexes are removed from the circulation.[267,268] According to this, immune complexes trigger their own removal by activating complement, which is then cleared from the circulation by binding to complement receptors on the surface of erythrocytes. The erythrocytes then transport the bound complexes of antigen, antibody, and complement to the liver and spleen.[267,268] Here macrophages remove the complexes from the erythrocyte surface and then degrade them. Another possible mechanism is the clearance of Aβ by LRP and degradation by Aβ-degrading enzymes such as neprilysin in the liver.[151] All these pathways could be investigated in more detail by immunohistochemistry, quantitative PCR and immune blots.

Such experiments could further help to dissect the contribution of the peripheral sink to immunotherapeutic approaches and promote to unravel the mechanism underlying immunotherapy. A better insight into the action of Aβ immunotherapy might help to design and test new combination therapies.[231,269] Especially in the field of AD research, mechanistical studies are required to pave the way for a disease-modifying or even causative treatment.

REFERENCES

1. Selkoe, D.J. Alzheimer's disease: genes, proteins, and therapy. *Physiol Rev* **81**, 741-66 (2001).

2. Stalder, A.K. et al. Invasion of hematopoietic cells into the brain of amyloid precursor protein transgenic mice. *J Neurosci* **25**, 11125-32 (2005).

3. Magaki, S., Yellon, S.M., Mueller, C. & Kirsch, W.M. Immunophenotypes in the circulation of patients with mild cognitive impairment. *J Psychiatr Res* **42**, 240-6 (2008).

4. Richartz-Salzburger, E. et al. Altered lymphocyte distribution in Alzheimer's disease. *J Psychiatr Res* **41**, 174-8 (2007).

5. Xue, S.R., Xu, D.H., Yang, X.X. & Dong, W.L. Alterations in lymphocyte subset patterns and co-stimulatory molecules in patients with Alzheimer disease. *Chin Med J (Engl)* **122**, 1469-72 (2009).

6. Rocca, W.A. et al. Frequency and distribution of Alzheimer's disease in Europe: a collaborative study of 1980-1990 prevalence findings. The EURODEM-Prevalence Research Group. *Ann Neurol* **30**, 381-90 (1991).

7. Plassmann, H., O'Doherty, J. & Rangel, A. Orbitofrontal cortex encodes willingness to pay in everyday economic transactions. *J Neurosci* **27**, 9984-8 (2007).

8. Gatz, M. et al. Complete ascertainment of dementia in the Swedish Twin Registry: the HARMONY study. *Neurobiol Aging* **26**, 439-47 (2005).

9. Wimo, A. & Prince, M. World Alzheimer ReporT 2010-The Global Economic Impact of Dementia (2010).

10. Abbott, A. Dementia: a problem for our age. *Nature* **475**, S2-4.

11. Citron, M. Strategies for disease modification in Alzheimer's disease. *Nat Rev Neurosci* **5**, 677-85 (2004).

12. Maurer, U. & Maurer, K. Alzheimer: the life of a physician and the career of a disease. *New York: Columbia University Press*, pp. 270 (2003).

13. Giacobini, E. & Becker, R.E. One hundred years after the discovery of Alzheimer's disease. A turning point for therapy? *J Alzheimers Dis* **12**, 37-52 (2007).

14. Alzheimer, A., Stelzmann, R.A., Schnitzlein, H.N. & Murtagh, F.R. An English translation of Alzheimer's 1907 paper, "Uber eine eigenartige Erkankung der Hirnrinde". *Clin Anat* **8**, 429-31 (1995).

15. Querfurth, H.W. & LaFerla, F.M. Alzheimer's disease. *N Engl J Med* **362**, 329-44.

16. Price, J.L. & Morris, J.C. Tangles and plaques in nondemented aging and "preclinical" Alzheimer's disease. *Ann Neurol* **45**, 358-68 (1999).

17. Jack, C.R., Jr. et al. Serial PIB and MRI in normal, mild cognitive impairment and Alzheimer's disease: implications for sequence of pathological events in Alzheimer's disease. *Brain* **132**, 1355-65 (2009).

18. WebMD, L. http://www.webmd.com/alzheimers/guide/making-diagnosis. (2005-2012).

19. Galasko, D. CSF tau and Abeta42: logical biomarkers for Alzheimer's disease? *Neurobiol Aging* **19**, 117-9 (1998).

20. Motter, R. et al. Reduction of beta-amyloid peptide42 in the cerebrospinal fluid of patients with Alzheimer's disease. *Ann Neurol* **38**, 643-8 (1995).

21. Shoji, M. et al. Combination assay of CSF tau, A beta 1-40 and A beta 1-42(43) as a biochemical marker of Alzheimer's disease. *J Neurol Sci* **158**, 134-40 (1998).

22. Tamaoka, A. et al. Amyloid beta protein 42(43) in cerebrospinal fluid of patients with Alzheimer's disease. *J Neurol Sci* **148**, 41-5 (1997).

23. Dubois, B. et al. Research criteria for the diagnosis of Alzheimer's disease: revising the NINCDS-ADRDA criteria. *Lancet Neurol* **6**, 734-46 (2007).

24. McKhann, G.M. et al. The diagnosis of dementia due to Alzheimer's disease: recommendations from the National Institute on Aging-Alzheimer's Association workgroups on diagnostic guidelines for Alzheimer's disease. *Alzheimers Dement* **7**, 263-9.

25. Slats, D. et al. CSF biomarker utilisation and ethical considerations of biomarker assisted diagnosis and research in dementia: perspectives from within the European Alzheimer's Disease Consortium (EADC). *J Neurol Neurosurg Psychiatry* **81**, 124-5.

26. Spies, P.E., Slats, D., Ramakers, I., Verhey, F.R. & Olde Rikkert, M.G. Experiences with cerebrospinal fluid analysis in Dutch memory clinics. *Eur J Neurol* **18**, 1014-6.

27. Mueller, S.G. et al. The Alzheimer's disease neuroimaging initiative. *Neuroimaging Clin N Am* **15**, 869-77, xi-xii (2005).

28. Mueller, S.G. et al. Ways toward an early diagnosis in Alzheimer's disease: the Alzheimer's Disease Neuroimaging Initiative (ADNI). *Alzheimers Dement* **1**, 55-66 (2005).

29. Visser, P.J. et al. Development of screening guidelines and clinical criteria for predementia Alzheimer's disease. The DESCRIPA Study. *Neuroepidemiology* **30**, 254-65 (2008).

30. Mucke, L. Neuroscience: Alzheimer's disease. *Nature* **461**, 895-7 (2009).

31. Selkoe, D.J. The molecular pathology of Alzheimer's disease. *Neuron* **6**, 487-98 (1991).

32. Blennow, K., de Leon, M.J. & Zetterberg, H. Alzheimer's disease. *Lancet* **368**, 387-403 (2006).

33. Obulesu, M., Venu, R. & Somashekhar, R. Tau mediated neurodegeneration: an insight into Alzheimer's disease pathology. *Neurochem Res* **36**, 1329-35.

34. Braak, E., Braak, H. & Mandelkow, E.M. A sequence of cytoskeleton changes related to the formation of neurofibrillary tangles and neuropil threads. *Acta Neuropathol* **87**, 554-67 (1994).

35. Aizenstein, H.J. et al. Frequent amyloid deposition without significant cognitive impairment among the elderly. *Arch Neurol* **65**, 1509-17 (2008).

36. Pike, K.E. et al. Beta-amyloid imaging and memory in non-demented individuals: evidence for preclinical Alzheimer's disease. *Brain* **130**, 2837-44 (2007).

37. Rodrigue, K.M. et al. beta-Amyloid burden in healthy aging: regional distribution and cognitive consequences. *Neurology* **78**, 387-95.

38. Yaari, R. & Corey-Bloom, J. Alzheimer's disease. in *Semin. Neurol. 2007 Thieme Medical Publishers* Vol. 27(1):32-41 (2007).

39. Ball, M.J. Neuronal loss, neurofibrillary tangles and granulovacuolar degeneration in the hippocampus with ageing and dementia. A quantitative study. *Acta Neuropathol* **37**, 111-8 (1977).

40. Ball, M.J. & Lo, P. Granulovacuolar degeneration in the ageing brain and in dementia. *J Neuropathol Exp Neurol* **36**, 474-87 (1977).

41. DeKosky, S.T. & Scheff, S.W. Synapse loss in frontal cortex biopsies in Alzheimer's disease: correlation with cognitive severity. *Ann Neurol* **27**, 457-64 (1990).

42. Scheff, S.W. & Price, D.A. Synapse loss in the temporal lobe in Alzheimer's disease. *Ann Neurol* **33**, 190-9 (1993).

43. Terry, R.D. et al. Physical basis of cognitive alterations in Alzheimer's disease: synapse loss is the major correlate of cognitive impairment. *Ann Neurol* **30**, 572-80 (1991).

44. Zlokovic, B.V. Neurovascular mechanisms of Alzheimer's neurodegeneration. *Trends Neurosci* **28**, 202-8 (2005).

45. Zlokovic, B.V., Deane, R., Sallstrom, J., Chow, N. & Miano, J.M. Neurovascular pathways and Alzheimer amyloid beta-peptide. *Brain Pathol* **15**, 78-83 (2005).

46. Keeney, J.T. et al. Cell Cycle Proteins in Brain in Mild Cognitive Impairment: Insights into Progression to Alzheimer Disease. *Neurotox Res*.

47. Zhu, X. et al. Differential activation of neuronal ERK, JNK/SAPK and p38 in Alzheimer disease: the 'two hit' hypothesis. *Mech Ageing Dev* **123**, 39-46 (2001).

48. Miklossy, J. Emerging roles of pathogens in Alzheimer disease. *Expert Rev Mol Med* **13**, e30.

49. Akiyama, H. et al. Inflammation and Alzheimer's disease. *Neurobiol Aging* **21**, 383-421 (2000).

50. Stone, J.G. et al. Frontiers in Alzheimer's disease therapeutics. *Ther Adv Chronic Dis* **2**, 9-23.

51. Hardy, J. & Selkoe, D.J. The amyloid hypothesis of Alzheimer's disease: progress and problems on the road to therapeutics. *Science* **297**, 353-6 (2002).

52. Hardy, J.A. & Higgins, G.A. Alzheimer's disease: the amyloid cascade hypothesis. *Science* **256**, 184-5 (1992).

53. Gotz, J., Chen, F., van Dorpe, J. & Nitsch, R.M. Formation of neurofibrillary tangles in P301l tau transgenic mice induced by Abeta 42 fibrils. *Science* **293**, 1491-5 (2001).

54. Lewis, J. et al. Enhanced neurofibrillary degeneration in transgenic mice expressing mutant tau and APP. *Science* **293**, 1487-91 (2001).

55. Kojro, E. & Fahrenholz, F. The non-amyloidogenic pathway: structure and function of alpha-secretases. *Subcell Biochem* **38**, 105-27 (2005).

56. Furukawa, K. et al. Increased activity-regulating and neuroprotective efficacy of alpha-secretase-derived secreted amyloid precursor protein conferred by a C-terminal heparin-binding domain. *J Neurochem* **67**, 1882-96 (1996).

57. Mattson, M.P., Guo, Z.H. & Geiger, J.D. Secreted form of amyloid precursor protein enhances basal glucose and glutamate transport and protects against oxidative impairment of glucose and glutamate transport in synaptosomes by a cyclic GMP-mediated mechanism. *J Neurochem* **73**, 532-7 (1999).

58. Meziane, H. et al. Memory-enhancing effects of secreted forms of the beta-amyloid precursor protein in normal and amnestic mice. *Proc Natl Acad Sci U S A* **95**, 12683-8 (1998).

59. Pardossi-Piquard, R. & Checler, F. The physiology of the beta-amyloid precursor protein intracellular domain AICD. *J Neurochem* **120 Suppl 1**, 109-24.

60. Nalivaeva, N.N., Beckett, C., Belyaev, N.D. & Turner, A.J. Are amyloid-degrading enzymes viable therapeutic targets in Alzheimer's disease? *J Neurochem* **120 Suppl 1**, 167-85.

61. Sharma, H.S., Castellani, R.J., Smith, M.A. & Sharma, A. The blood-brain barrier in Alzheimer's disease: novel therapeutic targets and nanodrug delivery. *Int Rev Neurobiol* **102**, 47-90.

62. Seubert, P. et al. Isolation and quantification of soluble Alzheimer's beta-peptide from biological fluids. *Nature* **359**, 325-7 (1992).

63. Stockley, J.H. & O'Neill, C. The proteins BACE1 and BACE2 and beta-secretase activity in normal and Alzheimer's disease brain. *Biochem Soc Trans* **35**, 574-6 (2007).

64. Mawuenyega, K.G. et al. Decreased clearance of CNS beta-amyloid in Alzheimer's disease. *Science* **330**, 1774.

65. Walsh, D.M. et al. Naturally secreted oligomers of amyloid beta protein potently inhibit hippocampal long-term potentiation in vivo. *Nature* **416**, 535-9 (2002).

66. Selkoe, D.J. Toward a comprehensive theory for Alzheimer's disease. Hypothesis: Alzheimer's disease is caused by the cerebral accumulation and cytotoxicity of amyloid beta-protein. *Ann N Y Acad Sci* **924**, 17-25 (2000).

67. Jack, C.R., Jr. et al. Hypothetical model of dynamic biomarkers of the Alzheimer's pathological cascade. *Lancet Neurol* **9**, 119-28.

68. Ertekin-Taner, N. Genetics of Alzheimer's disease: a centennial review. *Neurol Clin* **25**, 611-67, v (2007).

69. Finch, C.E. & Tanzi, R.E. Genetics of aging. *Science* **278**, 407-11 (1997).

70. Joshi, A., Ringman, J.M., Lee, A.S., Juarez, K.O. & Mendez, M.F. Comparison of clinical characteristics between familial and non-familial early onset Alzheimer's disease. *J Neurol*.

71. Selkoe, D.J. Translating cell biology into therapeutic advances in Alzheimer's disease. *Nature* **399**, A23-31 (1999).

72. Cruts, M. et al. Estimation of the genetic contribution of presenilin-1 and -2 mutations in a population-based study of presenile Alzheimer disease. *Hum Mol Genet* **7**, 43-51 (1998).

73. Hardy, J. The Alzheimer family of diseases: many etiologies, one pathogenesis? *Proc Natl Acad Sci U S A* **94**, 2095-7 (1997).

74. Bekris, L.M., Yu, C.E., Bird, T.D. & Tsuang, D.W. Genetics of Alzheimer disease. *J Geriatr Psychiatry Neurol* **23**, 213-27.

75. Chai, C.K. The genetics of Alzheimer's disease. *Am J Alzheimers Dis Other Demen* **22**, 37-41 (2007).

76. Ghiso, J. & Frangione, B. Amyloidosis and Alzheimer's disease. *Adv Drug Deliv Rev* **54**, 1539-51 (2002).

77. Jayadev, S. et al. Alzheimer's disease phenotypes and genotypes associated with mutations in presenilin 2. *Brain* **133**, 1143-54.

78. Van Nostrand, W.E., Melchor, J.P., Romanov, G., Zeigler, K. & Davis, J. Pathogenic effects of cerebral amyloid angiopathy mutations in the amyloid beta-protein precursor. *Ann N Y Acad Sci* **977**, 258-65 (2002).

79. Goate, A.M. Molecular genetics of Alzheimer's disease. *Geriatrics* **52 Suppl 2**, S9-12 (1997).

80. Corder, E.H. et al. Protective effect of apolipoprotein E type 2 allele for late onset Alzheimer disease. *Nat Genet* **7**, 180-4 (1994).

81. Cedazo-Minguez, A. Apolipoprotein E and Alzheimer's disease: molecular mechanisms and therapeutic opportunities. *J Cell Mol Med* **11**, 1227-38 (2007).

82. Holtzman, D.M. Role of apoe/Abeta interactions in the pathogenesis of Alzheimer's disease and cerebral amyloid angiopathy. *J Mol Neurosci* **17**, 147-55 (2001).

83. McGowan, E., Eriksen, J. & Hutton, M. A decade of modeling Alzheimer's disease in transgenic mice. *Trends Genet* **22**, 281-9 (2006).

84. Duff, K. et al. Increased amyloid-beta42(43) in brains of mice expressing mutant presenilin 1. *Nature* **383**, 710-3 (1996).

85. Borchelt, D.R. et al. Accelerated amyloid deposition in the brains of transgenic mice coexpressing mutant presenilin 1 and amyloid precursor proteins. *Neuron* **19**, 939-45 (1997).

86. Holcomb, L. et al. Accelerated Alzheimer-type phenotype in transgenic mice carrying both mutant amyloid precursor protein and presenilin 1 transgenes. *Nat Med* **4**, 97-100 (1998).

87. Citron, M. et al. Mutant presenilins of Alzheimer's disease increase production of 42-residue amyloid beta-protein in both transfected cells and transgenic mice. *Nat Med* **3**, 67-72 (1997).

88. Borchelt, D.R. et al. Familial Alzheimer's disease-linked presenilin 1 variants elevate Abeta1-42/1-40 ratio in vitro and in vivo. *Neuron* **17**, 1005-13 (1996).

89. Irizarry, M.C. et al. Abeta deposition is associated with neuropil changes, but not with overt neuronal loss in the human amyloid precursor protein V717F (PDAPP) transgenic mouse. *J Neurosci* **17**, 7053-9 (1997).

90. Irizarry, M.C., McNamara, M., Fedorchak, K., Hsiao, K. & Hyman, B.T. APPSw transgenic mice develop age-related A beta deposits and neuropil abnormalities, but no neuronal loss in CA1. *J Neuropathol Exp Neurol* **56**, 965-73 (1997).

91. Radde, R., Duma, C., Goedert, M. & Jucker, M. The value of incomplete mouse models of Alzheimer's disease. *Eur J Nucl Med Mol Imaging* **35 Suppl 1**, S70-4 (2008).

92. Herzig, M.C. et al. Abeta is targeted to the vasculature in a mouse model of hereditary cerebral hemorrhage with amyloidosis. *Nat Neurosci* **7**, 954-60 (2004).

93. Radde, R. et al. Abeta42-driven cerebral amyloidosis in transgenic mice reveals early and robust pathology. *EMBO Rep* **7**, 940-6 (2006).

94. Davis, J. et al. Early-onset and robust cerebral microvascular accumulation of amyloid beta-protein in transgenic mice expressing low levels of a vasculotropic Dutch/Iowa mutant form of amyloid beta-protein precursor. *J Biol Chem* **279**, 20296-306 (2004).

95. Oddo, S. et al. Triple-transgenic model of Alzheimer's disease with plaques and tangles: intracellular Abeta and synaptic dysfunction. *Neuron* **39**, 409-21 (2003).

96. Grueninger, F. et al. Phosphorylation of Tau at S422 is enhanced by Abeta in TauPS2APP triple transgenic mice. *Neurobiol Dis* **37**, 294-306.

97. Oddo, S., Caccamo, A., Kitazawa, M., Tseng, B.P. & LaFerla, F.M. Amyloid deposition precedes tangle formation in a triple transgenic model of Alzheimer's disease. *Neurobiol Aging* **24**, 1063-70 (2003).

98. Oddo, S. et al. Reduction of soluble A beta and Tau, but not soluble A beta alone, ameliorates cognitive decline in transgenic mice with plaques and tangles. *Journal of Biological Chemistry* **281**, 39413-39423 (2006).

99. Naslund, J. et al. Correlation between elevated levels of amyloid beta-peptide in the brain and cognitive decline. *JAMA* **283**, 1571-7 (2000).

100. Jucker, M. The benefits and limitations of animal models for translational research in neurodegenerative diseases. *Nat Med* **16**, 1210-4.

101. Brody, D.L. & Holtzman, D.M. Active and passive immunotherapy for neurodegenerative disorders. *Annu Rev Neurosci* **31**, 175-93 (2008).

102. Wisniewski, T. & Boutajangout, A. Immunotherapeutic approaches for Alzheimer's disease in transgenic mouse models. *Brain Struct Funct* **214**, 201-18.

103. Wisniewski, T. & Konietzko, U. Amyloid-beta immunisation for Alzheimer's disease. *Lancet Neurol* **7**, 805-11 (2008).

104. Schenk, D. et al. Immunization with amyloid-beta attenuates Alzheimer-disease-like pathology in the PDAPP mouse. *Nature* **400**, 173-7 (1999).

105. Weiner, H.L. et al. Nasal administration of amyloid-beta peptide decreases cerebral amyloid burden in a mouse model of Alzheimer's disease. *Ann Neurol* **48**, 567-79 (2000).

106. Sigurdsson, E.M., Scholtzova, H., Mehta, P.D., Frangione, B. & Wisniewski, T. Immunization with a nontoxic/nonfibrillar amyloid-beta homologous peptide reduces Alzheimer's disease-associated pathology in transgenic mice. *Am J Pathol* **159**, 439-47 (2001).

107. Maier, M. et al. Short amyloid-beta (Abeta) immunogens reduce cerebral Abeta load and learning deficits in an Alzheimer's disease mouse model in the absence of an Abeta-specific cellular immune response. *J Neurosci* **26**, 4717-28 (2006).

108. DeMattos, R.B. et al. Peripheral anti-A beta antibody alters CNS and plasma A beta clearance and decreases brain A beta burden in a mouse model of Alzheimer's disease. *Proc Natl Acad Sci U S A* **98**, 8850-5 (2001).

109. Bard, F. et al. Epitope and isotype specificities of antibodies to beta -amyloid peptide for protection against Alzheimer's disease-like neuropathology. *Proc Natl Acad Sci U S A* **100**, 2023-8 (2003).

110. Morgan, D. et al. A beta peptide vaccination prevents memory loss in an animal model of Alzheimer's disease. *Nature* **408**, 982-5 (2000).

111. Janus, C. et al. A beta peptide immunization reduces behavioural impairment and plaques in a model of Alzheimer's disease. *Nature* **408**, 979-82 (2000).

112. Dodart, J.C. et al. Immunization reverses memory deficits without reducing brain Abeta burden in Alzheimer's disease model. *Nat Neurosci* **5**, 452-7 (2002).

113. Bard, F. et al. Peripherally administered antibodies against amyloid beta-peptide enter the central nervous system and reduce pathology in a mouse model of alzheimer disease [In Process Citation]. *Nat Med* **6**, 916-9 (2000).

114. Hock, C. et al. Antibodies against beta-amyloid slow cognitive decline in Alzheimer's disease. *Neuron* **38**, 547-54 (2003).

115. Orgogozo, J.M. et al. Subacute meningoencephalitis in a subset of patients with AD after Abeta42 immunization. *Neurology* **61**, 46-54 (2003).

116. Nicoll, J.A.R. et al. Neuropathology of human Alzheimer disease after immunization with amyloid-[beta] peptide: a case report. *Nat Med* **9**, 448-452 (2003).

117. Gilman, S. et al. Clinical effects of Abeta immunization (AN1792) in patients with AD in an interrupted trial. *Neurology* **64**, 1553-62 (2005).

118. Masliah, E. et al. Abeta vaccination effects on plaque pathology in the absence of encephalitis in Alzheimer disease. *Neurology* **64**, 129-31 (2005).

119. Ferrer, I., Boada Rovira, M., Sanchez Guerra, M.L., Rey, M.J. & Costa-Jussa, F. Neuropathology and pathogenesis of encephalitis following amyloid-beta immunization in Alzheimer's disease. *Brain Pathol* **14**, 11-20 (2004).

120. Nicoll, J.A. et al. Abeta species removal after abeta42 immunization. *J Neuropathol Exp Neurol* **65**, 1040-8 (2006).

121. Serrano-Pozo, A. et al. Beneficial effect of human anti-amyloid-beta active immunization on neurite morphology and tau pathology. *Brain* **133**, 1312-27.

122. Holmes, C. et al. Long-term effects of Abeta42 immunisation in Alzheimer's disease: follow-up of a randomised, placebo-controlled phase I trial. *Lancet* **372**, 216-23 (2008).

123. Vellas, B. et al. Long-term follow-up of patients immunized with AN1792: reduced functional decline in antibody responders. *Curr Alzheimer Res* **6**, 144-51 (2009).

124. Pfeifer, M. et al. Cerebral hemorrhage after passive anti-Abeta immunotherapy. *Science* **298**, 1379 (2002).

125. Racke, M.M. et al. Exacerbation of cerebral amyloid angiopathy-associated microhemorrhage in amyloid precursor protein transgenic mice by immunotherapy is dependent on antibody recognition of deposited forms of amyloid beta. *J Neurosci* **25**, 629-36 (2005).

126. Kerchner, G.A. & Boxer, A.L. Bapineuzumab. *Expert Opin Biol Ther* **10**, 1121-30.

127. Boche, D. et al. Consequence of Abeta immunization on the vasculature of human Alzheimer's disease brain. *Brain* **131**, 3299-310 (2008).

128. Wilcock, D.M. et al. Passive immunotherapy against Abeta in aged APP-transgenic mice reverses cognitive deficits and depletes parenchymal amyloid deposits in spite of increased vascular amyloid and microhemorrhage. *J Neuroinflammation* **1**, 24 (2004).

129. Solomon, B., Koppel, R., Frankel, D. & Hanan-Aharon, E. Disaggregation of Alzheimer beta-amyloid by site-directed mAb. *Proc Natl Acad Sci U S A* **94**, 4109-12 (1997).

130. Solomon, B., Koppel, R., Hanan, E. & Katzav, T. Monoclonal antibodies inhibit in vitro fibrillar aggregation of the Alzheimer beta-amyloid peptide. *Proc Natl Acad Sci U S A* **93**, 452-5 (1996).

131. Bard, F. et al. Peripherally administered antibodies against amyloid beta-peptide enter the central nervous system and reduce pathology in a mouse model of Alzheimer disease. *Nat Med* **6**, 916-9 (2000).

132. Bacskai, B.J. et al. Non-Fc-mediated mechanisms are involved in clearance of amyloid-beta in vivo by immunotherapy. *J Neurosci* **22**, 7873-8 (2002).

133. Wilcock, D.M. et al. Intracranially administered anti-Abeta antibodies reduce beta-amyloid deposition by mechanisms both independent of and associated with microglial activation. *J Neurosci* **23**, 3745-51 (2003).

134. Das, P. et al. Amyloid-beta immunization effectively reduces amyloid deposition in FcRgamma-/- knock-out mice. *J Neurosci* **23**, 8532-8 (2003).

135. DeMattos, R.B., Bales, K.R., Cummins, D.J., Paul, S.M. & Holtzman, D.M. Brain to plasma amyloid-beta efflux: a measure of brain amyloid burden in a mouse model of Alzheimer's disease. *Science* **295**, 2264-7 (2002).

136. Matsuoka, Y. et al. Novel therapeutic approach for the treatment of Alzheimer's disease by peripheral administration of agents with an affinity to beta-amyloid. *J Neurosci* **23**, 29-33 (2003).

137. Deane, R. et al. RAGE mediates amyloid-beta peptide transport across the blood-brain barrier and accumulation in brain. *Nat Med* **9**, 907-13 (2003).

138. Sagare, A. et al. Clearance of amyloid-beta by circulating lipoprotein receptors. *Nat Med* **13**, 1029-31 (2007).

139. Sehgal, N. et al. Withania somnifera reverses Alzheimer's disease pathology by enhancing low-density lipoprotein receptor-related protein in liver. *Proc Natl Acad Sci U S A* **109**, 3510-5.

140. Baumgarth, N. A two-phase model of B-cell activation. *Immunol Rev* **176**, 171-80 (2000).

141. Szomolanyi-Tsuda, E. et al. Antiviral T-cell-independent type 2 antibody responses induced in vivo in the absence of T and NK cells. *Virology* **280**, 160-8 (2001).

142. Sigurdsson, E.M. et al. An attenuated immune response is sufficient to enhance cognition in an Alzheimer's disease mouse model immunized with amyloid-beta derivatives. *J Neurosci* **24**, 6277-82 (2004).

143. Li, Q.Y. et al. Virus-like peptide vaccines against Abeta N-terminal or C-terminal domains reduce amyloid deposition in APP transgenic mice without addition of adjuvant. *J Neuroimmune Pharmacol* **5**, 133-42.

144. Hartz, A.M., Miller, D.S. & Bauer, B. Restoring blood-brain barrier P-glycoprotein reduces brain amyloid-beta in a mouse model of Alzheimer's disease. *Mol Pharmacol* **77**, 715-23.

145. Zlokovic, B.V. Clearing amyloid through the blood-brain barrier. *J Neurochem* **89**, 807-11 (2004).

146. Zlokovic, B.V., Deane, R., Sagare, A.P., Bell, R.D. & Winkler, E.A. Low-density lipoprotein receptor-related protein-1: a serial clearance homeostatic mechanism controlling Alzheimer's amyloid beta-peptide elimination from the brain. *J Neurochem* **115**, 1077-89.

147. Deane, R., Wu, Z. & Zlokovic, B.V. RAGE (yin) versus LRP (yang) balance regulates alzheimer amyloid beta-peptide clearance through transport across the blood-brain barrier. *Stroke* **35**, 2628-31 (2004).

148. Shibata, M. et al. Clearance of Alzheimer's amyloid-ss(1-40) peptide from brain by LDL receptor-related protein-1 at the blood-brain barrier. *J Clin Invest* **106**, 1489-99 (2000).

149. Bell, R.D. et al. Transport pathways for clearance of human Alzheimer's amyloid beta-peptide and apolipoproteins E and J in the mouse central nervous system. *J Cereb Blood Flow Metab* **27**, 909-18 (2007).

150. Silverberg, G.D. et al. Amyloid efflux transporter expression at the blood-brain barrier declines in normal aging. *J Neuropathol Exp Neurol* **69**, 1034-43.

151. Tanzi, R.E., Moir, R.D. & Wagner, S.L. Clearance of Alzheimer's Abeta peptide: the many roads to perdition. *Neuron* **43**, 605-8 (2004).

152. Deane, R. & Zlokovic, B.V. Role of the blood-brain barrier in the pathogenesis of Alzheimer's disease. *Curr Alzheimer Res* **4**, 191-7 (2007).

153. Donahue, J.E. et al. RAGE, LRP-1, and amyloid-beta protein in Alzheimer's disease. *Acta Neuropathol* **112**, 405-15 (2006).

154. Miller, M.C. et al. Hippocampal RAGE immunoreactivity in early and advanced Alzheimer's disease. *Brain Res* **1230**, 273-80 (2008).

155. Kandimalla, K.K. et al. Pharmacokinetic analysis of the blood-brain barrier transport of 125I-amyloid beta protein 40 in wild-type and Alzheimer's disease transgenic mice (APP,PS1) and its implications for amyloid plaque formation. *J Pharmacol Exp Ther* **313**, 1370-8 (2005).

156. Jaeger, L.B. et al. Testing the neurovascular hypothesis of Alzheimer's disease: LRP-1 antisense reduces blood-brain barrier clearance, increases brain levels of amyloid-beta protein, and impairs cognition. *J Alzheimers Dis* **17**, 553-70 (2009).

157. Hawkes, C.A. & McLaurin, J. Selective targeting of perivascular macrophages for clearance of beta-amyloid in cerebral amyloid angiopathy. *Proc Natl Acad Sci U S A* **106**, 1261-6 (2009).

158. Johanson, C.E. et al. Multiplicity of cerebrospinal fluid functions: New challenges in health and disease. *Cerebrospinal Fluid Res* **5**, 10 (2008).

159. May, C. et al. Cerebrospinal fluid production is reduced in healthy aging. *Neurology* **40**, 500-3 (1990).

160. Rubenstein, E. Relationship of senescence of cerebrospinal fluid circulatory system to dementias of the aged. *Lancet* **351**, 283-5 (1998).

161. Pascale, C.L. et al. Amyloid-beta transporter expression at the blood-CSF barrier is age-dependent. *Fluids Barriers CNS* **8**, 21.

162. Iliff, J.J. et al. A Paravascular Pathway Facilitates CSF Flow Through the Brain Parenchyma and the Clearance of Interstitial Solutes, Including Amyloid beta. *Sci Transl Med* **4**, 147ra111.

163. Levites, Y. et al. Anti-Abeta42- and anti-Abeta40-specific mAbs attenuate amyloid deposition in an Alzheimer disease mouse model. *J Clin Invest* **116**, 193-201 (2006).

164. Levites, Y. et al. Insights into the mechanisms of action of anti-Abeta antibodies in Alzheimer's disease mouse models. *FASEB J* **20**, 2576-8 (2006).

165. Heppner, F.L. et al. Prevention of scrapie pathogenesis by transgenic expression of anti-prion protein antibodies. *Science* **294**, 178-82 (2001).

166. Britschgi, M. & Wyss-Coray, T. Systemic and acquired immune responses in Alzheimer's disease. *Int Rev Neurobiol* **82**, 205-33 (2007).

167. Bleesing, J.H. Assays for B Cell and Germinal Center Development. *John Wiley & Sons* **7.35.1-7.35.21**(2004).

168. Hardy, R.R. & Hayakawa, K. B cell development pathways. *Annu Rev Immunol* **19**, 595-621 (2001).

169. Kracker, S. & Radbruch, A. Immunoglobulin class switching: in vitro induction and analysis. *Methods Mol Biol* **271**, 149-59 (2004).

170. Fehr, T. et al. Correlation of anti-viral B cell responses and splenic morphology with expression of B cell-specific molecules. *Int Immunol* **12**, 1275-84 (2000).

171. Nevens, J.R., Mallia, A.K., Wendt, M.W. & Smith, P.K. Affinity chromatographic purification of immunoglobulin M antibodies utilizing immobilized mannan binding protein. *J Chromatogr* **597**, 247-56 (1992).

172. Hauptman, S.P. & Tomasi, T.B., Jr. Mechanism of immunoglobulin A polymerization. *J Biol Chem* **250**, 3891-6 (1975).

173. Grathwohl, S.A. et al. Formation and maintenance of Alzheimer's disease beta-amyloid plaques in the absence of microglia. *Nat Neurosci* **12**, 1361-3 (2009).

174. Hartman, R.E. et al. Treatment with an amyloid-beta antibody ameliorates plaque load, learning deficits, and hippocampal long-term potentiation in a mouse model of Alzheimer's disease. *J Neurosci* **25**, 6213-20 (2005).

175. Kawarabayashi, T. et al. Age-dependent changes in brain, CSF, and plasma amyloid (beta) protein in the Tg2576 transgenic mouse model of Alzheimer's disease. *J Neurosci* **21**, 372-81 (2001).

176. Schagger, H. & von Jagow, G. Tricine-sodium dodecyl sulfate-polyacrylamide gel electrophoresis for the separation of proteins in the range from 1 to 100 kDa. *Anal Biochem* **166**, 368-79 (1987).

177. Shapiro, S.S. & Wilk, M.B. An analysis of variance test for normality. *Biometrika* **52(3-4)**, 591-611 (1965).

178. Brown, A.M. A new software for carrying out one-way ANOVA post hoc tests. *Comput Methods Programs Biomed* **79**, 89-95 (2005).

179. Klinman, D.M. Polyclonal B cell activation in lupus-prone mice precedes and predicts the development of autoimmune disease. *J Clin Invest* **86**, 1249-54 (1990).

180. Sfriso, P. et al. Infections and autoimmunity: the multifaceted relationship. *J Leukoc Biol* **87**, 385-95.

181. Amezcua Vesely, M.C., Bermejo, D.A., Montes, C.L., Acosta-Rodriguez, E.V. & Gruppi, A. B-Cell Response during Protozoan Parasite Infections. *J Parasitol Res* **2012**, 362131.

182. Vos, Q. & Hodes, R.J. Immunoglobulin (Ig) mu, kappa transgenic mice express transgenic idiotype on endogenously rearranged IgM and IgA molecules by secretion of chimeric molecules. *J Exp Med* **176**, 951-61 (1992).

183. Era, T. et al. Differentiation of growth signal requirement of B lymphocyte precursor is directed by expression of immunoglobulin. *EMBO J* **10**, 337-42 (1991).

184. Mason, D.Y., Jones, M. & Goodnow, C.C. Development and follicular localization of tolerant B lymphocytes in lysozyme/anti-lysozyme IgM/IgD transgenic mice. *Int Immunol* **4**, 163-75 (1992).

185. Togo, T. et al. Occurrence of T cells in the brain of Alzheimer's disease and other neurological diseases. *J Neuroimmunol* **124**, 83-92 (2002).

186. Rogers, J., Luber-Narod, J., Styren, S.D. & Civin, W.H. Expression of immune system-associated antigens by cells of the human central nervous system: relationship to the pathology of Alzheimer's disease. *Neurobiol Aging* **9**, 339-49 (1988).

187. Ohsugi, T. & Kumasaka, T. Low CD4/CD8 T-cell ratio associated with inflammatory arthropathy in human T-cell leukemia virus type I Tax transgenic mice. *PLoS One* **6**, e18518.

188. Roshal, M., Wood, B.L. & Fromm, J.R. Flow cytometric detection of the classical hodgkin lymphoma: clinical and research applications. *Adv Hematol* **2011**, 387034.

189. Stuve, O. et al. Altered CD4+/CD8+ T-cell ratios in cerebrospinal fluid of natalizumab-treated patients with multiple sclerosis. *Arch Neurol* **63**, 1383-7 (2006).

190. Ochsenbein, A.F. et al. Protective long-term antibody memory by antigen-driven and T help-dependent differentiation of long-lived memory B cells to short-lived plasma cells independent of secondary lymphoid organs. *Proc Natl Acad Sci U S A* **97**, 13263-8 (2000).

191. Brundler, M.A. et al. Immunity to viruses in B cell-deficient mice: influence of antibodies on virus persistence and on T cell memory. *Eur J Immunol* **26**, 2257-62 (1996).

192. Thomsen, A.R. et al. Cooperation of B cells and T cells is required for survival of mice infected with vesicular stomatitis virus. *Int Immunol* **9**, 1757-66 (1997).

193. Andersson, J., Coutinho, A., Lernhardt, W. & Melchers, F. Clonal growth and maturation to immunoglobulin secretion in vitro of every growth-inducible B lymphocyte. *Cell* **10**, 27-34 (1977).

194. Kearney, J.F., Cooper, M.D. & Lawton, A.R. B cell differentiation induced by lipopolysaccharide. IV. Development of immunoglobulin class restriction in precursors of IgG-synthesizing cells. *J Immunol* **117**, 1567-72 (1976).

195. Yuan, D. & Vitetta, E.S. Structural studies of cell surface and secreted IgG in LPS-stimulated murine B cells. *Mol Immunol* **20**, 367-75 (1983).

196. Hefendehl, J.K. et al. Long-term in vivo imaging of beta-amyloid plaque appearance and growth in a mouse model of cerebral beta-amyloidosis. *J Neurosci* **31**, 624-9.

197. Roher, A.E. et al. Structural alterations in the peptide backbone of beta-amyloid core protein may account for its deposition and stability in Alzheimer's disease. *J Biol Chem* **268**, 3072-83 (1993).

198. Aslund, A. et al. Novel pentameric thiophene derivatives for in vitro and in vivo optical imaging of a plethora of protein aggregates in cerebral amyloidoses. *ACS Chem Biol* **4**, 673-84 (2009).

199. Thinakaran, G. & Koo, E.H. Amyloid precursor protein trafficking, processing, and function. *J Biol Chem* **283**, 29615-9 (2008).

200. Vermes, L.M. [Cerebrospinal fluid proteins: III. Normal values of immunoglobulins G, A and M (variations related to race, sex and age)]. *Arq Neuropsiquiatr* **41**, 25-49 (1983).

201. Banks, W.A. et al. Passage of amyloid beta protein antibody across the blood-brain barrier in a mouse model of Alzheimer's disease. *Peptides* **23**, 2223-6 (2002).

202. Ritchie, K.A., Brinster, R.L. & Storb, U. Allelic exclusion and control of endogenous immunoglobulin gene rearrangement in kappa transgenic mice. *Nature* **312**, 517-20 (1984).

203. Rusconi, S. & Kohler, G. Transmission and expression of a specific pair of rearranged immunoglobulin mu and kappa genes in a transgenic mouse line. *Nature* **314**, 330-4 (1985).

204. Storb, U. Transgenic mice with immunoglobulin genes. *Annu Rev Immunol* **5**, 151-74 (1987).

205. Weaver, D., Costantini, F., Imanishi-Kari, T. & Baltimore, D. A transgenic immunoglobulin mu gene prevents rearrangement of endogenous genes. *Cell* **42**, 117-27 (1985).

206. Alt, F.W. et al. Ordered rearrangement of immunoglobulin heavy chain variable region segments. *EMBO J* **3**, 1209-19 (1984).

207. Kitamura, D., Roes, J., Kuhn, R. & Rajewsky, K. A B cell-deficient mouse by targeted disruption of the membrane exon of the immunoglobulin mu chain gene. *Nature* **350**, 423-6 (1991).

208. Nussenzweig, M.C. et al. Allelic exclusion in transgenic mice that express the membrane form of immunoglobulin mu. *Science* **236**, 816-9 (1987).

209. Reth, M., Petrac, E., Wiese, P., Lobel, L. & Alt, F.W. Activation of V kappa gene rearrangement in pre-B cells follows the expression of membrane-bound immunoglobulin heavy chains. *EMBO J* **6**, 3299-305 (1987).

210. Stall, A.M., Kroese, F.G., Gadus, F.T., Sieckmann, D.G. & Herzenberg, L.A. Rearrangement and expression of endogenous immunoglobulin genes occur in many murine B cells expressing transgenic membrane IgM. *Proc Natl Acad Sci U S A* **85**, 3546-50 (1988).

211. Lamers, M.C. et al. Immune status of a mu, kappa transgenic mouse line. Deficient response to bacterially related antigens. *Eur J Immunol* **19**, 459-68 (1989).

212. Goodnow, C.C. Transgenic mice and analysis of B-cell tolerance. *Annu Rev Immunol* **10**, 489-518 (1992).

213. Nussenzweig, M.C. et al. A human immunoglobulin gene reduces the incidence of lymphomas in c-Myc-bearing transgenic mice. *Nature* **336**, 446-50 (1988).

214. Muller, W. et al. Membrane-bound IgM obstructs B cell development in transgenic mice. *Eur J Immunol* **19**, 923-8 (1989).

215. Herzenberg, L.A. et al. Depletion of the predominant B-cell population in immunoglobulin mu heavy-chain transgenic mice. *Nature* **329**, 71-3 (1987).

216. Kitamura, D. et al. A critical role of lambda 5 protein in B cell development. *Cell* **69**, 823-31 (1992).

217. Keyna, U., Beck-Engeser, G.B., Jongstra, J., Applequist, S.E. & Jack, H.M. Surrogate light chain-dependent selection of Ig heavy chain V regions. *J Immunol* **155**, 5536-42 (1995).

218. Waisman, A. et al. IgG1 B cell receptor signaling is inhibited by CD22 and promotes the development of B cells whose survival is less dependent on Ig alpha/beta. *J Exp Med* **204**, 747-58 (2007).

219. Hao, Z. & Rajewsky, K. Homeostasis of peripheral B cells in the absence of B cell influx from the bone marrow. *J Exp Med* **194**, 1151-64 (2001).

220. Li, F., Jin, F., Freitas, A., Szabo, P. & Weksler, M.E. Impaired regeneration of the peripheral B cell repertoire from bone marrow following lymphopenia in old mice. *Eur J Immunol* **31**, 500-5 (2001).

221. Riley, R.L., Kruger, M.G. & Elia, J. B cell precursors are decreased in senescent BALB/c mice, but retain normal mitotic activity in vivo and in vitro. *Clin Immunol Immunopathol* **59**, 301-13 (1991).

222. Stephan, R.P., Sanders, V.M. & Witte, P.L. Stage-specific alterations in murine B lymphopoiesis with age. *Int Immunol* **8**, 509-18 (1996).

223. Zharhary, D. Age-related changes in the capability of the bone marrow to generate B cells. *J Immunol* **141**, 1863-9 (1988).

224. Kline, G.H., Hayden, T.A. & Klinman, N.R. B cell maintenance in aged mice reflects both increased B cell longevity and decreased B cell generation. *J Immunol* **162**, 3342-9 (1999).

225. Lepesheva, G.I. et al. Comparative structural-functional characterization of recombinant and natural adrenodoxin. Interaction with cytochrome P450scc. *Biochemistry (Mosc)* **64**, 1079-88 (1999).

226. Lepesheva, G.I., Strushkevich, N.V. & Usanov, S.A. Conformational dynamics and molecular interaction reactions of recombinant cytochrome p450scc (CYP11A1) detected by fluorescence energy transfer. *Biochim Biophys Acta* **1434**, 31-43 (1999).

227. Medved, L.V. et al. Thermal stability and domain-domain interactions in natural and recombinant protein C. *J Biol Chem* **270**, 13652-9 (1995).

228. Wiessner, C. et al. The second-generation active Abeta immunotherapy CAD106 reduces amyloid accumulation in APP transgenic mice while minimizing potential side effects. *J Neurosci* **31**, 9323-31.

229. Sturchler-Pierrat, C. et al. Two amyloid precursor protein transgenic mouse models with Alzheimer disease-like pathology. *Proc Natl Acad Sci U S A* **94**, 13287-92 (1997).

230. Hsiao, K. et al. Correlative memory deficits, Abeta elevation, and amyloid plaques in transgenic mice. *Science* **274**, 99-102 (1996).

231. Wang, A., Das, P., Switzer, R.C., 3rd, Golde, T.E. & Jankowsky, J.L. Robust amyloid clearance in a mouse model of Alzheimer's disease provides novel insights into the mechanism of amyloid-beta immunotherapy. *J Neurosci* **31**, 4124-36.

232. Patton, R.L. et al. Amyloid-beta peptide remnants in AN-1792-immunized Alzheimer's disease patients: a biochemical analysis. *Am J Pathol* **169**, 1048-63 (2006).

233. Schroeter, S. et al. Immunotherapy reduces vascular amyloid-beta in PDAPP mice. *J Neurosci* **28**, 6787-93 (2008).

234. Weller, R.O., Subash, M., Preston, S.D., Mazanti, I. & Carare, R.O. Perivascular drainage of amyloid-beta peptides from the brain and its failure in cerebral amyloid angiopathy and Alzheimer's disease. *Brain Pathol* **18**, 253-66 (2008).

235. Siemers, B.M., Friedrich, S. & Dean, R.A. Safety, tolerability and biomarker effects of an A[beta] monoclonal antibody administered to patients with Alzheimer's disease. in *Alzheimers Dement* Vol. 4(suppl 2):T774 (2008).

236. Kaufer, D. & Gandy, S. APOE {epsilon}4 and bapineuzumab: Infusing pharmacogenomics into Alzheimer disease therapeutics. *Neurology* **73**, 2052-3 (2009).

237. Bachmeier, C.J., Beaulieu-Abdelahad, D., Mullan, M.J. & Paris, D. Epitope-dependent effects of Beta-amyloid antibodies on Beta-amyloid clearance in an in vitro model of the blood-brain barrier. *Microcirculation* **18**, 373-9.

238. Lemere, C.A. et al. Evidence for peripheral clearance of cerebral Abeta protein following chronic, active Abeta immunization in PSAPP mice. *Neurobiol Dis* **14**, 10-8 (2003).

239. Vasilevko, V., Xu, F., Previti, M.L., Van Nostrand, W.E. & Cribbs, D.H. Experimental investigation of antibody-mediated clearance mechanisms of amyloid-beta in CNS of Tg-SwDI transgenic mice. *J Neurosci* **27**, 13376-83 (2007).

240. Pardridge. Transnasal and intraventricular delivery. in *Peptide Drug Delivery to the Brain*, Vol. 1991:112 (Raven Press, 1991).

241. McGeer, P.L. & McGeer, E.G. Inflammation and the degenerative diseases of aging. *Ann N Y Acad Sci* **1035**, 104-16 (2004).

242. Rogers, J. et al. Complement activation by beta-amyloid in Alzheimer disease. *Proc Natl Acad Sci U S A* **89**, 10016-20 (1992).

243. Rogers, J. et al. Complement activation and beta-amyloid-mediated neurotoxicity in Alzheimer's disease. *Res Immunol* **143**, 624-30 (1992).

244. Strohmeyer, R., Shen, Y. & Rogers, J. Detection of complement alternative pathway mRNA and proteins in the Alzheimer's disease brain. *Brain Res Mol Brain Res* **81**, 7-18 (2000).

245. Zanjani, H. et al. Complement activation in very early Alzheimer disease. *Alzheimer Dis Assoc Disord* **19**, 55-66 (2005).

246. Brazil, M.I., Chung, H. & Maxfield, F.R. Effects of incorporation of immunoglobulin G and complement component C1q on uptake and degradation of Alzheimer's disease amyloid fibrils by microglia. *J Biol Chem* **275**, 16941-7 (2000).

247. Wyss-Coray, T. et al. Prominent neurodegeneration and increased plaque formation in complement-inhibited Alzheimer's mice. *Proc Natl Acad Sci U S A* **99**, 10837-42 (2002).

248. Schwab, C., Hosokawa, M. & McGeer, P.L. Transgenic mice overexpressing amyloid beta protein are an incomplete model of Alzheimer disease. *Exp Neurol* **188**, 52-64 (2004).

249. D'Andrea, M.R., Cole, G.M. & Ard, M.D. The microglial phagocytic role with specific plaque types in the Alzheimer disease brain. *Neurobiol Aging* **25**, 675-83 (2004).

250. Chauhan, N.B. & Siegel, G.J. Efficacy of anti-Abeta antibody isotypes used for intracerebroventricular immunization in TgCRND8. *Neurosci Lett* **375**, 143-7 (2005).

251. Radaev, S. & Sun, P. Recognition of immunoglobulins by Fcgamma receptors. *Mol Immunol* **38**, 1073-83 (2002).

252. Carty, N.C. et al. Intracranial administration of deglycosylated C-terminal-specific anti-Abeta antibody efficiently clears amyloid plaques without activating microglia in amyloid-depositing transgenic mice. *J Neuroinflammation* **3**, 11 (2006).

253. Bacskai, B.J. et al. Imaging of amyloid-beta deposits in brains of living mice permits direct observation of clearance of plaques with immunotherapy. *Nat Med* **7**, 369-72 (2001).

254. Das, P., Murphy, M.P., Younkin, L.H., Younkin, S.G. & Golde, T.E. Reduced effectiveness of Abeta1-42 immunization in APP transgenic mice with significant amyloid deposition. *Neurobiol Aging* **22**, 721-7 (2001).

255. Maier, M., Seabrook, T.J. & Lemere, C.A. Modulation of the humoral and cellular immune response in Abeta immunotherapy by the adjuvants monophosphoryl lipid A (MPL), cholera toxin B subunit (CTB) and E. coli enterotoxin LT(R192G). *Vaccine* **23**, 5149-59 (2005).

256. Nimmerjahn, F., Bruhns, P., Horiuchi, K. & Ravetch, J.V. FcgammaRIV: a novel FcR with distinct IgG subclass specificity. *Immunity* **23**, 41-51 (2005).

257. Nimmerjahn, F. et al. FcgammaRIV deletion reveals its central role for IgG2a and IgG2b activity in vivo. *Proc Natl Acad Sci U S A* **107**, 19396-401.

258. Yamada, K. et al. Abeta immunotherapy: intracerebral sequestration of Abeta by an anti-Abeta monoclonal antibody 266 with high affinity to soluble Abeta. *J Neurosci* **29**, 11393-8 (2009).

259. Brendza, R.P. & Holtzman, D.M. Amyloid-beta immunotherapies in mice and men. *Alzheimer Dis Assoc Disord* **20**, 118-23 (2006).

260. Bonetta, L. Door Slams on RAGE. (http://www.alzforum.org, 2011).

261. Deane, R. et al. A multimodal RAGE-specific inhibitor reduces amyloid beta-mediated brain disorder in a mouse model of Alzheimer disease. *J Clin Invest* **122**, 1377-92.

262. Deane, R.J. Is RAGE still a therapeutic target for Alzheimer's disease? *Future Med Chem* **4**, 915-25.

263. Diez, M. et al. Neuropeptide alterations in the hippocampal formation and cortex of transgenic mice overexpressing beta-amyloid precursor protein (APP) with the Swedish double mutation (APP23). *Neurobiol Dis* **14**, 579-94 (2003).

264. Lalonde, R., Dumont, M., Staufenbiel, M., Sturchler-Pierrat, C. & Strazielle, C. Spatial learning, exploration, anxiety, and motor coordination in female APP23 transgenic mice with the Swedish mutation. *Brain Res* **956**, 36-44 (2002).

265. Gengler, S., Hamilton, A. & Holscher, C. Synaptic plasticity in the hippocampus of a APP/PS1 mouse model of Alzheimer's disease is impaired in old but not young mice. *PLoS One* **5**, e9764.

266. Heppner, F.L. et al. Experimental autoimmune encephalomyelitis repressed by microglial paralysis. *Nat Med* **11**, 146-52 (2005).

267. Nelson, R.A., Jr. The immune-adherence phenomenon; an immunologically specific reaction between microorganisms and erythrocytes leading to enhanced phagocytosis. *Science* **118**, 733-7 (1953).

268. Waxman, F.J. et al. Complement depletion accelerates the clearance of immune complexes from the circulation of primates. *J Clin Invest* **74**, 1329-40 (1984).

269. Obregon, D. et al. CD40L disruption enhances Abeta vaccine-mediated reduction of cerebral amyloidosis while minimizing cerebral amyloid angiopathy and inflammation. *Neurobiol Dis* **29**, 336-53 (2008).

ACKNOWLEDGEMENT

I want to thank a group of very special people that have supported me in many different ways.

Prof. F.L. Heppner, my main supervisor. I want to express my sincere gratitude for the guidance and support he showed me throughout my dissertation and especially for giving me the opportunity to pursue my PhD thesis in his elite institute. His perpetual energy and enthusiasm in research motivated me. In addition, he was always accessible and willing to help his students with their research.

I thank Prof. U. Kalinke for his valuable advice in science discussion especially with respect to B cell proliferation assays and ELISA development. I also show my gratitude to his lab (especially to Dr. Claudia Detje) for performing the *in vivo* VSV infection of *AB9µ*, *DelS* and control mice.

I thank Dr. L. Li for her support during the first year of this doctoral thesis work and her input on the first experiments (B cell and immune cell phenotyping, ELISA and genotyping).

I thank Kerstin Kopp for technical support and beyond that for fruitful discussions and encouragement during the span of my doctoral research.

I am much indebted to Dr. Stefan Prokop for his valuable advice in science discussion and experimental design. I also gratefully thank him for his constructive comments on this thesis. I am thankful that in the midst of all his work, he accepted to be a member of the reading committee.

Many thanks go in particular to Dr. Jason Millward, post doc and friend. Although not being responsible for me and working in another lab, he always helped me, answered my questions and most importantly used his precious times to read this thesis and gave his critical and constructive comments about it.

Many thanks go to Annette Wolf who was involved in the generation of both transgenic mouse strains and helped me to understand all cloning steps described in this thesis.

The generous support from NeuroCure is greatly appreciated. They granted me the scholarship and furthermore funded the visit of several conferences and seminars.

Finally, I want to express my gratitude to all the other members of the neuropathology lab, to the senior scientists, to my fellow graduate students, to all the technical assistants, and to the general support staff. There is no telling how much my dissertation profited from working in such a network that is at the same time friendly and professional. In particular, I want to thank my fellow students - Maren Bradtmöller, Josephine Held, Susann Handrick, Gina Eom, Stefanie Kraft, Lisa Wagner, Juliane Obst and Natalia Drost – for coffee breaks and chatting while sharing the ups and downs that come with doing a PhD.

SELBSTÄNDIGKEITSERKLÄRUNG

Ich, Nicole Hentschel, erkläre, dass ich die vorgelegte Dissertation mit dem Thema: Mechanisms of Immunotherapy in **Alzheimer`s disease - Testing the peripheral sink hypothesis by restricting Aβ-antibodies to the periphery** selbst verfasst und keine anderen als die angegebenen Quellen und Hilfsmittel benutzt, ohne die (unzulässige) Hilfe Dritter verfasst und auch in Teilen keine Kopien anderer Arbeiten dargestellt habe.

Datum Unterschrift